Page

LISTE DES TABLEAUX

Page

LISTE DES FIGURES

Page

LISTE DES ABRÉVIATIONS, SIGLES ET ACRONYMES

SMC	Mode de glissement
PID	Contrôleur proportionnel intégral dérivative
EHS	Système électrohydraulique
LVDT	Transformateur variable linéaire
ERL	Loi d'atteinte exponentielle
SMHC	Contrôleur hybride mode de glissement
FSMHC	Contrôleur hybride mode de glissement à logique floue
PSM	Contrôleur mode de glissement de la position
FSM	Contrôleur mode de glissement de la force
DAQ	Acquisition de données
SMPIDHC	Contrôleur hybride mode de glissement et proportionnel intégral dérivative
PIDHC	Contrôleur hybride proportionnel intégral dérivative
SMPIDHC	Contrôleur hybride mode de glissement et proportionnel intégral dérivative
FPID	Contrôleur proportionnel intégral dérivative à logique floue
AFPID	Contrôleur adaptatif proportionnel intégral dérivative à logique floue
PIDDL	Contrôleur double boucle proportionnel intégral dérivative à double boucle
FPIDDL	Contrôleur double boucle proportionnel intégral dérivative à logique floue
AFPIDDL	Contrôleur adaptative double boucle proportionnel intégral dérivative à logique floue
FERLSMHC	Contrôleur hybride mode de glissement avec une loi d'atteinte exponentielle et logique floue
SMPIDHCERL	Contrôleur hybride mode de glissement et proportionnel intégral dérivative avec une loi d'atteinte exponentielle

SMPIDHCERL	Contrôleur hybride mode de glissement et proportionnel intégral dérivative avec une loi d'atteinte exponentielle
SMHCERL	Contrôleur hybride mode de glissement avec une loi d'atteinte exponentielle

LISTE DES SYMBOLES ET UNITÉS DE MESURE

M_s	Masse du corps du véhicule, Kg
M_u	Masse de l'ensemble suspension-pneu, Kg
x_r	Perturbations da la route, Cm
x_s	Position verticale du corps du véhicule, cm
x_u	Position verticale du pneu du véhicula, cm
B_p	Coefficient de frottement visqueux da la suspension passive, $N.s/m$
K_p	Rigidité da la suspension passive N/m
B_r	Coefficient d'amortissement du pneu $N.s/m$
k_r	Rigidité du pneu, N/m
β	Coefficient de compressibilité da l'huile, N/m^2
L	Coefficient da fuite interne du vérin hydraulique, $m^5/N\ s$
$Q_{1,2}$	Débits à travers les orifices da la servovalve,cm^2/s
P_s	Pression à la sortie de la pompe, N/cm^2
P_L	Pression différentielle à la charge, N/cm^2
$P_{1,2}$	Pression dans les deux chambres de l'actionneur hydraulique, N/cm^2
A	Section du piston du vérin hydraulique, m^2
ρ	Masse volumique da l 'huile, kg/m^3
V_O	Volume d'huile dans une des chambres moitié ouverte, m^3
τ	Constante de temps da la servovalve, sec
k_v	Gain constant de la servovalve, m^2/V
C_D	Coefficient d'écoulement, sans dimension

α	Constante exponentielle, sans dimension
U	Signal d'entrée de la servovalve, Volt

INTRODUCTION

Les systèmes électrohydrauliques sont très utilisés dans plusieurs applications industrielles. L'espace occupé par un système hydraulique pour produire la même puissance est très petit par rapport à celui des systèmes électriques ou mécaniques.
Plus particulièrement, les industries de l'aéronautique, de la marine, des machines lourdes, de l'automobile et de la robotique utilisent les systèmes électrohydrauliques dans des applications qui requièrent un grand niveau de précision en contrôle de force ou de position.
Dans la marine, les systèmes électrohydrauliques en acier inoxydable sont les plus avancés et les plus modernes. Ils sont utilisés pour la propulsion, la stabilisation et la direction. Ils sont conçus pour rencontrer la demande croissante de l'énergie dans les espaces limitées pour les systèmes embarquées dans les sous-marins.

Les systèmes hydrauliques en automobile, sont intégrés dans le système de freinage, de suspension active, de transmission et de pilotage. De tels systèmes exigent un asservissement rapide tant pour la force que pour la position. Les composants principaux sont la pompe, l'accumulateur, le réservoir, la servovalve et l'actionneur. La pompe est un élément essentiel pour alimenter le circuit hydraulique en huile. L'accumulateur est utilisé pour compenser la variation de pression dans les cas où il y une demande de débit due à une variation de charge. Le réservoir est utilisé pour stocker l'huile de tout le système. La servovalve est l'élément actif qui contrôle le débit, le sens découlant et la pression dans le circuit hydraulique.
L'actionneur est conçu pour transformer l'énergie hydraulique en une énergie mécanique en transition où en rotative.

La servovalve peut être contrôlée en boucle ouverte ou fermée dépendamment de l'application. La modélisation de la servovalve illustre clairement la nonlinéarité des systèmes hydrauliques contrôlés par des servovalves. Le fait que l'équation du débit dépend de la racine carrée de la pression et que la pression est multipliée par le mouvement transitionnel du tiroir de la servovalve et la fonction de signe rendent le contrôle plus complexe. Les stratégies de contrôle de ce type de systèmes passent par l'emploi de lois de commande non classiques. Ces lois de

commande nonlinéaires devraient s'adapter avec la variation des paramètres du système ou la variation des charges. Dans un système hydraulique, la température de l'huile, la viscosité, la variation des charges, la dégradation de l'huile avec le temps impliquent des méthodes de contrôle plus avancées et adaptives. Ces méthodes de contrôle utilisent des algorithmes mathématiques pour générer un signal de contrôle qui tient compte de la variation des paramètres du système.

Pour les contrôleurs simples comme le PID, la stratégie de contrôle n'exige pas des modèles mathématiques compliqués. La mise en marche de ce type de contrôle est facile et direct comme il n'est pas nécessaire d'intégrer les équations mathématiques non différentiables et nonlinéaires dans les lois de contrôle. Il existe dans l'industrie des contrôleurs classiques qui font un asservissement direct pour une seule variable. Les contrôleurs classiques comme le PID, le placement de pôles et la commande linéaire quadratique ont des procédures systématiques à suivre pourtant la commande nonlinéaire, dans certains cas, n'a pas de procédures précises à appliquer et impose des conditions différentes et limitations sur les systèmes théoriques.

La configuration de ce type des contrôleurs est facile, leur efficacité rend leur usage plus populaire dans différents secteurs industriels. La variation des paramètres du système n'a pas de grand effet sur l'efficacité de ces contrôleurs. Due au développement rapide dans ce domaine, les contrôleurs classiques comme le PID appliquent des algorithmes de contrôle adaptif en trouvant les paramètres optimaux de ces contrôleurs pour des applications plus réalistes en industrie. Malgré l'avancement de ces contrôleurs, ils sont loin de satisfaire une demande croissante de contrôleurs rapides, efficaces, adaptifs et intelligents. Ce constat a constitué au développement des nouveaux contrôleurs nonlinéaires basés sur les modèles mathématiques des systèmes hydrauliques contrôlés par des servovalves.

Les applications industrielles, munies des systèmes de contrôles nonlinéaires avancés, déploient des théories de contrôle destinées à résoudre les modules mathématiques ayant une structure nonlinéaire, nondifférentiable ou bien une incertitude dans les paramètres. Le but de

modéliser ces systèmes de telle façon est de rapprocher le plus possible le module théorique de celui de la réalité que représente ce système sans être obligé de simplifier où de passer par des alternatives équivalentes.

La commande nonlinéaire a une capacité pour s'adapter avec tout changement en utilisant des méthodes, des structures et même des lois adaptives pour mettre à jour les paramètres internes. Le choix de la théorie de la commande nonlinéaire dépend de la dynamique du système, de ses équations et même de l'objectif du contrôle. Il est nécessaire, pour certains systèmes, de faire des changements de variables dans les équations avant d'appliquer certaines théories.

Les théories de contrôle nonlinéaire les plus populaires sont le mode de glissement, le backstepping, la linéarisation approximative par feedback, les réseaux de neurones artificiels et la logique floue. Le mode de glissement est une méthode systématique commençant par le choix de la surface de glissement. Une fois la surface est dérivée, le signal de control peut être extrait si la condition nécessaire est rencontrée. Le mode de glissement a un effet indésirable représentée par le broutement inhérent produit par la fonction de commutation dans la loi de commande. La commande produite devrait prendre en considération les effets indésirables du broutement sur les actionneurs hydrauliques, les servovalves et la performance générale de contrôleur. Cette méthode sera exploitée dans le cadre de notre thèse où nous avons adopté le système de suspension active électrohydraulique comme une base de recherche.

Vu que la majorité des composants hydrauliques existent déjà dans les systèmes automobiles, l'exploitation et l'intégration de la suspension active devient plus facile sur ces systèmes. Par conséquent, les systèmes électrohydrauliques sont devenus incontournables dans le processus de freinage, le pilotage, la suspension active, le levage et toute autre opération exigeant une forte puissance. Les systèmes automobiles aujourd'hui se développent rapidement avec une gamme de technologies avancées, ultra rapide et respectueux de l'environnementale. Cette technologie s'adapte bien avec les méthodes de contrôle nonlinéaire qui exigent l'utilisation des ordinateurs ultra rapides, des composants électroniques, hydrauliques et mécaniques fiables.

En général, la suspension active, dans une automobile, constitue deux masses, des vérins de suspension et des ressorts. Les deux masses sont la masse de corps de véhicule (siège du passager) et la masse des pneus. Les vérins de suspension sont installés entre le corps et les pneus pour atténuer les perturbations de la route. Le groupe des vérins est muni par des ressorts de suspension et asservis par un système électrohydraulique.

L'objectif principal de cette recherche est de développer une méthode de contrôle d'une suspension active avec plusieurs sous objectifs. Le premier sous objectif est de faire un contrôle de position et de force en utilisant des stratégies de contrôle applicables sur un système embarqué. Le deuxième est de réaliser une structure hybride qui combine les deux contrôleurs développés précédemment pour le contrôle de position et de force.
Le troisième est de faire un contrôle adaptatif basé sur des contrôleurs conventionnels qui peut être applicable dans une structure hybride.

Dans un premier temps, nous avons adopté le contrôle par mode de glissement pour faire un contrôle de la position verticale des passagers. La position du siège a été isolée des perturbations générées par les imperfections de la route. Le désavantage du mode de glissement, comme le broutement, a été contourné en adaptant une fonction mathématique récemment développée (Fallaha et al, 2011).La méthode a été appliquée et a donné des résultats intéressants tant en simulation qu'en temps réel ouvrant la porte à l'étape suivante. Le contrôle de force a été développé de la même façon. Une force désirée a été générée à partir des variables du système selon certains critères et normes imposés sur les fabricants d'automobiles. Le suivi de la force désirée a été fait indépendamment du contrôle de position de l'étape précédente.

Une fois, le contrôleur de force développé et réglé, les éléments essentiels des deux contrôleurs de position et de force ont été intégrés efficacement dans une structure hybride.
Dans un second temps, la structure hybride a été développée afin de surmonter la difficulté des autres structures existantes. La simplicité et l'efficacité sont des éléments essentiels pour qu'une méthode de contrôle soit applicable. Le contrôle hybride assure le confort des passagers

lors de la conduite avec une tenue de route plus sécuritaire. Un algorithme a été adopté avec le mode de glissement pour améliorer la performance de structure suggérée. La stabilité de la méthode a été vérifiée ainsi que la robustesse en utilisant des réponses fréquentielles.

Le contrôle hybride peut contenir des contrôleurs adaptives, c'est pour cela que nous avons développé deux contrôleurs adaptifs par l'intermédiaire des contrôleurs de logique floue. Les contrôleurs adaptifs ont été validés en temps réel sur le système de suspension active pour les intégrer dans la structure hybride.

Les objectifs spécifiques de notre thèse sont les suivantes :

- ✓ la modélisation mathématique des systèmes électrohydrauliques à suspension active pour les tests en simulation ainsi que pour les tests en temps réel. L'objectif est de créer un modèle hybride compensant des éléments essentiels manquants comme les ressorts dans le banc d'essai de suspension active;
- ✓ Le développement d'une loi de commande nonlinéaire impliquant une structure de contrôle hybride pour contrôler la position et la force sur le banc à suspension active.
- ✓ L'évaluation expérimentale de la performance des lois de commande nonlinéaire développées précédemment en présence de bruit sur les mesures pour différentes structures hybrides;
- ✓ L'évaluation numérique en temps réel des techniques existantes récemment développées, comme la loi d'atteinte exponentielle et le contrôleur de logique floue basé sur les surfaces de glissement, en vue d'améliorer notre structure hydride développé précédemment;
- ✓ La comparaison entre les structures de contrôle hybride utilisant des contrôleurs nonlinéaires et conventionnels pour évaluer la performance;
- ✓ Le développement de contrôleur adaptatif dans le but de contrôler conjointement la position et la force comme piste de développement futur dans le domaine de commande hybride.

La thèse est structurée de la façon suivante :

Dans le premier chapitre, une revue de littérature est présentée illustrant les travaux précédents effectués dans ce domaine et liés avec notre thèse. L'originalité de nos contributions a été élaborée dans le même chapitre.

Dans un deuxième chapitre, le mode de glissement est détaillé dans le but de faciliter la compréhension du modèle de commande nonlinéaire utilisé dans cette thèse. Les chapitres suivants sont consacrés aux trois articles rédigés dans le cadre de cette thèse. Ces articles contiennent les contributions originales de la thèse.

Le troisième chapitre contient le premier article publié dans la revue " Transactions of the Institute of Measurement and Control" :
«Shaer, B., Kenné, J.-P. Kaddissi, C., Fallaha, C. A chattering-free fuzzy hybrid sliding mode control of an electrohydraulic active suspension. *Transactions of the Institute of Measurement and Control* 2016; DOI: 0142331216652468».
Dans cet article, nous présentons une structure de contrôle hybride composée des deux contrôleurs non linéaires. La technique pour réduire le broutement produit par le mode de glissement ainsi que les contrôleurs sont testés et validés en simulation et en temps réel.

L'article du quatrième chapitre est soumis dans la revue "International Journal of Robust and Nonlinear Control". Nous présentons dans cet article des structures de contrôle hybride linéaire et nonlinéaire. Le modèle de banc d'essai a été développé et validé en utilisant des séries d'équations nonlinéaires. La comparaison de la structure proposée est faite avec le contrôleur PID pour des fins de validation. Les tests en temps réel sont présentés et comparés avec d'autres contrôleurs pour la validation.
«Shaer B, Kenné JP, Kaddissi C, Honorine AM. Real-Time Hybrid Control of Electrohydraulic Active Suspension. publié dans le journal " *International Journal of Robust and Nonlinear Control 2016*".

L'article du cinquième chapitre est soumis à la revue " IEEE Transactions on Control Systems Technology". Dans cet article, on présente un contrôleur de position du banc d'essai à

suspension active. Le contrôleur PIDDL est modifié et validé en temps réel. Un contrôleur de logique flou est développé pour faire la mise à jour des gains des contrôleurs PIDDL et PID. Les résultats des tests sont validés et comparés avec ceux de PID pour valider l'approche proposée.

«Shaer, B., Kenné, JP., Kaddissi C., Zaher, A., Serial Fuzzy Self-Tuning PID Dual Loop Position Controller For Active Suspension, soumis dans le journal " IEEE Transactions on Control Systems Technology 2017".

Finalement, dans la conclusion, nous avons résumé le travail fait dans le cadre de cette thèse et les contributions originales apportées.

CHAPITRE 1

REVUE DE LITÉRATURE

1.1 Introduction

De nos jours, Les systèmes électrohydrauliques sont construits d'une façon intégrée en utilisant des composants hydrauliques assez performants. La modélisation de ces systèmes est le premier pas afin de faire un contrôle efficace correspondant aux enjeux et aux défis de l'industrie. La demande de forte puissance mécanique passe souvent par l'installation d'un système électrohydraulique contrôlé par des différentes méthodes. Les méthodes classiques sont plus faciles et rapides, par contre elles ne rencontrent pas les exigences croissantes des utilisateurs. Face à cette réalité, les chercheurs dans ce domaine continuent à développer des méthodes nonlinéaires et non standards plus avancées pour la progression des contrôleurs performants. Dans ce cas, cette modélisation et ce processus de développement sont plus complexes et constituent un défi à relever dans cette thèse.

1.2 Systèmes électrohydrauliques en général

Les systèmes électrohydrauliques, comme tous les systèmes, ont des composants essentiels dont on obtient la puissance mécanique voulue. Les systèmes électrohydrauliques sont composés des actionneurs hydrauliques en rotation ou en translation. Pour les actionneurs hydrauliques en rotation, le système de suspension active est composé d'une pompe bidirectionnelle à cylindrée variable. Cette cylindrée peut être variée par le biais d'une servovalve et d'un actionneur. Deux réglages sont faits à ce niveau, le premier se fait par un limiteur de pression installé sur le refoulement, le deuxième c'est un régulateur de pression installé directement sur la pompe. Pour les actionneurs hydrauliques en translation, la pression est gardée à une valeur de consigne par l'accumulateur, le limiteur de pression et la servovalve. Cette servovalve reçoit un signal de commande électrique pour déplacer un tiroir afin de déterminer l'ouverture de l'orifice et par conséquence le débit.

La servovalve détermine la direction du débit fourni à l'actionneur hydraulique. Le vérin représente un actionneur hydraulique en translation vu qu'il change l'énergie hydraulique en énergie mécanique représentée par un mouvement linéaire. Dans le cas d'une absence de signal, la servovalve prend une position initiale par laquelle le débit envoyé vers le vérin dépend du type de l'orifice.

La suspension active utilise l'actionneur hydraulique en translation qui contient des vérins et des ressorts pour atténuer les perturbations produites par les irrégularités de la route. La modélisation d'un système à suspension active est basée sur celle d'un system électrohydraulique. La différence est représentée par la dynamique du vérin de suspension et celle des ressorts. Des équations décrivent la dynamique du système électrohydraulique sont présentées dans Merritt (1967).

La modélisation portant sur ces équations se base sur les lois de la physique. Un changement des variables est par la suite appliqué pour avoir le modèle d'état du système. Le livre Tomas (1994) contient également la modélisation des différents composants d'une automobile. Si on prend en considération chaque élément dans la modélisation, on aura un ensemble des équations nonlinéaires. Le fait de trouver une loi de commande pour stabiliser ce type des systèmes nonlinéaires sans avoir des singularités, broutement où bien des complications de toutes sortes est impossible. Alors, il faut passer toujours par des fonctions simplificatrices telles que dans Kaddissi et al (2009) où des algorithmes de contrôle divisant les systèmes nonlinéaires en plusieurs sous-systèmes soit pour la modélisation ou bien pour la commande.

Selon l'objectif de contrôle, les systèmes hydrauliques sont conçus pour produire une force désirée, suivre un trajet de position voulu ou bien faire les deux en même temps. Les applications en robotique sont de bons exemples pour le contrôle de position et de la force. Les tâches en robotique sont résumées par le suivi d'une trajectoire spécifiée dans un espace déterminé avec des forces de contact précises. Nous commençons la revue de littérature par un survol des méthodes de contrôle en position et en force. Le contrôle hybride est par la suite

consacré dans le reste de la revue, pour montrer les étapes de développement des contrôleurs hybrides visant la force et la position en même temps.

1.3 La commande de position des systèmes électrohydrauliques

Dans un contrôle de position, le processus d'asservissement peut être affecté par plusieurs facteurs comme le frottement (Bonchis et al, 2001), la perturbation externe et la dynamique non modelé (Mihajlov et al, 2002) ainsi que l'incertitude des paramètres (Mintsa et al, 2011). Certains chercheurs ont adopté des méthodes simples avec une seule technique comme les contrôleurs PID et les théories de contrôle nonlinéaire simple (Heinrichs et al, 1997). Malgré leur efficacité et popularité, les méthodes simples n'atteignent pas les spécifications imposées par l'industrie et les conditions variables de certains paramètres. C'est pour cela que les chercheurs font recours aux méthodes de contrôle de position en utilisant plusieurs techniques en même temps.

Ces méthodes assurent le bon contrôle, surtout que la majorité des applications exigent des courses contrôlées et précises. (Campos et al, 1999) ont adopté un ensemble de techniques basées sur le temps et sur la transformation de découplage des entrées pour les forces en arrière et en avant d'une véhicule. Leur méthode a été appliquée sur un système de suspension active de 4 degrés de liberté. Ces auteurs ont utilisé des filtres passe haut et bas dans les boucles internes pour réduire les forces perturbatrices pourtant les déplacements tangages et lacets sont contrôlés et stabilisés par une boucle externe. Les résultats de simulation ont montré une mauvaise suspension pour les fréquences plus élevées que la fréquence de résonance des pneus.

Le contrôleur de position peut être intégré à d'autres contrôleurs en utilisant des méthodes adaptatives. Cela représente une partie des étapes de développement où les paramètres sont estimés et mis à jour pour avoir une meilleure performance. Une fois les méthodes de contrôle sont développées, les chercheurs prennent en considération les incertitudes qui perturbent les paramètres des systèmes en temps réel. Ils se réfèrent aux algorithmes adaptatifs pour estimer et mettre à jour les paramètres de ces systèmes.

Les systèmes de la suspension sans exception se distinguent par rapport à leurs fonctions nonlinéaires et nondifférentiables. Ces caractéristiques rendent la tâche de commande adaptative plus compliqués. Mentionnerons par exemple que la variation de la température et la pression sont les causes principales pour l'incertitude dans les systèmes à suspension active. Pour résoudre ce problème, (Han et al, 2005) ont utilisé un contrôleur basé sur le PID et la logique floue avec un auto-rajustement universel. La turbine à vapeur contrôlé par ce dernier contrôleur pour asservir la position et pour éliminer le broutement. En principe ces types des contrôleurs sont efficaces mais ils sont loin d'atteindre des objectifs de contrôle différents. Dans le même thème, plusieurs chercheurs ont développé une structure nommée hybride en référence à une structure où il y deux contrôleurs développés pour faire des tâches différents.

En général, la structure d'un contrôleur hybride est limitée par les capacités des composants hydrauliques et les contrôleurs utilisés. Shi et al (2008) ont combiné un retour d'état de la pression et de débit du système. La pression est utilisée dans la boucle externe et le débit dans l'interne pour réduire l'interaction entre eux. Deux signaux de commande permettent de suivre l'ensemble la pression et le débit en même temps. Cette stratégie de contrôle a permis d'attendre la performance désirée. Dans la littérature, les solutions suggérées sont soit des contrôleurs simples, contrôleurs hybrides ou bien des méthodes adaptatives intégrées dans les contrôleurs.

Dans ce sens, (Kalyoncu et Haydim, 2009) ont ajouté des paramètres spéciaux au modèle mathématique comme la fuite interne. Ils ont négligé la fuite est négligée dans le modèle du système pour des fins de simplicité. Pourtant (Kalyoncu et Haydim, 2009) ont montré que l'ajout de la fuite interne a améliorait la performance du contrôleur de position d'un système électrohydraulique.

Les contrôleurs de position intégrant plusieurs techniques comme le block intégral, le mode de glissement et le contrôle $H\infty$ (Alexander et al, 2009) ont développé un control de position pour suivre une trajectoire de référence chaotique. Ce contrôleur a été développé pour

compenser les nonlinéarités inhérentes de l'actuateur et rejeter la perturbation appariée. Avec une telle structure, le contrôleur n'était pas capable de donner un signal de contrôle exempt de broutement de hautes fréquences.

Le développement de contrôleur de position a atteint un autre niveau dans le travail de Shao et al (2009). Ils ont commencé par un modèle d'identification en utilisant un bloc d'identification en temps réel de Matlab RTW. Ensuite, ils ont intégré deux contrôleurs en parallèle pour former un contrôleur hybride. Le premier c'est un contrôleur proportionnel. Le deuxième c'est un contrôleur PID accompagné d'un contrôleur en logique floue. La transition entre ces deux contrôleurs est réalisée par un interrupteur où l'erreur de position est essentielle dans ce processus. La position zéro de l'interrupteur est vue comme un seuil de commutation pour éviter les perturbations non désirées. Ce dernier bascule entre les contrôleurs quand l'erreur dépasse une consigne prédéterminé pour garantir une commutation stable.

D'une façon similaire, une autre structure de quatre boucles est suggérée par (Priyandoko et al, 2009) pour un contrôleur hybride en temps réel. La méthode proposée est original par la façon dont il a élaboré le problème de contrôle. Ils ont ajusté la dynamique du système par l'intermédiaire de boucles rétroactives. En résumé, les perturbations de basse fréquence ont été supprimées et les perturbations de hautes fréquences étaient hors contrôle.

Pour remédier à ce problème, (Çetin et Akkaya, 2010) ont trouvé que les méthodes adaptatives avec un contrôleur de structure hybride pouvaient donner de bons résultats pour le contrôle de position. Par conséquence un contrôleur hybride à logique floue accompagné par des règles couplées pourrait asservir parfaitement un système hydraulique. La réponse de système était relativement rapide pourtant de grande forces ont été générées par l'actuateur. Cela a ouvert la porte à d'autres chercheurs pour développer des contrôleurs de position avec des gains variables basés sur les variables du système.

1.4 La commande adaptative de position des systèmes électrohydrauliques

La nonlinéarité et l'incertitude des systèmes électrohydrauliques étaient difficiles à contrôler, un contrôleur devrait s'adapter en variant ses gains ou en changeant des paramètres dans le système. Dans le contrôle de position, des contrôleurs conventionnels et classiques sont développés en utilisant des méthodes intuitives comme la logique floue.

La logique floue (Callai et al, 2005) est utilisée comme un outil efficace pour changer les gains d'un contrôleur PID. Pour ne pas dépendre de la connaissance de l'expert, (Callai et al, 2005) as adapté quatre techniques pour réduire au maximum le besoin de correction par l'expert. Une des structures se base sur le décalage des fonctions d'appartenance, cela est différent du travail fait par Jantzen (1998). Une autre structure qui utilise des compensateurs pour renforcer le signal de commande contre les points d'opération différents. Ces contrôleurs sont faits pour mettre à jour les gains, pourtant d'autres chercheurs ont pris un autre chemin pour régler le problème d'incertitude des paramètres Solihin (2007). La mise à jour des gains est faite par des facteurs flous de pondération ajoutés à la sortie du contrôleur.

Dans les règles de contrôle par logique floue, les chercheurs font recours au décalage des fonctions d'appartenance vu qu'il relocalise le signal d'entrée dans une autre échelle (Bakri et al, 2012). Dans leur travail, un contrôle par logique floue adaptative a été développé par le décalage des fonctions d'appartenance pour les entrées et les sorties en même temps. Le paramètre ajusté est l'univers du discours qui détermine combien il faut décaler les fonctions d'appartenances. La méthode essais-erreurs est utilisée pour changer l'univers du discours et avoir de bons résultats, par contre les contrôleurs développés manquent de robustesse.
Pour résoudre ce problème, Maghfiroh (2013) a développé une structure hybride basée sur la logique floue pour avoir un contrôleur plus robuste qui s'adapte à la variation des références. Le contrôleur proposé a donné des résultats meilleurs que ceux d'un contrôleur PID avec des gains fixes.

Malgré leur importance et leur popularité, les contrôleurs conventionnels comme le PID n'ont pas subi des modifications de structure au fils des années. Récemment, le contrôleur PID dual loop (PIDDL) a été conçu par Desantis (1996) comme une extension des contrôleurs PID classique. À notre connaissance, le contrôleur PIDDL n'a pas encore été implanté dans le domaine de commande des systèmes électrohydrauliques malgré leurs performances. Cela nous a motivés dans notre thèse à développer un contrôleur à logique flou pour mettre à jour les gains de contrôleur PIDDL. Le contrôleur PIDDL est modifié à travers plusieurs étapes et testé sur le banc d'essai à suspension active pour contrôler la position du siège du passager.

1.5 La commande de force des systèmes électrohydrauliques

Avec le contrôle de position, le contrôle de force se manifeste comme une nécessité avec la demande croissante par l'industrie d'avoir des contrôleurs plus volatiles. Alleyne et Liu (2000) ont commencé à développer des contrôleurs de force simple par l'intermédiaire de la fonction lyapunov. Le fait de simplifier le modèle peut créer des erreurs de précision et en l'ajoutant lors du suivi des références. Dans le même ouvrage de (Alleyne et Liu, 2000) qui ont proposé le contrôle de pression/force à partir d'une seule dérivation de la fonction lyapunov pour avoir directement le signal de contrôle. Pourtant avec le mode de glissement, plusieurs dérivations sont exigées, selon le choix de la surface de glissement, pour avoir enfin le signal de contrôle.

Si le choix de la surface de glissement est fait avec plusieurs dérivations de la même variable, l'expression mathématique donnant le signal de contrôle sera lourde et longue (Hedrick et Yip, 2000). Le fait de choisir adéquatement la surface de glissement pourrait empêcher ce problème mais tout dépend de l'expérience du développeur. Le contrôle de force peut se présenter comme un contrôle de la pression où de l'accélération Shoorehdeli et al (2006). Ils ont suggéré une fonction Lyapunov avec une un gain variable pour construire la loi de commande. Le fait de régler ce gain peut étendre le contrôle des systèmes sur une grande échelle. Malgré que la théorie de lyapunov garantisse la stabilité, la performance est limitée. Pour remédier à ce problème, Hudha (2006) a développé un contrôleur hybride en série. Dans ce contrôleur, la boucle interne est utilisée pour tracer une référence de force produite par une boucle externe.

La performance du contrôleur est bonne pour le suivi de force mais elle n'est pas suffisante en termes du déplacement de masse du véhicule.

Dans les applications aéronautiques où le contrôle de force est critique (Karpenko and Sepehri, 2012), l'asservissement de force par un simple retour d'états est difficile à atteindre. La rétroaction quantifiée nonlinéaire s'est présentée comme une solution pour atteindre une erreur minimale de force asservie dans le cas d'une dynamique de charge variable. Comme la demande pour le contrôle de force et position augmente, le contrôle hybride s'est présenté comme un contrôle alternatif pour compromettre les objectifs contradictoires. L'approche hybride est le remplaçant pratique des approches homogènes pour traiter efficacement des problèmes au niveau des variations de la structure suite aux différents modes d'opération, d les variations des paramètres du système accompagnant les états de transition et de la commutation entre les modèles pour modéliser un phénomène transitoire.

Le contrôle hybride réfère non seulement à une structure avec deux contrôleurs, mais aussi aux contrôleurs de deux références différentes à suivre ou un système intégrant des signaux discrets et continus (Fainekos et al, 2005). Dans les travaux de (Lane et al, 1997), une comparaison est faite entre deux contrôleurs hybrides. Le premier contrôleur hybride utilise la structure variable de contrôle et le deuxième utilise un contrôle multi variables hybride et adaptatif. Le contrôleur hybride ajoute les deux signaux de contrôle pour former le signal hybride. Avec un tel design, c'est difficile de contrôler le signal hybride car les deux signaux de contrôle n'ont pas des bornes ni de contrôle sur les deux branches.

Dans le même esprit, le contrôle hybride développé par (Assadsangabi et al, 2009), a utilisé deux références : le modèle de skyhook idéal et le modèle de Ground Skyhook. La connaissance des perturbations d'une route est un prérequis pour le modèle hybride; ce modèle est construit en ajoutant des signaux de contrôle intermédiaires. Malgré les résultats satisfaisants obtenus par (Assadsangabi et al, 2009), les auteurs n'ont pas pu avoir l'accélération de masse désirée.

Pour réduire l'accélération de la masse, (Priyandoko et al, 2009) a utilisé quatre boucles de réseaux de neurones pour construire la dynamique inverse d'un actionneur. Avec les réseaux de neurones, le contrôleur proposé était capable de suivre une référence de force et de récompenser la perturbation. En général, (Priyandoko et al, 2009) ont résolu le problème de (Assadsangabi et al, 2009) en réduisant l'accélération de masse. Les résultats de suivi de force sont intéressants mais l'erreur en position est assez grande. Fateh (2010) a trouvé que la solution devrait assurer un ensemble de règles, reconnues comme était les règles d'impédance. Un compromis entre la tenue de route et le confort a été établi en variant les coefficients d'impédance. Des coefficients d'une valeur grande fournissent un confort assez élevé et une bonne tenue de la route. Le désavantage de cette méthode est que l'énergie est dissipée au niveau des pneus et cela peut engendrer des déformations des pneus et une fatigue assez élevée à ce niveau.

D'autres méthodes de contrôle de force ont suggéré l'utilisation des composants hydrauliques comme un actuateur de contrôle. Le contrôleur fait par (Chen et al, 2012) contient un régulateur de pression et une servovalve de débit pour former un actuateur de contrôle. Un contrôleur par logique floue a donné des résultats intéressants dans les limites imposés. En résumé, le contrôle de force a été réalisé par trois types des contrôleurs comme les contrôleurs simples, les contrôleurs faits par l'ajout des composants hydrauliques et les contrôleurs hybrides.

1.6 La commande de position et de force des systèmes électrohydrauliques

Dans la revue de littérateur mentionné précédemment, les contrôleurs de force et de position sont développés séparément afin de déterminer la force et la position successivement.
L'ensemble des contrôleurs est fourni par des méthodes adaptatives pour surmonter les variations des paramètres durant les tests en temps réel. Récemment, la structure hybride a été considérée en recherche étant donné que ces structures ont montré leur efficacité vis-à-vis des autres méthodes. Cette structure réfère à une combinions de deux contrôleurs ou plus pour tracer plusieurs variables en même temps.

Dans les applications intégrant des systèmes électrohydrauliques où le contrôle de la position et de force sont de la même importance, les contrôleurs hybrides donnent des meilleurs résultats. Dans ce sens, (Ursu et al, 2006) ont développé trois lois de contrôle pour faire un contrôle de position et de force pour un système électrohydraulique en utilisant la technique de backstepping. D'autres chercheurs comme (Ferreira et al, 2006) utilisent deux gains indépendants pour former un contrôleur hybride, dont chaque contrôleur formant le contrôleur hybride possède sa propre structure de logique floue. La loi de contrôle est appliquée à une presse hydraulique durant trois phases d'opération. Dans ces phases, le contrôle de position et de force est fait en utilisant un gain fixe.

Bien que l'utilisation des gains fixes avec un système précis de vision a donné de bons résultats, plusieurs chercheurs préfèrent les gains variables afin d'avoir des réponses rapides avec des gains PID variables. Cela a été fait par (Sun and Er. 2004) qui as conçu un contrôleur hybride pour tracer des trajectoires désirées en robotique. Le contrôleur est divisé en deux couches. La couche supérieur est développée avec un contrôleur floue de type Takagie-Sugeno dont la sortie est un gain graduel tandis que la couche inférieure constitue un contrôleur floue de type mamdani pour contrôler le système linéarisé localement d'un bras robotique.

En résumé, les contrôleurs des gains variables donnent de bonne performance et les algorithmes de contrôle adaptatif deviennent nécessaires en présence d'incertitude dans les paramètres. Shi et al (2011) ont concentré leurs recherches sur ces points en construisant un contrôleur de deux boucles avec un algorithme pour rejeter les perturbations en ligne. L'algorithme de double boucle à rejet automatique de la perturbation (ADRC) est formé de trois blocs: un bloc transitoire, un observateur et un block pour calculer le signal de commande composé des variables transitoires et leurs estimées. Le système est découplé de deux boucles, une pour la position et l'autre pour la force successive. L'ADRC a montré une performance robuste adaptative et précise.

Malgré que les théories de contrôle de la position et de force d'un système électrohydraulique soient assez répandues, l'idée de découpler une structure de contrôle est de plus en plus

présente dans ce champ. Cela est récemment fait par (Wos and Dindorf, 2014) où deux diagrammes parallèles de contrôle hybride sont construits afin de faire un contrôle de force et de position. Les contrôleurs adaptatifs sont développés avec des gains variables. Le contrôleur de position est le proportionnelle dérivative, pourtant sur l'autre branche, le contrôleur de force intègre un bloc d'identification. Le bloc de force est nécessaire pour une mise à jour de la force du système. Avec un contrôleur aussi compliqué, la position est bien tracée mais l'erreur de force est devenue significative pour des fréquences plus élevées.

Comme nous l'avons déjà mentionné, il y a une variété de contrôleurs hybrides employant des contrôleurs linéaires et nonlinéaires. Le fait d'employer un contrôleur nonlinéaire produit des problèmes non désirés comme le bruit, l'apparition des éléments d'une dynamique nonlinéaire et le broutement (Gao and Hung, 1993). Un contrôleur basé sur le mode de glissement a été développé par (Gao and Hung, 1993) afin de réduire le dépassement, l'erreur de suivi et d'avoir une réponse rapide d'un système électrohydraulique. Trois lois d'atteinte sont développées par Gao and Hung (1993): la loi constante d'attente, la loi constante d'atteinte plus proportionnelle et la loi d'atteint avec puissance. En pratique, ils ont trouvé que une combinaison de lois de atteint constant et plus proportionnelle donne le meilleur résultat. Cette combinaison a donné une bonne performance et a réduit le broutement.

Due à la robustesse de cette dernière combinaison, le mode à structure variable (VSM) et le mode de glissement conventionnel ont été employé dans plusieurs applications (Hwang et Lan, 1994). Dans le travail de (Hwang et Lan, 1994), la loi de contrôle a été construite d'une façon structurelle permettant à la surface de glissement d'avoir plus de flexibilité toute en contrôlant le temps d'atteinte.

Dans le même esprit, Hwang (1996) a introduit une nouvelle loi en utilisant un gain variable dans le temps et une couche limite pour remplacer les lois conventionnelles de mode de glissement. Les paramètres de pondération sont utilisés pour déterminer quelle variable devrait être suivie. Un mauvais choix des variables de pondération peut produire soit moins de sensibilité ou bien une réponse transitoire assez grande. Malgré le choix d'utiliser une couche limite variable dans la loi de contrôle, le broutement est toujours présent avec des valeurs

significatives. L'inconvénient de mode de glissement est le broutement élevé résultant de la commutation du signale de contrôle quand la surface de glissement est autour de zéro.

Le broutement dépend du gain de commutation et de la largeur de la couche limite. Plus le gain est élevé, plus le broutement est produit. C'est pour cela qu'une variable couche limite est suggérée par (Young et al, 1996) afin de réduire le broutement. Une autre solution a été suggérée pour ce cas dans les travaux de (Hwang et Lan, 1994) et (Fung etYang, 1998) en utilisant un gain de commutation variable. Dans le même sens, (Zhiming et al, 2003) ont utilisé le mode de glissement avec contrôleur basé sur la logique floue en forme de modèle cérébelleux pour réduire le broutement de contrôleurs de position d'un système électrohydraulique. L'incertitude issue de la dynamique non modélisée et la perturbation externe sont apprentie par un réseau de neurones afin de développer une loi de commande adaptative appropriée.

La méthode d'apprentissage est compliquée et dépend de la connaissance de l'expert. De plus, elle est difficile d'être appliqué en pratique. Des études plus récentes suppose que si la méthode soit capable de réduire le gain de commutation, elle représente donc une bonne solution pour l'élimination de broutement (Utkin et Lee, 2006). C'est pour cela que (Utkin et Lee, 2006) ont exprimé le gain de commutation en forme d'une fonction de contrôle équivalente.

En conséquence, (Fallaha et al, 2011) ont proposé une loi d'atteinte générale pour la méthode de mode de glissement basé sur la loi de puissance développé par (Gao et Hung, 1993). Cette loi, connue sous le nom de la loi exponentielle, a résolu les problèmes du temps d'atteinte et la robustesse. Elle était suffisant pour réduire/éliminer le broutement et a était capable de bien s'adapter avec les variations dans la surface de glissement. Cette nouvelle approche est appliquée à un bras robotique flexible (systèmes multiple-entrées et multiple-sorties). Cette loi devient, dans une condition spéciale, la loi conventionnelle d'atteint de la commande de mode de glissement.

Dans des travaux récemment publiés, (Mahmoodabadi et al, 2014) ont suggéré un contrôleur hybride adaptatif avec un PID robuste accompagné d'un contrôle superviseur basé sur le mode de glissement pour assurer un broutement minimal. Les gains de contrôleurs PID sont optimisés et mis à jour par un algorithme génétique. Le broutement est réduit par un contrôle de mode de glissement découplé employant des méthodes comme les fonctions des transferts. Le contrôleur proposé regroupe trois signaux de commande afin de former son propre signal. Les interférences entre les contrôleurs mettent à jour les gains de PID. Les résultats sont intéressants mais la structure est assez compliquée.

1.7 Contributions originales

De la revue de littérature précédente, nous avons comme but de développer un contrôleur qui rejoint les avantages de plusieurs contrôleurs en modélisation et en commande.

a) Modèle électrohydraulique à suspension active

Le modèle de système électrohydraulique représentant la suspension active est testé en simulation vu que le modèle contient tous les éléments nécessaires. Pourtant, le modèle de banc d'essai ne correspond pas à un modèle idéal de la suspension active. Pour rapprocher le modèle du banc à un modèle de suspension active, nous avons déterminé les éléments non installés pour les ajouter dans le modèle réel. Ces éléments sont les deux ressorts représentant la suspension passive. Les équations du modèle de banc d'essai ont été modifiées pour avoir un modèle hybride. Avec un tel modèle, nous avons réussi à tester et valider les méthodes de contrôle proposées par des séries des tests.

b) Au niveau de la commande de suspension active électrohydraulique

Dans notre thèse, nous utilisons la commande par mode de glissement pour suivre des trajectoires désirées de la position et de la force d'un système électrohydraulique à suspension active.

- Le développement d'une structure de contrôle hybride en ajoutant deux contrôleurs pour suivre des trajectoires de la position et la force d'un siège d'un passager. Cette nouvelle structure est construite en forme simple et efficace pour obtenir le meilleur

asservissement en position avec une force minimal transmise au passager à travers le siège. Une telle structure hybride est faite pour surmonter les problèmes des structures classiques existantes. Les filtres passe bas sont utilisés pour atténuer les signaux de commande de haute fréquence et passer les signaux de commande de basse fréquence. En outre, on applique un contrôle adaptatif pour changer la fréquence de coupure du filtre dominant en variant le gain de ce filtre. Une combinaison des signaux plus lisse a été atteinte en donnant aux filtres la liberté de choisir le signal de contrôle qui correspond mieux à la performance désirée.

- Le développement d'un contrôleur en logique floue pour déterminer la valeur optimale du gain de filtre à chaque instant durant la simulation. Les fonctions d'appartenance de ce contrôleur sont basées sur les surfaces de glissement. Ces surfaces sont déjà calculées instantanément pour la position et la force. Les gains calculés sont dépendants des variables significatives et critiques dans le système.

- L'évaluation numérique d'une loi d'atteinte exponentielle (ERL) afin d'éliminer ou de réduire le broutement. L'ERL pour le mode de glissement a été introduit par (Fallaha et al, 2011). Son efficacité en réduisant le broutement a été prouvé en robotique. On a adapté et appliqué cette technique afin de démontrer son efficacité en temps réel dans un système électrohydraulique.
- Le développement d'un contrôleur adaptatif pour la mise à jour des gains des contrôleurs conventionnels comme PID et PIDDL. Le contrôleur est testé en temps réel sur le banc de la suspension active. Un lien a été créé entre les contrôleurs responsables de la mise à jour des gains essentiels des contrôleurs PID et PIDDL.
  Le contrôleur développé peut être placé dans la structure hydride pour un travail de développement futur pour contrôler l'ensemble de la position et la force.

CHAPITRE 2

LA COMMANDE PAR MODE DE GLISSEMENT

2.1 Introduction

Dans la formulation d'un problème de contrôle, on constate une différence entre le banc d'essai réel et son modèle mathématique utilisé pour des fins de contrôle. Cette différence est due à l'incertitude dans les paramètres, perturbation externe, une dynamique non-modélisés. Le fait de développer un contrôleur pour caractérise les incertitudes dans le système et la présence des perturbations est une tâche difficile sans faire des compromis.

Cela a amené les développeurs à chercher dans les méthodes robustes qui sont supposé à résoudre ce problème. Le contrôle par mode de glissement est l'un des méthodes conçu pour ça. Nous allons aborder la théorie de la commande par mode de glissement pour les systèmes SISO. La méthode et les principes de cette théorie, connue comme Sliding Mode, seront exposés en détail. La théorie sera appliquée sur un système électrohydraulique à suspension active d'une voiture pour mettre en questions la validité de cette méthode et d'autres structures de contrôles. La méthode connue pour sa robustesse et son broutement inhérent a été intégré efficacement dans une structure hybride proposée afin de faire un contrôle de la position et la force.

2.2 Théorie de contrôle par mode de glissement

Le mode de glissement est conçu pour asservir un vecteur d'états d'un système à une région où un hyperplan nommé le surface de glissement$S = 0$. Le choix de surface, influence la stabilité du système. Une fois la surface de glissement atteint l'espace$S = 0$, le vecteur d'états glisse autour du point d'équilibre. Cette méthode est nommée mode de glissement car le vecteur dans la phase de glissement glisse autour de cette line avec une loi discontinue. Grace à cette loi, la surface de glissement est atteinte dans un temps fini.

La tâche la plus importante est de développer un contrôle discontinu qui guide les états de système vers la surface de glissement et les garder sur cette surface.

La fonction lyapunov est utilisée pour caractériser cette tâche. La méthode laypunov est généralement utilisée pour déterminer les propriétés de stabilité d'un point d'équilibre sans résoudre les équations d'états. On suppose que $V(X)$ est une fonction scalaire et continuellement différentiable défini dans un domaine D. la fonction $V(X)$ est positivement définie si $V(0) = 0$ et $V(X) > 0$ pour tout x.

Par contre, elle est négativement définie si $V(0) = 0$ et $V(X) < 0$ pour tout$x$.
La fonction générale de lyapunov qui caractérise le mouvement des trajectoires d'états vers la surface de glissement est défini en termes de la surface. Pour chaque structure de contrôle discontinue, on choisit les gains de sorte que cette fonction laypunov est négativement définie pour garantir la convergence des états vers la surface de glissement.
Les vecteurs tangents d'états se dirigent vers la surface, c'est ainsi que ces états sont guidés et conservés sur la surface.
Un système nonlinéaire d'une entrée peut être représenté par:

$$x^n = f(x,t) + b(x,t)\, u(t) \tag{2.1}$$

$x(t)$: Est le vecteur d'état, $u(t)$ est le signal de commande. x^n est la dérivative de vecteur d'état jusqu' au ordre $\mathrm{n}-1$. Les fonctionnes $f(x,t)$et $b(x,t)$ sont des fonctions nonlinéaires et non définie mais ils sont bornées par des fonctionnes de x définies et continues. Le problème de contrôle est ramener l'état $x(t)$ à sa valeur désirée $x_d(t)$ dans la présence de incertitude sur les fonctions $f(x)$, $b(x)$. Une surface variable dans le temps $s(t)$ est définie dans l'espace R^n.

$$s(x,t) = (\frac{d}{dt} + \delta)^{n-1}\, \tilde{x}(t) \tag{2.2}$$

δ est un constant strictement positive et prise comme une bande passante, $\tilde{x}(t)$ est l'erreur de sortie $x(t) - x_d(t)$. Le problème d'asservissement d'un vecteur $x_d(t)$ de dimension n peut être remplacé par un problème de stabilisation de premier ordre par rapport à $s(t)$. La

surface $s(x,t)$ de l'équation (2.2) est appelée la surface de glissement. L'expression de l'erreur sera dérivé n $-$ 1 fois pourtant la surface $s(x,t)$ sera dérivé une seul fois pour avoir l'entrée de la commande. Par conséquence, les bornes sur la surface $s(x,t)$ peuvent se traduire en forme des bornes sur l'erreur$\tilde{x}(t)$. Le scalaire s représente une mesure réelle de la performance d'asservissement.

On suppose que les conditions initiales $\tilde{x}(t) = 0$.

$$\forall\, t \geq 0, |s(t)| \leq \emptyset \tag{2.3}$$

$$\Longrightarrow \forall\, t \geq 0, \left|\tilde{x}(t)^i\right| \leq (2\delta)^i \varepsilon \qquad i = 0,1,\ldots n,-1$$

Où $\varepsilon = \frac{\emptyset}{\delta^{n-1}}$ Slotine et Li (1990) en faisant cela on a changé le problème de n ordre à un problème de stabilisation de premier ordre. Donc, on peut garder le scalaire s à zéro en choisissant la loi de contrôle de (2.1) de sorte que:

$$\frac{1}{2}\frac{d}{dt}s^2 \leq -\eta|s| \tag{2.4}$$

Où η est constant strictement positive. En satisfaisant cette condition, la surface devienne un ensemble invariant. Autrement dit, les trajectoires mouvant à partir d'une condition initiale font rester dans l'ensemble en tout temps. L'équation (2.4), cela implique que les perturbations ou les incertitudes peuvent être tolérées en gardant la surface dans l'ensemble invariant.

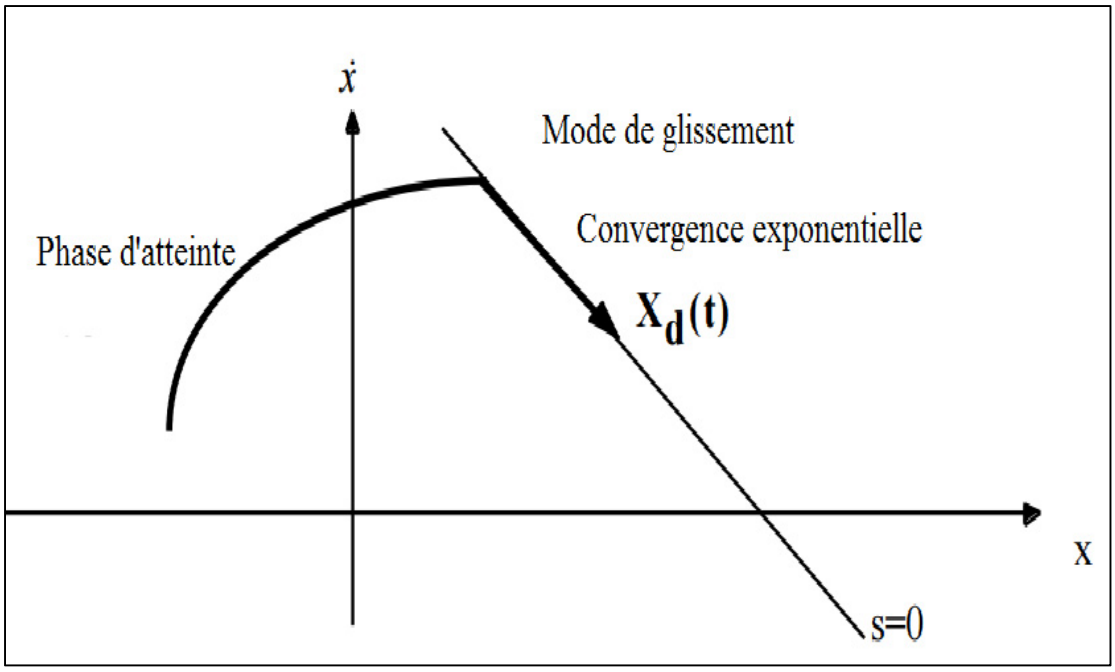

Figure 2.1 Une représentation graphique des équations (2.2), (2.4) pour n=2 (tiré de Slotine et Li (1991))

Finalement, en satisfaisant (2.2), cela garantit que si $x(t=0)$ est proche de $x_d(t=0)$. La surface $s(t)$ sera atteint dans un temps fini plus petit que $\frac{s(t=0)}{\eta}$. On suppose que :

$s(t-0)>0$ et $t_{atteint}$ est le temps nécessaire pour atteindre la surface.

En intégrant (3.4) entre $t=0$ et $t=t_{atteint}$ donne :

$0-s(t=0)=s(t=t_{atteint})-s(t=0)\leq -\eta(t_{atteint}-0)$.

Cela implique que:

$$t_{atteint}\leq s(t=0)/\eta.$$

On obtient les mêmes résultats dans le cas $s(t=0)>0$

$$t_{atteint}\leq \frac{s(t=0)}{\eta}$$

Donc, en partant de n'importe quel point, les trajectoires d'états attentent la surface à temps variable dans un période de temps finie plus petite que $s(t=0)/\eta$ et glissent sur la surface vers $x_d(t)$ d'une façon exponentielle avec un constant de temps équivalent à $\frac{1}{\lambda}$.

En résumé, l'idée est de choisir $s(t)$ selon l'équation (2.2). Cette surface devrait satisfaire l'équation (2.4) pour que la loi de commande stabilise le système.

2.3 Design de contrôleur par mode de glissement

Les procédures pour développer un contrôleur est divisé en deux étapes. Premièrement, il faut choisir la surface de glissement et calculer la loi de contrôle pour satisfaire la condition (2.4). Pour la présence de l'imprécision et la perturbation, la loi de contrôle devrait être discontinuée sur $s(t)$. Cela produit du broutement à cause de l'implémentation imparfaite de l'algorithme de commutation (Figure 2.2). Le broutement est un phénomène indésirable surtout qu'il endommage les équipements et créée des dynamiques de hautes fréquences dans le modèle de système.

Dans un second lieu, la loi discontinue u devrait être plus lisse pour avoir un contrôle optimal et garantir une commutation lisse entre les bandes passantes et la précision de l'asservissement.

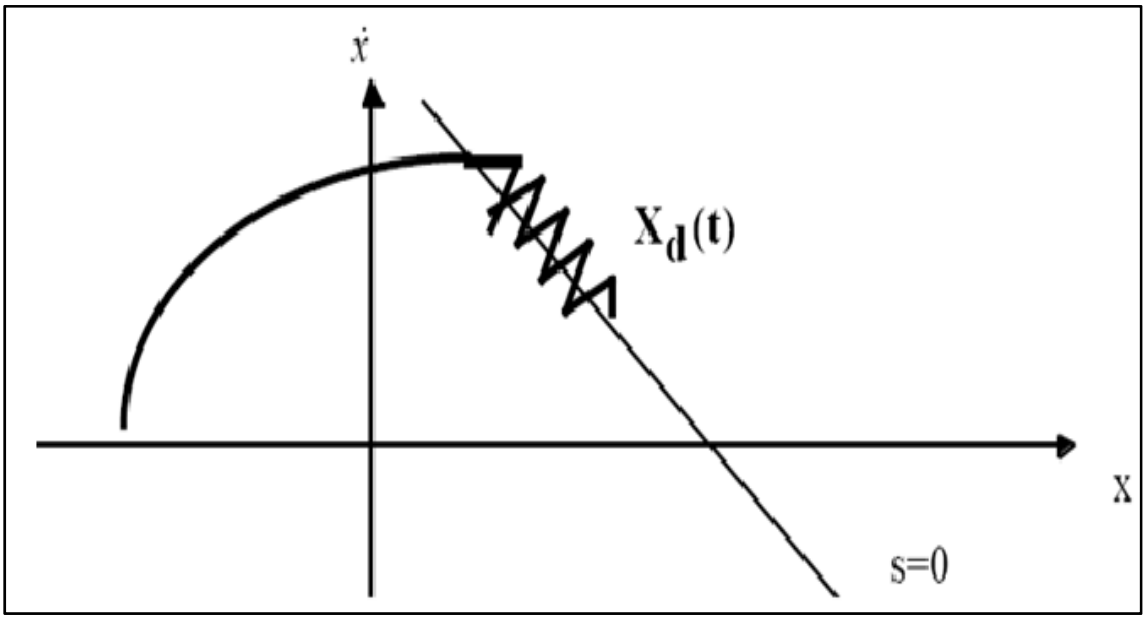

Figure 2.2 Le broutement dans le mode de glissement (tiré du (Kurfess 2004))

Pour un système de deuxième ordre:

$$\ddot{x}(t) = f(x,t) + u(t) \tag{2.5}$$

Où $f(x,t)$est une fonction nonlinéaire et variable dans le temps; son estimation est $\hat{f}(x,t)$.

$u(t)$ est l'entrée commande, $x(t)$ est les états à asservir et $x_d(t)$ est les états désirés.
L'erreur d'estimation sur $f(x,t)$ est supposé d'être borné par une fonction définie $F = F(x,t)$.

$$\left|\hat{f}(x,t) - f(x,t)\right| \leq F(x,t) \tag{2.6}$$

On définit la variable de glissement selon l'équation (4.2).

$$s(t) = \left(\frac{d}{dt} + \gamma\right) = \tilde{x}(\dot{t}) + \gamma\, \tilde{x}(t) \tag{2.7}$$

La dérivation de variable de glissement donne:

$$\dot{s}(t) = \ddot{x}(t) - \ddot{x}_d(t) + \gamma\dot{\tilde{x}}(t) \tag{2.8}$$

En remplaçant l'équation (2.5) dans l'équation (2.8):

$$\dot{s}(t) = f(x,t) + u(t) - \ddot{x}_d(t) + \gamma\dot{\tilde{x}}(t) \tag{2.9}$$

L'approximation de la loi de contrôle $\hat{u}(t)$ pour avoir $\dot{s}(t) = 0$ est:

$$\hat{u}(t) = -\hat{f}(x,t) + \ddot{x}_d(t) - \gamma\dot{\tilde{x}}(t) \tag{2.10}$$

$\hat{u}(t)$ Peut être interprété comme le meilleur estimé de la loi de contrôle équivalent:

$$\frac{1}{2}\frac{d}{dt}(s(t)^2) \leq -\eta|s(t)| \qquad\qquad \eta > 0 \tag{2.11}$$

On prend la loi de contrôle:

$$u(t) = \hat{u}(t) - k(x,t)sgn(s(t)) \qquad \eta > 0 \qquad (2.12)$$

En choisissant $k(x,t)$ suffisamment grand:

$$k(x,t) = F(x,t) + \eta$$

On s'assurer que la condition (4.11) est rencontrée:

$$\frac{1}{2}\frac{d}{dt}(s(t)^2) = s(t)\dot{s}(t) = \left(f(x,t) - \hat{f}(x,t)\right)s(t) - k(x,t)|s(t)| \leq -\eta|s(t)| \quad \eta > 0 \qquad (2.13)$$

Alors en utilisant (2.12), on confirme que les trajectoires du système atteignent la surface $s(t)$ dans un temps fini et que l'erreur se converge exponentiellement à zéro.

De ce qui procède, on voit clairement l'avantage de changer un problème original à un problème de stabilisation de premier ordre par rapport à $s(t)$.

On suppose qu'un système de deuxième ordre a la forme suivante:

$$\ddot{x}(t) = f(x,t) + b(x,t)u(t) \qquad (2.14)$$

Où $b(x,t)$ est borné:

$$0 \leq b(x,t)_{min} \leq b(x,t) \leq b(x,t)_{max}$$

Le gain de contrôle $b(x,t)$ et ses bornes peuvent être dépendant des états ou variables dans le temps.

$$\hat{b}(x,t) = \sqrt{b(x,t)_{min}b(x,t)_{max}}$$

Les bornes peuvent être reformulées sous la forme suivante:

$$\beta^{-1} \leq \frac{\hat{b}}{b} \leq \beta \text{ où } \beta = \sqrt{\frac{b_{max}}{b_{min}}}$$

où β est la marge du gain de design.
La loi de contrôle est conçue pour être robuste par rapport à une incertitude bornée.
La loi de contrôle devient:

$$u(t) = \hat{b}(x,t)^{-1}[\hat{u}(t) - k(x,t)sgn(s(t))] \quad (2.15)$$

Avec un $k(x,t)$ qui satisfait la condition de glissement:

$$k(x,t) \geq \beta(x,t)(F(x,t) + \eta) + (\beta(x,t) - 1)|\hat{u}(t)| \quad (2.16)$$

La loi de contrôle du système d'ordre plus élevé peut être calculée selon la même approche.

2.4 Conclusion

Dans ce chapitre, on a présenté le mode de glissement par un exemple simple. La méthode est connue pour sa robustesse contre la perturbation. Le développement de lois de contrôle est méthodologique pourtant la difficulté se manifestes avec les systèmes nonlinéaires contenant des fonctions nondifférentiables. Ces fonctions devraient être remplacées par des fonctions différentiable pour pouvoir dériver ces fonctions. Le broutement est l'un des avantages de cette méthode, cela a été résolue et testé dans les chapitres 3 et 4.

CHAPITRE 3

A CHATTERING-FREE FUZZY HYBRID SLIDING MODE CONTROL OF AN ELECTROHYDRAULIC ACTIVE SUSPENSION

Bassel Shaer[1], Jean-Pierre Kenné[1], Claude Kaddissi[1] and Charles Fallaha[1]

[1] Department of Mechanical Engineering, École de technologie supérieure, Université du Québec à Montréal (UQAM), Montreal, Canada

Article publié dans «Transactions of the Institute of Measurement and Control», juin 2016

Abstract

This paper introduces a new hybrid controller for position and force control of an electrohydraulic car active suspension. In most hybrid controllers, a switching function is normally used in order to take advantage of two separate controllers. Switching between the two controllers produces a chattering in the system, in addition to the chattering that could be inherent to the controller itself, which deteriorates the system performance. In this work, we resolved the switching limitations dilemma by transitioning from one controller to another through two low-pass filters. These filters are used with variable gains to improve the new hybrid position/force controller performance that we developed. The produced control signal is a structured combination, in which the signal coming from the position controller reduces the effect of road perturbations on passengers by bringing the car's vertical motion to zero. Simultaneously, the signal from the force controller tracks a reference force, and thus, reduces the force transmitted to passengers.

To eliminate the chattering that is inherent to the sliding mode controller, we introduced an exponential reaching law function to the hybrid sliding mode controller. This exponential function also reduced the response time, consequently speeding up the system reaction to suppress perturbations. In addition to that, a recent sliding surface-based controller is applied to vary the filters' gains and get better performance. The frequency analysis is done to verify

the controller performance. The proposed hybrid controller is also validated in real time on active suspension workbench and compared to a classical PID controller.

Keywords: Position and force control, hybrid control, exponential reaching law, active suspension, sliding mode control.

3.1 Introduction

Electrohydraulic systems (EHS) are very commonly used in industry. These are very powerful systems, thanks to their produced forces, high-speed reversal and low control signal versus the space they occupy. On the other hand, the components of any EHS are highly nonlinear due to many factors: oil viscosity, friction, temperature, oil contamination and leakage, which really complicate the mathematical modeling and control of such systems. Recent research studies on EHS have focused on position tracking, with some consideration given to the powerful produced force. Applications employing an EHS call for ever greater precision in position and finite force tracking. Position control in servomechanism was applied to precisely track a desired position. Tracking performance is reduced by many factors, such as friction in (Bonchis et al., 2001), external perturbations and unmodeled dynamics (Mihajlov et al., 2002), and parameter uncertainty (Mintsa et al., 2011).

For position controllers, (Alexander et al., 2009) used various robust control techniques, such as integral-block, sliding-mode, and H-infinity controls. These methods are combined to track a position reference. The controller is too complicated; the inherent chattering is too high with high frequency components.

Along with position control, researchers pay particular attention to the force control in these systems. They simplify the modeling in order to control the force produced by means of a Lyapunov function, as in (Alleyne and Liu, 2000).

In the work by (Alleyne and Liu, 2000), pressure/force control is restricted to one derivation with a Lyapunov function, and with the control signal appearing after the derivation. Conversely, with the force control in sliding mode, many derivations could be needed,

depending on the sliding surface choice. If more than one derivation is needed in the sliding surface in order to obtain the control signal, the mathematical expression of the latter becomes very cumbersome, as illustrated in (Hedrick and Yip, 2000). Adequately choosing the sliding surface could prevent this problem (Karpenko and Sepehri, 2012).

As the need for force control and position control increases due to industry requirements, a hybrid control is used as a compromise between the control's objectives. The hybrid controller usually refers to a structure with two controllers, two references or mixed continuous and discrete signals.

In (Lane et al., 1997), a comparison between two classical hybrid controllers is suggested in order to specify the robot motion and contact forces simultaneously. The hybrid controllers use the sliding mode and self-tuning adaptive controller to realize their objectives. The hybrid structure adds the two control signals to form the hybrid one. With such a design, it is difficult to control the mixed signals as there are neither limitations nor controls on each path. Within the framework of hybrid control, in (Assadsangabi et al., 2009), they proposed two references for the position and the force respectively.

Although satisfactory results were achieved by (Assadsangabi et al., 2009), they nevertheless fell short of what is needed in terms of mass accelerations. To reduce mass accelerations, (Priyandoko et al., 2009) used four neural network loops to form an inverse dynamic of the actuator, in order to track a force reference, and to compensate for the disturbances. Generally, (Priyandoko et al., 2009) resolved the problem of (Assadsangabi et al., 2009) by reducing the mass acceleration. The force tracking obtained was good, but the position error was still high.

(Fateh, 2010) found that the solution must verify a given set of rules, known as the impedance rules. A compromise between handling and comfort was achieved by varying the impedance coefficients. A high impedance coefficient provides high comfort in terms of road handling but the energy is dissipated at the tire level leading to tire deformation. As we have seen above, there is a wide variety of hybrid controllers employing linear and nonlinear controllers. Using

nonlinear controllers causes undesired problems such as noisy, nonlinear dynamics and chattering (Gao and Hung, 1993).

In (Gao and Hung, 1993), three reaching laws were developed: constant reaching law, constant plus proportional reaching law and power reaching law. In experiments, they found that a combination of constant plus proportional reaching laws is the best choice for reducing chattering and achieving a steady performance. Due to the robustness of the latter, a variable structure mode (VSM) control and a conventional sliding mode (SMC) control are employed in many applications, such as in the case of (Hwang and Lan, 1994), where the control law was structurally built, allowing the sliding surface to be flexible and the reaching time to be controlled.

Like with every control method that has its drawbacks, the problem with SMC is the high chattering resulting from the switching of the control signal when the sliding surface is around zero. Chattering depends on the named switching gain and the boundary layer width. However, the higher the gain, the higher the chattering it produces as well. As a solution to reduce the chattering, a variable boundary layer width is suggested in (Young et al., 1996).

Another solution is suggested for chattering reduction by using a variable switching gain as in (Hwang and Lan, 1994; Fung and Yang, 1998) or using fuzzy cerebellar model articulation controller along with the sliding mode controller (Zhiming et al., 2003).

In more recent research studies, it is suggested that any method capable of reducing or varying the switching gain represents a good solution for chattering suppression (Utkin and Lee, 2006). Thus, (Fallaha et al., 2011) proposed a general reaching law in a sliding mode approach based on the power law developed in (Gao and Hung, 1993). This general reaching law, known as the exponential law, solved the problems of reaching time and robustness. It was sufficient to suppress chattering and to adapt smoothly with the variation of the sliding surface. This new approach was applied to a flexible robotic arm (multiple-input and multiple-output system).

What is interesting in this developed law is the fact that it became, in its special case, the conventional reaching law in a sliding mode control.

In our paper, we used the sliding mode to control the force/position of an electrohydraulic active suspension. Thus, two nonlinear controllers were integrated in a hybrid structure in order to track both the position and force of a passenger seat. Such a hybrid structure overcomes the existing classical structure as it contains filters. The low-pass filters are used to attenuate the high control signal frequencies and to pass the low control signal frequencies. In addition to that, we applied an adaptive control to change the cut-off frequency of the dominant filters by varying the filter gain. A smooth combination was reached by letting the filter set choose the best-fit control signal. A fuzzy logic controller, based on the calculated position and force sliding surfaces, was employed to control the filters' gain in order to improve performance. This constitutes our first contribution.

This new structure is demonstrated in a simple and efficient way to achieve a best tracking position with minimum transmitted force to the passenger. An exponential reaching law (ERL) was used to subdue chattering. The ERL for sliding mode control was introduced recently by (Fallaha et al.,2011) . Its effectiveness in reducing chattering was proven so far in a limited number of applications and mainly in robotics. We applied this chattering reduction technique and adapted it in order to demonstrate its efficiency in real time in electrohydraulic systems. This constitutes our second contribution. The rest of the paper is organized as follows: In the next section, we demonstrate the system modeling in detail. The third section describes the main contribution of our work. It elaborates the hybrid control, the hybrid control with ERL, and finally, the hybrid control with both ERL and fuzzy control. In the fourth section, we present the results of the step-by-step controller developed, compared to a PID controller in simulation.

The experimental study in real time is done in the fifth section. The last section is devoted to conclusions and future work perspectives.

3.2 Electrohydraulic Active Suspension Mathematical Modeling

The model presented in Figure 3.1 relates to an active suspension bench, and the quarter-car model is composed of two masses, the first being the passenger mass, and the second, representing the tire's mass, modeled as a damper with a spring. The control cylinder, combined with a spring, is placed between the two masses. This part works functions as a passive suspension when no control is applied. The active part is comprised of the control cylinder, the servovalve and the controller.

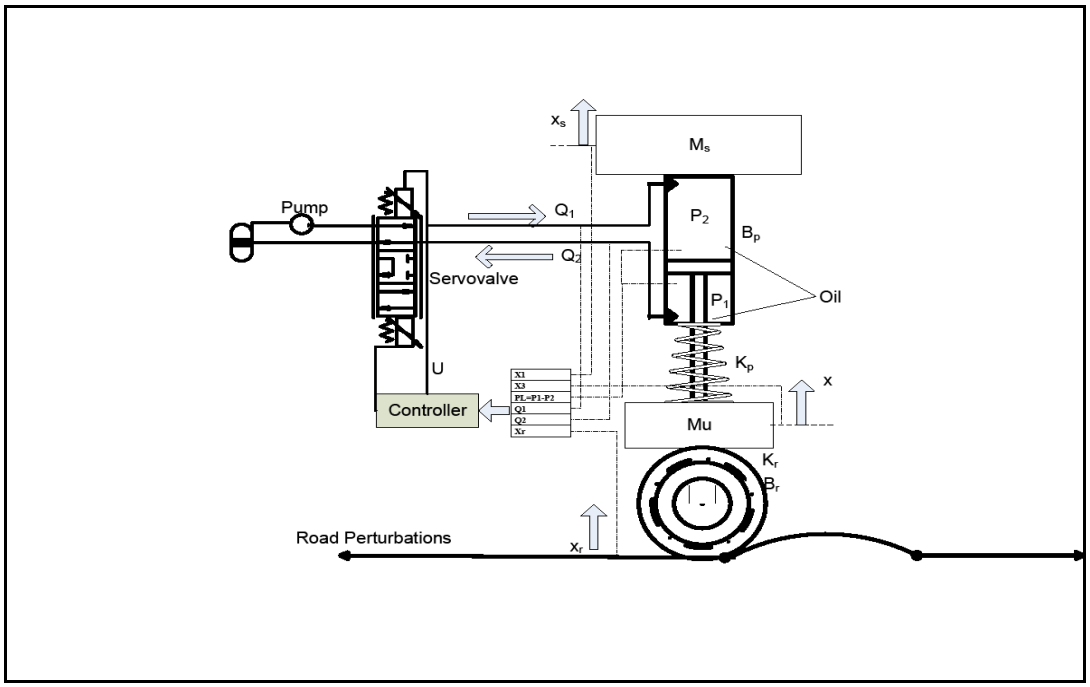

Figure 3.1 Active suspension bench

The servovalve equation is represented as a first-order system (Merritt, 1967):

$$\dot{x}_v = \frac{1}{\tau}(-x_v + ku) \tag{3.1}$$

Where x_v is the spool valve position (refer to Annexe I, Tableau-A I-1 for active suspension parameters).

The flow rate to and from the servovalve through the valve orifices, assuming symmetric and matched orifices with a small leakage, is given by:

$$Q_1 = Q_2 = C_d x_v \sqrt{\frac{P_s - P_L * sigm(x_v)}{\rho}} \tag{3.2}$$

where $P_L = P_1 - P_2$ is the load pressure. The sign function, which expresses the change in the fluid flow direction, can be replaced by a differentiable function for numerical simulations. This function helps avoid the differentiability problems as suggested in (Kaddissi et al., 2009). The sigmoid function is defined as: $sigm\,(x_v) = \frac{1-e^{-\alpha x_v}}{1+e^{-\alpha x_v}}$.

We therefore have:

$$\text{sigm}(x) = \begin{cases} 1 & \text{if } ax \to \infty \\ 0 & \text{if } ax \to 0 \\ -1 & \text{if } ax \to -\infty \end{cases} \text{ and } \frac{d\,(\text{sigm}(ax_v))}{dt} = \frac{2\,ae^{-\alpha x_v}}{(1+e^{-\alpha x_v})^2}.$$

The compressibility equation that represents the load pressure dynamics is as follows:

$$\dot{P}_L = \frac{2\beta}{V_0}\left\{C_d x_v \sqrt{\frac{P_s - P_L * sigm(x_v)}{\rho}} - L * P_L - A(\dot{x}_s - \dot{x})\right\} \tag{3.3}$$

We now proceed to identify the car dynamics, using Newton's second law:

$$\begin{aligned} M_s\ddot{x}_s &= -K_p\,(x_s - x) - B_p(\dot{x}_s - \dot{x}) + AP_L \\ M_u\ddot{x} &= K_p(x_s - x) + B_p(\dot{x}_s - \dot{x}) - k_r(x - x_r) - B_r(\dot{x} - \dot{x}_r) \\ &\quad - AP_L \end{aligned} \tag{3.4}$$

Rewriting Equations (3.3) and (3.4) in terms of the chosen variable $x_i : i = 1..6$, we obtain a model such as in (Kaddissi et al., 2009), who proposed a change in variables in order to include the suspension deflection, which is the difference between the car body position and the tire position.

One of the control's objectives is to prevent this variable from hitting the imposed limits. The new variable states are: $y_1 = x_1,\ y_2 = x_2,\ y_3 = x_1 - x_3,\ y_4 = x_2 - x_4,\ y_5 = x_5,\ y_6 = x_6$ (refer to Annexe I, Tableau-A I-2 for Systems variables).
The model can be rewritten as follows:

$$\begin{aligned}
\dot{y}_1 &= y_2 \\
\dot{y_2} &= -a_0 y_3 - b_0 y_4 + a_1 y_5 \\
\dot{y_3} &= y_4 \\
\dot{y_4} &= -A_1\, y_3 - A_2 y_4 + A_3 y_5 + b_1 \dot{y}_r + h_1 y_r \\
\dot{y}_5 &= \frac{J_1}{f(.)}(-A y_4 - L y_5 - C_d\, y_6 g(.)) \\
\dot{y}_6 &= \frac{1}{\tau}(-y_6 + ku)
\end{aligned} \tag{3.5}$$

Where: $A_1 = a_0 + d_0,\ A_2 = b_0 + d_1,\ A_3 = c_1 + a_1,\ f(.) = V_0^2 - A^2 y_3^2,$

$$g(.) = \sqrt{\frac{P_s - sigm(y_6) y_5}{\rho}}.$$

Now that the system modeling and the variables changes are done, we have the final model on which we will apply a position, force and hybrid control separately in next section.

3.3 Fuzzy hybrid sliding mode (FHSM) control with exponential reaching law (ERL)

The work of (Lin and Kanellakopoulos, 1997) integrated a variable bandwidth filter in order to soften or stiffen the suspension settings. In other words, the filter was reacting on one of the system variables. Our structure forms a basis for controllers using adaptive filters at the control signal level. In such controllers, the control algorithm could change the filters' bandwidths,

depending on the system parameters, references to be tracked and load variations, etc. In the hybrid structure, the filters attenuate the high frequencies control signals and change the influence of every controller, depending on the force and position errors produced in the systems.

When the position error is too big, the position controller will react with high amplitude signals yielding to high force errors. On the other hand, the force controller will react and contribute to the total control signal by reducing the effect of the position control signal. The force controller interferes in the control via a force-based gain, when the force transmitted to the passenger is high. The filters become more efficient as their parameters depend on the sliding surface generated via the system parameters. The added fuzzy controller plays an adaptive role when one of the sliding surfaces dominates the other, to keep the equilibrium between them. Thus, in the total control law, the equilibrium occurs when using two variable gains K_1 and α_1. These gains adjust the percentage of anticipation of every controller depending on the sliding surfaces.

To design a hybrid structure, we developed a position controller, and then a force controller, separately. In a second step, we integrated the two controllers to form a hybrid position/force controller. Then we enhanced the hybrid controller by adding an exponential reaching law and a set of fuzzy rules. The whole approach is detailed in the following subsections.

3.3.1 Position sliding mode (PSM) control

For the position control, we used the sliding mode, which is a nonlinear control strategy in which an invariant set exists and attracts every trajectory to the sliding surface. Therefore, $S = 0$ is a positive invariant set that attracts the error trajectories. The control problem is then reduced to:

- Driving the tracking errors to this surface.
- Ensuring that the tracking errors remain on this surface.

We will develop the control signal with the original coefficient of the system model. We first choose the surface S as:

$$S = c_1 y_1 + c_2 \dot{y_1} + c_3 \ddot{y_1} + c_4 \dddot{y_1} \tag{3.6}$$

We then calculate the derivative of y_1 and replace it in the (3.6):

$$\begin{aligned}
\dot{y_1} &= y_2 \\
\ddot{y}_1 = \dot{y_2} &= -a_0 y_3 - b_0 y_4 + a_1 y_5 \\
\dddot{y_1} = \ddot{y_2} &= -a_0 \dot{y_3} - b_0 \dot{y_4} + a_1 \dot{y_5} \\
&= -a_0 y_4 - b_0[-A_1 y_3 - A_2 y_4 + A_3 y_5] \\
&+ a_1 \frac{J_1}{f(.)}[-A y_4 - L y_5 - C_d y_6 g(.)] \\
&= b_0 A_1 y_3 - \left(a_0 - b_0 A_2 + a_1 \tfrac{J_1}{f(.)} A\right) y_4 + \left(-A_3 b_0 - a_1 L \tfrac{J_1}{f(.)}\right) y_5 \\
&- \frac{a_1 C_d J_1 g(.) y_6}{f(.)}
\end{aligned} \tag{3.7}$$

Replacing (3.7) in (3.6) yields:

$$\begin{aligned}
S = {} & c_1 y_1 + c_2 y_2 + (-c_3 a_0 + c_4 b_0 A_1) y_3 - (c_4 a_0 + c_3 b_0 - \mathrm{c_4 b_0 A_2} \\
& + \frac{\mathrm{c_4 a_1 J_1 A}}{f(.)}) \mathrm{y_4} - \left(A_3 b_0 c_4 - c_3 a_1 + \frac{c_4\, a_1\, J_1\, L}{f(.)}\right) * y_5 \\
& - \frac{c_4\, a_1\, C_d\, J_1\, g(.)}{f(.)}\, y_6
\end{aligned} \tag{3.8}$$

The reaching condition in (Edwards and Spurgeon, 1998) has to be verified:

$$S\dot{S} < 0 \tag{3.9}$$

The reaching condition ensures that the Lyapunov function derivative is strictly negative, meaning that S will converge to zero. Usually, to ascertain that (3.9) is true, $\dot{S}$ is chosen as follows:

$$\dot{S} = -K_{sw}\, sign(S) \tag{3.10}$$

By deriving (3.8) and replacing it in (3.10), we obtain:

$$\begin{aligned}\dot{S} = {} & c_1 y_2 + c_2 \dot{y_2} + (-c_3 a_0 + c_4 b_0 A_1)\dot{y_3} - (c_4 a_0 + c_3 b_0 - c_4 b_0 A_2)\dot{y_4} \\ & - c_4 a_1 J_1 A \frac{\dot{y_4} f(.) - y_4 \dot{f(.)}}{f(.)^2} - (A_3 b_0 c_4 - c_3 a_1)\dot{y_5} \\ & - c_4 a_1 J_1 L \frac{\dot{y_5} f(.) - \dot{f(.)} y_5}{f(.)^2} \\ & - c_4 a_1 C_d J_1 \frac{\left[g(.)\left[\frac{1}{\tau}\left(-y_6 + kU_{P_{smc}}\right)\right] + \dot{g(.)} y_6\right] f(.)}{f(.)^2} \\ & + c_4 a_1 C_d J_1 \frac{g(.) y_6 \dot{f(.)}}{f(.)^2} = -K_{sw}\, sign(S)\end{aligned} \tag{3.11}$$

We calculate the derivative of $g(.)$ and replace it in (3.11):

$$\dot{g(.)} = \frac{1}{\sqrt{\rho}} * \frac{-[\dot{sigm}(y_6) y_5 + sigm(y_6)\dot{y_5}\,]}{2\sqrt{P_s - sigm(y_6) y_5}}$$

$$= \frac{1}{\sqrt{\rho}} * \frac{-\left[\frac{2a_2 e^{-a_2 y_6}}{(1+e^{-a_2 y_6})^2}\frac{y_5}{\tau}\left(-y_6 + kU_{P_{smc}}\right) + sigm(y_6)\dot{y_5}\right]}{2\sqrt{P_s - sigm(y_6) y_5}}$$

$$\begin{aligned}= {} & \frac{\frac{2a_2 e^{-a_2 y_6}}{(1+e^{-a_2 y_6})^2}\frac{y_5 y_6}{\tau}}{2\sqrt{\rho(P_s - sigm(y_6) y_5)}} - \frac{\frac{2a_2 e^{-a_2 y_6}}{(1+e^{-a_2 y_6})^2}\frac{k y_5}{\tau}}{2\sqrt{\rho(P_s - sigm(y_6) y_5)}} U_{P_{smc}} \\ & - \frac{sigm(y_6)\dot{y_5}}{2\sqrt{\rho(P_s - sigm(y_6) y_5)}} \\ = {} & H(.) - I(.) - J(.) U_{P_{smc}}\end{aligned} \tag{3.12}$$

$H(.),\ I(.),\ J(.)$ are given by:

$$H(.) = \frac{\frac{2a_2 e^{-a_2 y_6}}{(1+e^{-a_2 y_6})^2}\frac{y_5 y_6}{\tau}}{2\sqrt{\rho(P_s - sigm(y_6) y_5)}}$$

$$I(.) = \frac{sigm(y_6)\dot{y_5}}{2\sqrt{\rho(P_s - sigm(y_6) y_5)}} \tag{3.13}$$

$$J(.) = \frac{\frac{2a_2 e^{-a_2 y_6}}{(1+e^{-a_2 y_6})^2}\frac{k y_5}{\tau}}{2\sqrt{\rho(P_s - sigm(y_6)y_5)}}$$

Let:

$$\begin{aligned} A_{41} &= -c_4 a_0 + c_3 b_0 - c_4 b_0 A_2 \\ A_{42} &= A_3 b_0 c_4 - c_3 a_1 \end{aligned} \tag{3.14}$$

Replacing (3.12) and (3.14) in (3.11):

$$\begin{aligned} \dot{S} &= c_1 y_2 + c_2 \dot{y_2} + (-c_3 a_0 + c_4 b_0 A_1)\dot{y_3} \\ &-A_{41}\dot{y_4} - c_4 a_1 J_1 A \frac{\dot{y_4} f(.) - y_4 \dot{f(.)}}{f(.)^2} - A_{42}\dot{y_5} - c_4 a_1 J_1 L \frac{\dot{y_5} f(.) - \dot{f(.)} y_5}{f(.)^2} \\ &-c_4 a_1 C_d J_1 \frac{k g(.) f(.) U_{P_{smc}}}{\tau f(.)^2} - c_4 a_1 C_d J_1 \frac{y_6 f(.)\left[H(.) - I(.) - J(.) U_{P_{smc}}\right]}{f(.)^2} \\ &-c_4 a_1 C_d J_1 \frac{\frac{-y_6 f(.) g(.)}{\tau} - g(.) y_6 \dot{f(.)}}{f(.)^2} = -K_{sw}\, sign(S) \end{aligned} \tag{3.15}$$

Rearranging (3.15) to have:

$$\begin{aligned} \dot{S} &= c_1 y_2 + c_2 \dot{y_2} + (-c_3 a_0 + c_4 b_0 A_1)\dot{y_3} - A_{41}\dot{y_4} - c_4 a_1 J_1 A \frac{\dot{y_4} f(.) - y_4 \dot{f(.)}}{f(.)^2} \\ &-c_4 a_1 J_1 L \frac{\dot{y_5} f(.) - \dot{f}(.) y_5}{f(.)^2} - A_{42}\dot{y_5} + c_4 a_1 C_d J_1 \left[-\frac{k g(.)}{\tau f(.)} + \frac{y_6 J(.)}{f(.)}\right] U_{P_{smc}} \\ &-c_4 a_1 C_d J_1 \frac{y_6 [H(.) - I(.)]}{f(.)} - c_4 a_1 C_d J_1 \frac{\frac{-y_6 f(.) g(.)}{\tau} - g(.) y_6 \dot{f}(.)}{f(.)^2} \\ &= -K_{sw} sign(S) \end{aligned} \tag{3.16}$$

In a reduced form $\dot{S}$ becomes:

$$\dot{S} = \eta + \mu \mathrm{U}_{\mathrm{psmc}} = -K_{sw} sign(s) \tag{3.17}$$

$$\Longrightarrow U_{P_{smc}} = -\frac{\eta}{\mu} - \frac{K_{sw}}{\mu} sign(s)$$

Finally, the total control signal for the position control is:

$$U_{P_{smc}} = U_{P_{eq}} + U_{P_{sw}} \tag{3.18}$$

The control signal $U_{P_{smc}}$ should be able to stabilize and keep the sprung mass near the zero position as much as possible. Obviously, with the switching control signal $U_{P_{sw}}$, we will have chattering due to a discontinuous part (sign function). The simulation in the next section clearly shows the controller performance and the chattering in control signals.

3.3.2 Force sliding mode (FSM) control

Since the position control results are generally obtained at the cost of increasing the force transmitted to passengers, the results are presented in the first subsection of the fifth section; it is of interest to study the impact of force control on system performance. Force tracking is also accomplished by using the sliding mode controller (SMC). The sliding surface is chosen as:

$$S = C_1\left(F - F_{ref}\right) = C_1 A(y_5 - y_{5ref}) \tag{3.19}$$

The reference force F_{ref} is chosen as in the work of (Sohl and Bobrow, 1999), and is derived from:

$$F_{ref} = M_s Acc_{ref} - K_v\left(\dot{y}_1 - \dot{y}_{1_{ref}}\right) - K_p(y_1 - y_{1_{ref}}) \tag{3.20}$$

Equation (3.20) is derived from (3.4). When the tracking error of position $y_1 - y_{1_{ref}} = 0$ and the tracking speed error is $\dot{y}_1 - \dot{y}_{1_{ref}} = 0$, Equation (3.20) becomes $M_s Acc_{ref}$. At the same time, the force produced by the piston is $F_{ref} = AP_L$. We can write, for the force produced by the piston, $F_{ref} = AP_L = -M_s Acc_{ref}$.

This means that the force produced by the active part (piston) AP_L equals the force transmitted to the passenger by the sprung mass. The force F_{ref} is a reference force we want to track, as we are not able to reduce it to zero. We therefore set this pattern to be tracked as a reference force. We derive $\dot{S}$ in the same way as we did in (3.10), to obtain the following control signal:

$$\begin{aligned} \dot{S} &= C_1 A\left(\dot{y}_5 - \dot{y}_{5ref}\right) \\ &= C_1 A\left[\frac{J_1}{f(.)}\left(-Ay_4 - Ly_5 + C_d y_6 g(.)\right)\right. \\ &\left. - \dot{y}_{5ref}\right] \quad = -K_{sw}\, sign(s) \end{aligned} \tag{3.21}$$

From (3.5), we have $\dot{y}_6 = \frac{1}{\tau}(-y_6 + kU_{F_{smc}})$. This yields to:

$$y_6 = -\tau\dot{y}_6 + kU_{Fsmc} \tag{3.22}$$

Replacing (3.22) in (3.21), we obtain:

$$\begin{aligned} \dot{S} &= C_1 A\left[\frac{J_1}{f(.)}\left(-Ay_4 - Ly_5 + C_d g(.)\left(-\tau\dot{y}_6 + kU_{F_{smc}}\right)\right) - \dot{y}_{5ref}\right] \\ &= \frac{C_1 A J_1}{f(.)}\left(-Ay_4 - Ly_5 - C_d g(.)\tau\dot{y}_6 + C_d g(.)kU_{F_{smc}}\right) - C_1 A y_{5ref} \\ &= -K_{sw} sign(S) \end{aligned} \tag{3.23}$$

Therefore, the equivalent control can be written as:

$$U_{f_{equ}} = -\frac{C_1 A\frac{J_1}{f(.)}(-Ay_4 - Ly_5 - C_d g(.)\tau\dot{y}_6) - C_1 A y_{5ref}}{\frac{C_1 A J_1 C_d g(.)k}{f(.)}} \tag{3.24}$$

The switching control is:

$$U_{F_{sw}} = -\frac{f(.)}{C_1 A J_1 C_d g(.) k} K_{sw} sign(s) \quad (3.25)$$

The total control signal for force tracking $U_{F_{smc}}$ is:

$$U_{F_{smc}} = U_{fequ} + U_{F_{sw}}$$

3.3.3 Hybrid sliding mode (HSM) control

The schema in Figure 3.2 shows how we took advantage of both controllers developed in the first two subsections of the fourth section. The principle of combining two controllers with two filters derives from the idea that every controller has some advantages, but at the cost of performance reduction elsewhere. Thus, the other controller compensates for the disadvantage of the first controller. This controller is designed such as to achieve both a reduction of passengers' vertical motion and a reduction of the force transmitted to the passenger. The position/force controller outputs go through two low-pass filters. Low-pass filters are used in order to prevent the high frequency control signal from getting through, likely causing the appearance of some nonlinear terms.

A singularity problem will appear if the filters are not used. The phase in the filter adds a delay to the control signal to avoid any singularity. The filters' gains α_1, α_3 are important for prioritizing one controller over another. These gains are limited, but could vary in a range where they make the corresponding filter more efficient. In other words, the selected controller will be more dominant and flexible in dealing with our system. Every controller tries to reach its objective. The main goal of the position controller is to deal with the sprung mass position. This objective will be reinforced by the corresponding gain choice. Fixed gain filters will react in the same manner against errors during simulation whereas the variable gains (α_1, K_1) add more flexibility and adaptability to the control law U_{tot}. The total control law will be calculated such as to reduce the most significant errors by employing the sliding surfaces in the fuzzy controller.

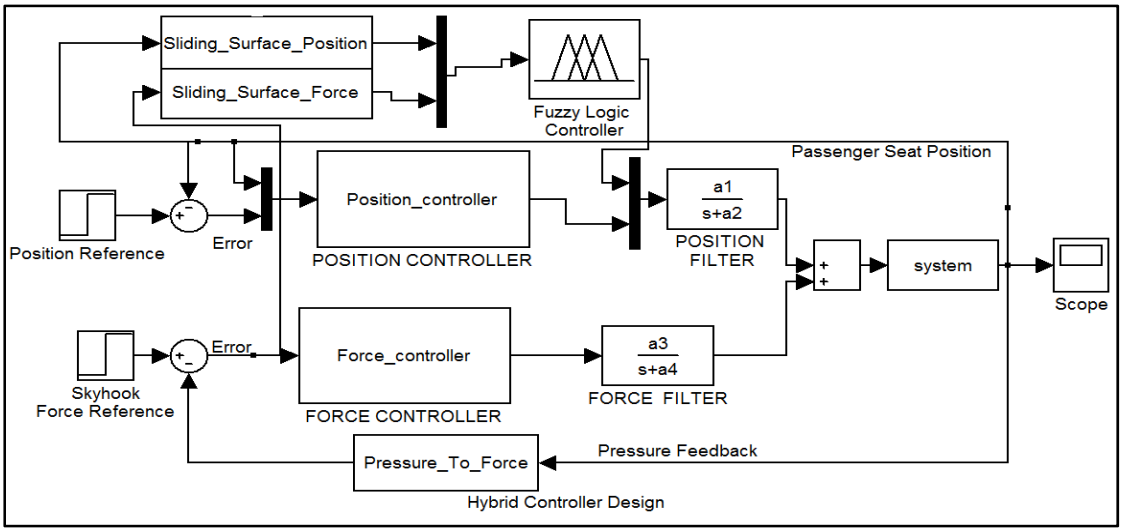

Figure 3.2 Hybrid controller schema

The control signal is given by:

$$U_{tot} = \frac{\alpha_1}{s+\alpha_2} U_{P_{smc}} + K_1 \frac{\alpha_3}{s+\alpha_4} U_{F_{smc}} \tag{3.26}$$

α_1, α_3 are the gains of the low-pass filter that give priority to the corresponding filter. α_2, α_4 are designed to select the bandwidth. For its part, the force controller participates in the control law through its predetermined percentage gain. Indeed, the gain α_3 is linked to another variable positive gain K_1 by which the transmitted force to passengers is integrated into the control law. The variable gain is related to the $F_{passenger}$ in order to linearly increase the priority in the control force part:

$$K_1 = \frac{F_{passenger}}{force\ threshold} = \frac{M_s \ddot{x}_s}{force\ threshold} \tag{3.27}$$

The force controller reacts directly to reduce this extra produced force. Increasing these parameters to high values could generate instability in the system response. The bandwidth of the filters should also be greater than that of the active suspension system in order to allow full control of a wide range of the system's bandwidth, such as in (Wright, 1983).

3.3.4 Exponential reaching law (ERL)

As we will see in Figure 3.5, we have control signals with pronounced chattering, which is inherent to the sliding mode control. This chattering appears in the reaching phase, where the system trajectory starts sliding along the surface $S = 0$. The chattering is due to the discontinuity in the switching control signal, and the conventional control law is not enough to suppress it. Thus, (Gao and Hung, 1993) used a sliding surface with a power rate in the reaching law. This strategy is efficient for chattering reduction, but it increased the reaching time.

To remedy this problem, (Fallaha et al., 2011) suggested an exponential reaching law (ERL) in order to reduce the chattering with a fast reaching time. This exponential law was applied to a robotic arm with 3 degrees of freedom, but has not been tested with other systems. As the chattering in control signals may damage hydraulic actuators, and given the demonstrated efficiency of ERL-based control, we found it worthwhile implementing this approach to the electrohydraulic system. The results were encouraging, and chattering was reduced, and even removed, in some cases. The exponential reaching law states that:

$$\dot{S} = -\frac{k}{\rho_0 + (1-\rho_0) * \mathrm{e}^{(-\alpha|s|^2)}} sign(S)$$

The convergence law is a general case of the conventional law when $0 \leq \rho_0 \leq 1$. This makes the exponential law more flexible by changing ρ_0. When $\rho_0 = 0$, we obtain the conventional convergence law. Because the convergence law offers flexibility in reducing chattering and decreasing the reaching time, we applied it to all three controllers. It produced good results in eliminating the chattering, as we see in the hybrid controller simulations. When applying the exponential reaching law to the position and force controllers in the hybrid structure separately, we actually vary the switching gain. By proceeding as such, the resulting control signal changes the reaching time and actively anticipates the sliding surface controller's performance. This can be seen in the simulation results. In hybrid control, the issue considered is how much

ERL could reduce the force tracking error and isolate the sprung mass position from road irregularities.

3.3.5 Fuzzy hybrid sliding mode (FHSM) control with ERL

We noticed in the simulation results (as we will see in the fourth section), that the position control plays a dominant role. That is why a variation in the filter gain α1 related to the position controller provides a variable weighting factor, making the control signal more efficient. Thus a sliding surface-based fuzzy logic controller was developed in order to vary the gain α1. The fuzzy controller output is scaled to change α1 in the system stability limit. The fuzzy control is applied to our last ERL sliding mode hybrid controller used in the fourth subsection of the fourth section.

Using sliding surfaces as fuzzy inputs is an interesting principle in hybrid control, which achieves better stability, and could merge the errors and their rates into one type (Kim and Lee, 1995). The fuzzy inputs and outputs are classified into four equal-span gaussian membership functions scaled within a range of 6 (Han et al. 2005). The fuzzy rules are summarized in Tableau 2.1, and also illustrated in Figure 3.3. When we have a big force and position sliding surfaces, we need to increase the filter gain α1 to a maximum, and vice versa. Accordingly, the smaller sliding surfaces lead to small values of α1. The fuzzy symbols are **VB**: Very Big, **B**: Big, **Z**: Zero, **L**: Low, **VL**: Very Low.

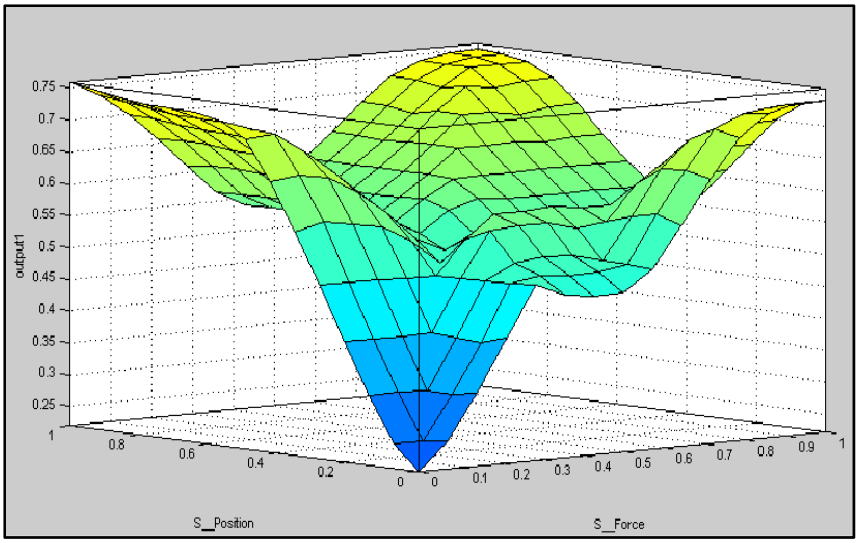

Figure 3.3 Control surfaces of fuzzy inputs

Tableau 3.1 Fuzzy rules

Force Sliding Surface / Position Sliding Surface	VB	B	Z	L	VL
VB	VB	VB	B	L	L
B	B	B	L	VL	VL
Z	L	L	Z	Z	Z
L	L	L	Z	VL	VL
VL	VL	VL	Z	VL	VL

3.4 Simulation results

The proposed electrohydraulic active suspension mathematical model and the designed controllers were developed and implemented using Simulink/Matlab. The simulation was performed with a short sampling time (0.001 sec). The controller variables are listed in Annexe I, Tableau-A I-3. In Figure 3.4, the road profile is a sinusoidal-shaped single bump with an amplitude of $h = 0.1\,m$, length $\lambda = 13\,m$ and vehicle velocity $v = 25\,m/s$ (Baumal et al., 1998):

$$x_r = \left\{ \begin{array}{cc} \frac{h}{2}(1-\cos(wt-24)) & 0 \le t \le \frac{2\lambda}{v} \\ 0 & otherwise \end{array} \right\} \tag{3.28}$$

3.4.1 Hybrid sliding mode control

In Figure 3.4, the passenger seat position is deviated to 5 cm in the position controller. A reduction of more than 5 cm is achieved, but a relatively high force (2000 N) is reached. This shows that the position controller exhibits a good performance in terms of position reduction, but at the cost of increasing the force transmitted to passengers. However, this force is high with the position controller (Figure 3.5), in comparison with the same force obtained when using the force controller. The control signal presents significant chattering (Figure 3.6), especially around the zero crossings. This chattering, at the proximity of the sliding surface, is due to the high frequency switching of the function $sign(S)$ in both controllers.

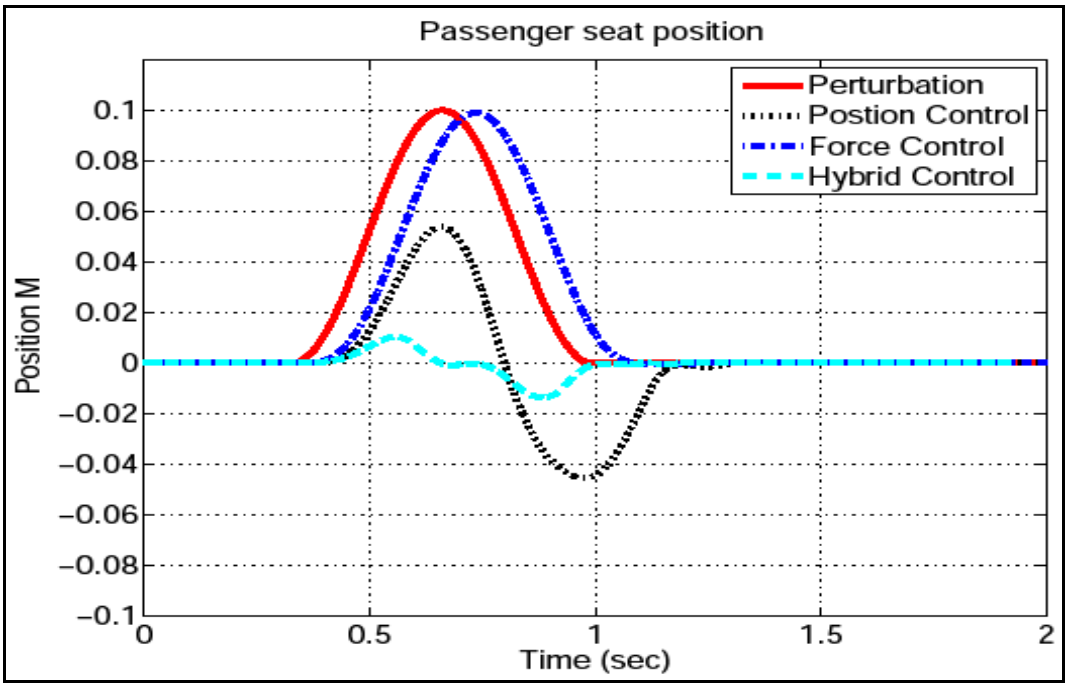

Figure 3.4 Sprung mass position when SMC position control is applied

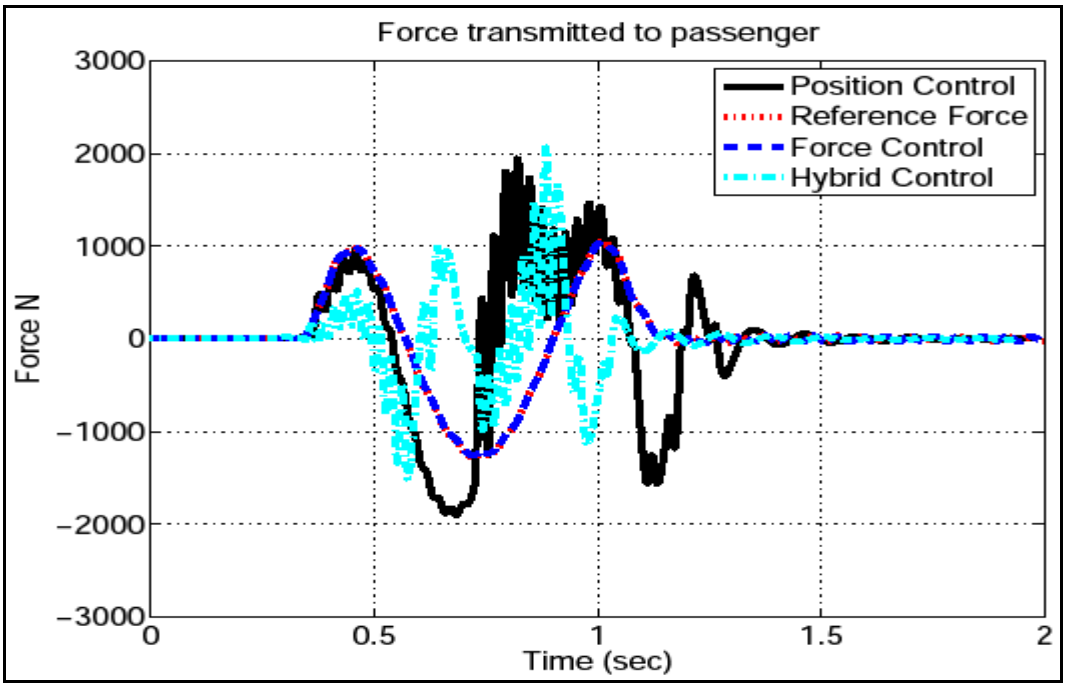

Figure 3.5 Force transmitted to passenger

The force controller demonstrated a significant force reduction, and the amplitude of the force transmitted to the passenger was reduced to 1250 N (Figure 3.5). In comparison with the position controller, the passenger force was reduced by 35%, and in comparison with the passive suspension, by 50%, which is a good indicator of the controller's efficiency. In terms of the passenger seat displacement, there was no significant improvement or deterioration (Figure 3.4). Figure 3.6 shows the corresponding control signal with a maximum of 0.5 volt and a small chattering. For the hybrid control, the force transmitted to the passenger is limited to 2046 N (Figure 3.5), which is high enough in comparison with the force controller performance.

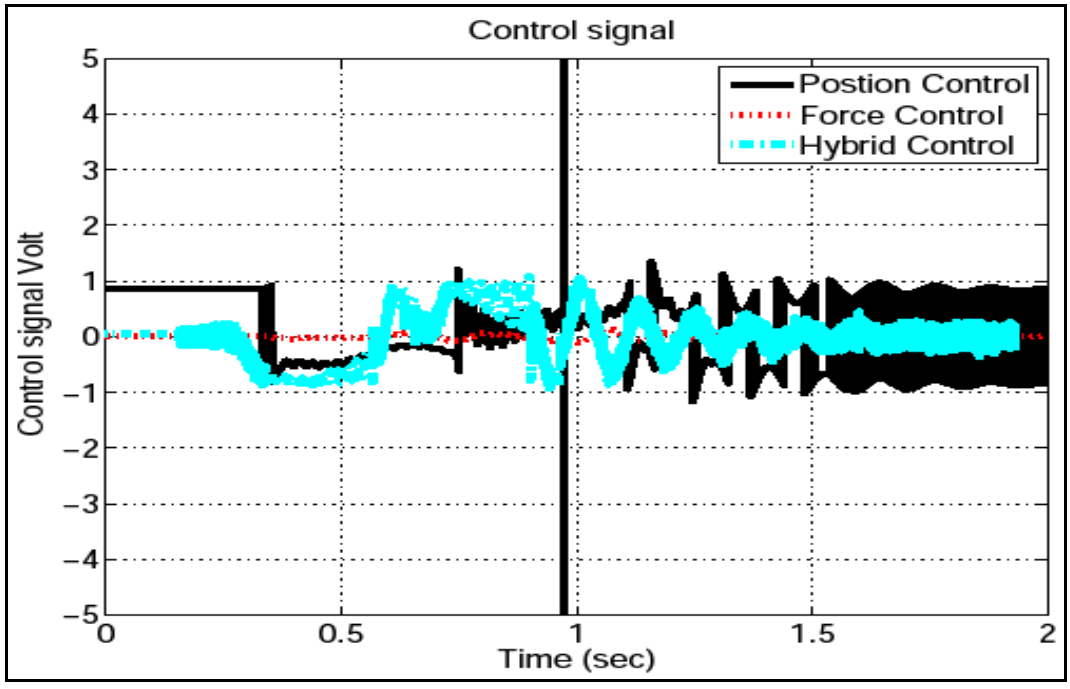

Figure 3.6 Control signal when SMC position control is applied

The hybrid control is able to reduce the perturbation from 10 cm to less than 2 cm, which is another good indicator of the controller robustness and performance as illustrated in Figure 3.4.

The hybrid controller signal reached a maximum of 1 volt with chattering whereas the position controller had exceeded that value with a huge chattering, as can be seen in Figure 3.6.

In the next sections, the hybrid controller will be improved to reach a better force tracking, more perturbation reduction and less chattering. The hybrid controller is modified such as to essentially reduce the maximum transmitted force.

3.4.2 Hybrid sliding mode control with ERL

The simulation shows that using a variable switching gain with an exponential reaching law is more efficient than using a fixed switching gain. In Figure 3.7, for the same perturbation, the position with an ERL controller has been slightly degraded from 1.4 cm to 1.57 cm. On the other hand, the force transmitted to the passenger is 1550 N, which is better than without ERL (2046N).

In Figure 3.8, the force tracking error is not just smaller than without ERL, but it is also smoother. This reduction in force error guarantees an improvement in passenger comfort. The ERL effect appears clearly in the shape of a control signal which became free of chattering (Figure 3.9 and Figure 3.10). When comparing to the results of the work done by (Hwang, 1996), the chattering exists with significant values in spite of using variable boundary to reduce the chattering in the control signal. Thus, ERL has proven an efficiency as it is also easy to apply.

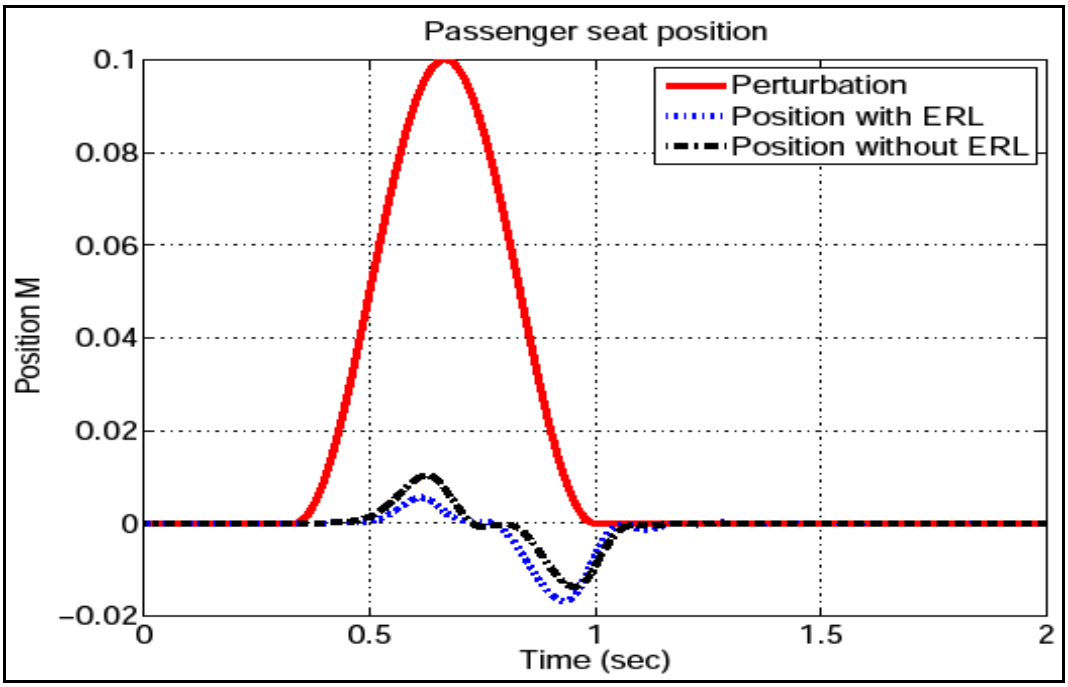

Figure 3.7 Sprung mass position when exponential reaching law hybrid controller is applied

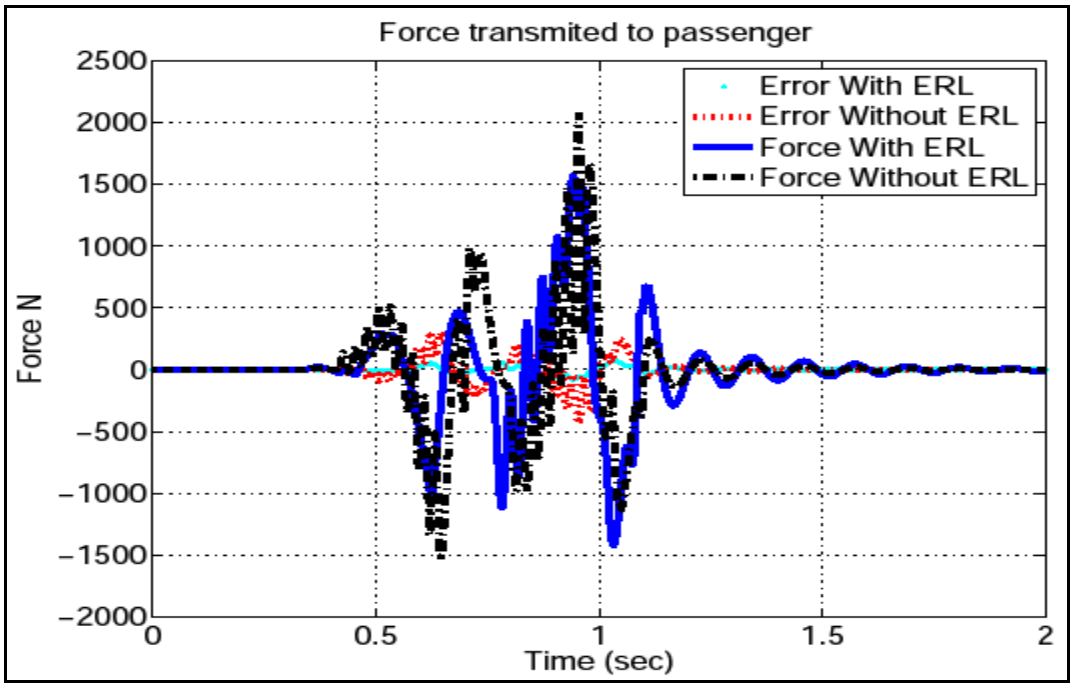

Figure 3.8 Force transmitted to passenger when exponential reaching law hybrid controller is applied

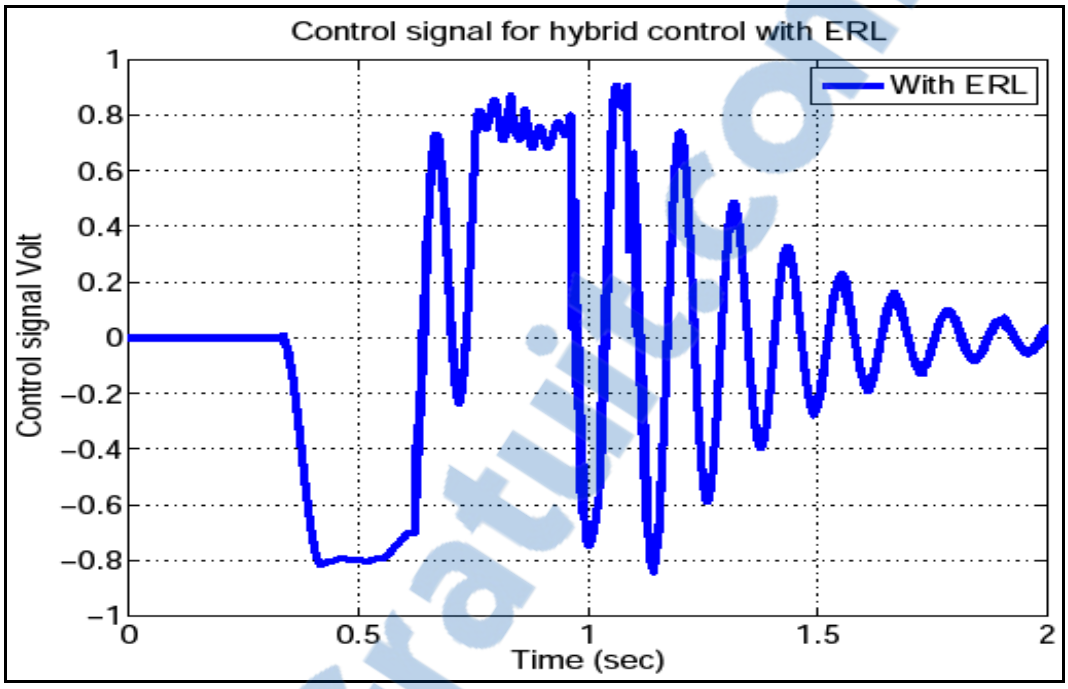

Figure 3.9 Control signal when hybrid controller is applied with ERL

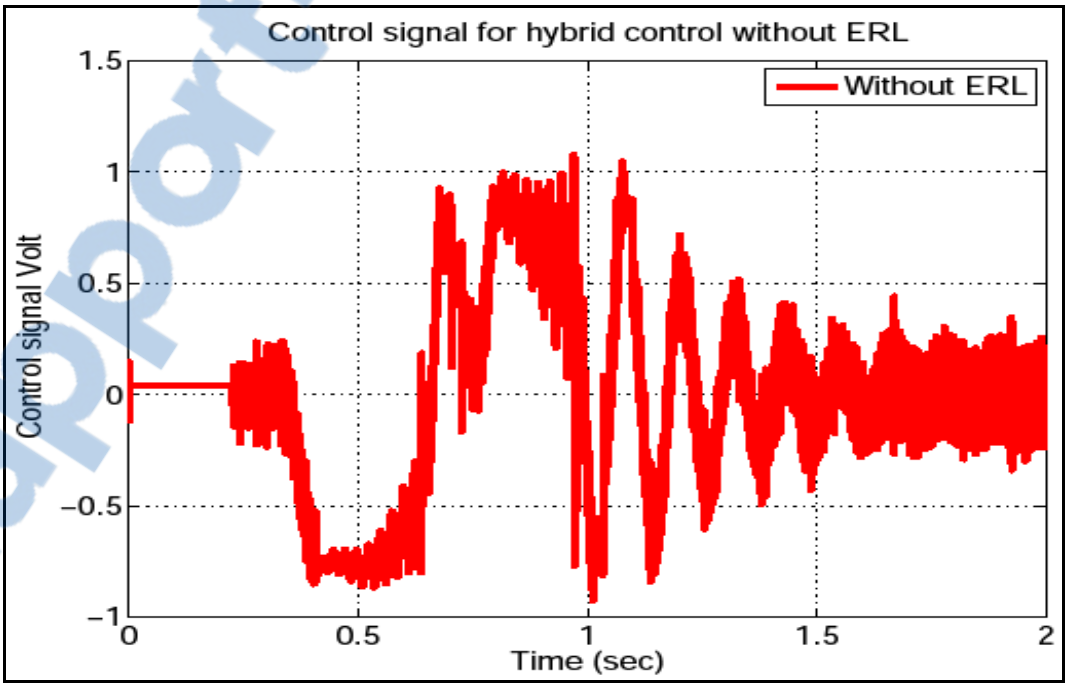

Figure 3.10 Control signal when hybrid controller is applied without ERL

3.4.3 Fuzzy hybrid sliding mode control with ERL

As expected, when varying the gain of the position controller filter, the results of the added fuzzy control appeared directly in the simulation. The position of the sprung mass, when using a Fuzzy SMHC with ERL controller, was reduced by 18.02% (1.29 cm) in comparison with the position without using fuzzy logic (1.57 cm) (Figure 3.11).

Furthermore, the maximum force transmitted to passengers improved by 18.5% (1304N), in comparison with the force without using FLC (Figure 3.12). Referring to Figure 3.12, the force tracking error was also reduced.

For road handling, the tire deflection y_r presented in Figure 3.13 has minimum values when using a Fuzzy ERL SMHC controller. It returns to zero faster than the ERL SMHC controller. The suspension travel y_3 in Figure 3.14 is kept within a limited range for design considerations for both controllers.

The sliding surfaces in Figure 3.15 are calculated during simulation in order to find the control laws. They are reused in the fuzzy controller to change the filter gain α1. Both sliding surfaces stabilize in 2 secs, but the force sliding surface takes more time. Although the position error is very small, the force error is still significant. The fuzzy controller output α1 in Figure 3.16 is proportional with the position sliding surfaces. The filter gain increases when the position sliding surface is high, and it returns to a fixed value when the position surface is reduced. As we used ERL hybrid controllers, we do not expect to encounter chattering (Figure 3.17).

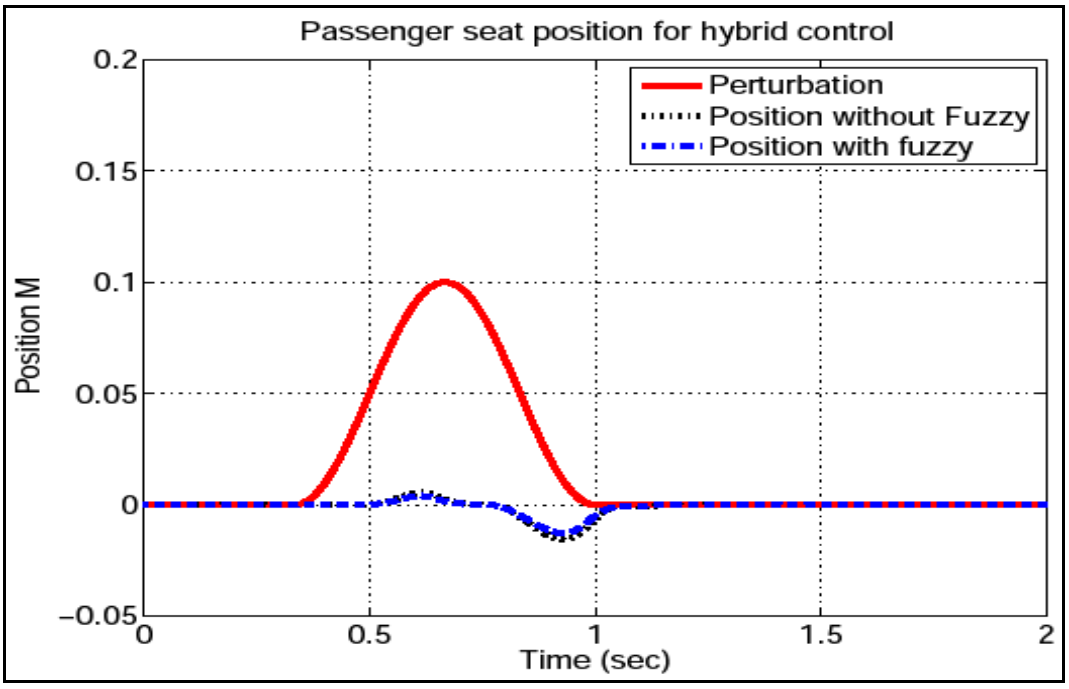

Figure 3.11 Sprung mass position when fuzzy ERL hybrid controller and ERL hybrid controller are applied

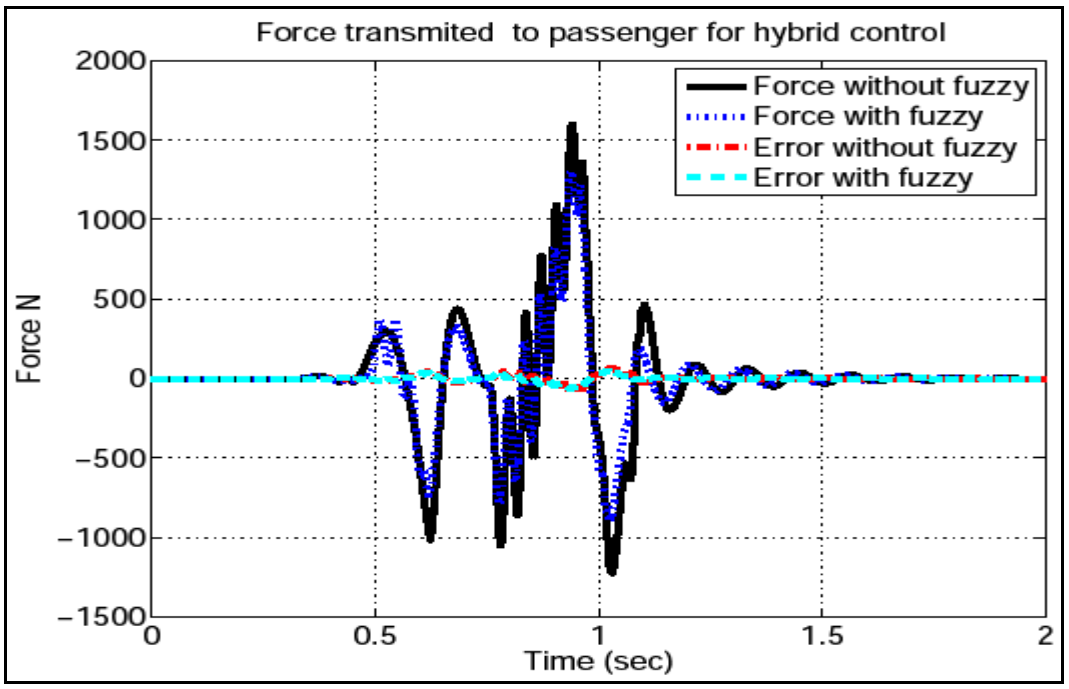

Figure 3.12 Force transmitted to passenger

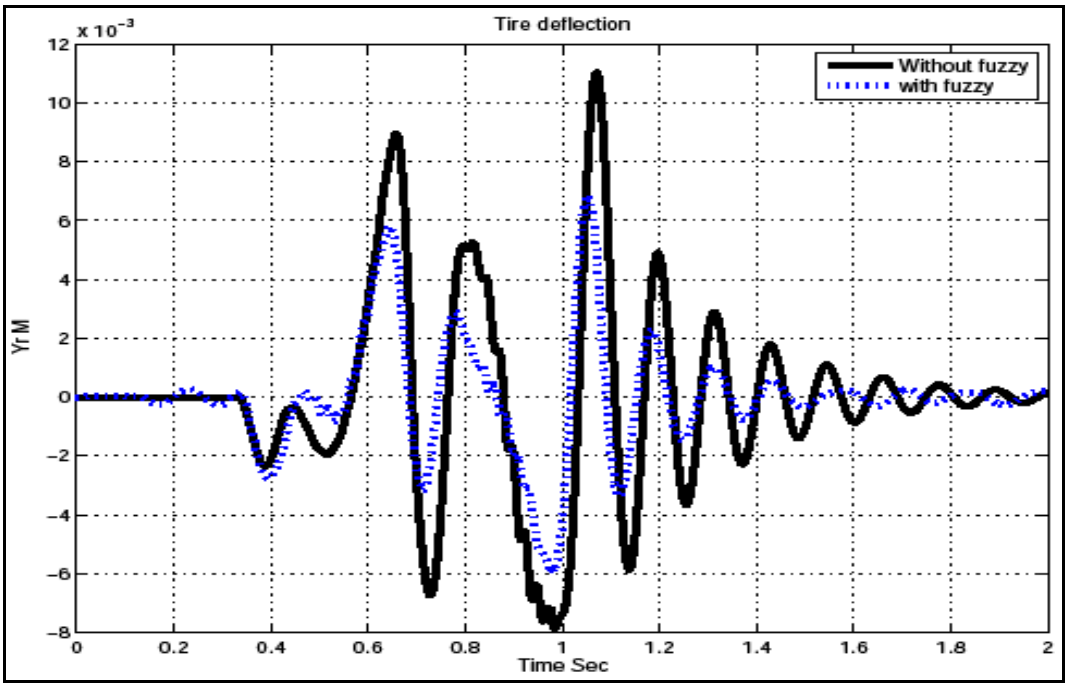

Figure 3.13 Tire deflection

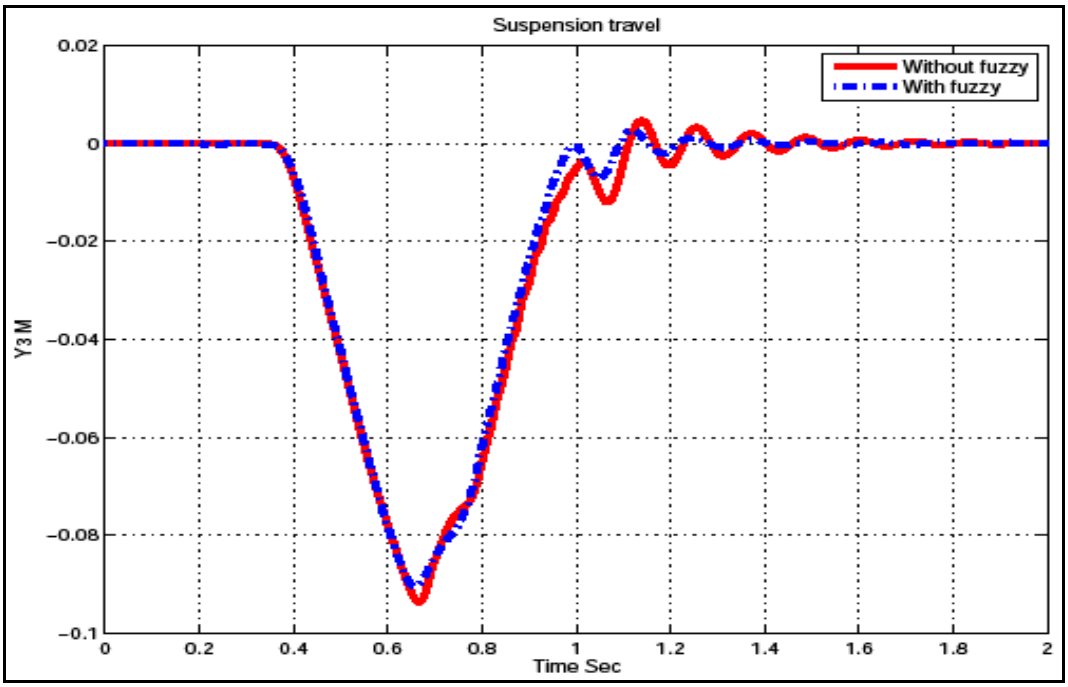

Figure 3.14 Suspension travel

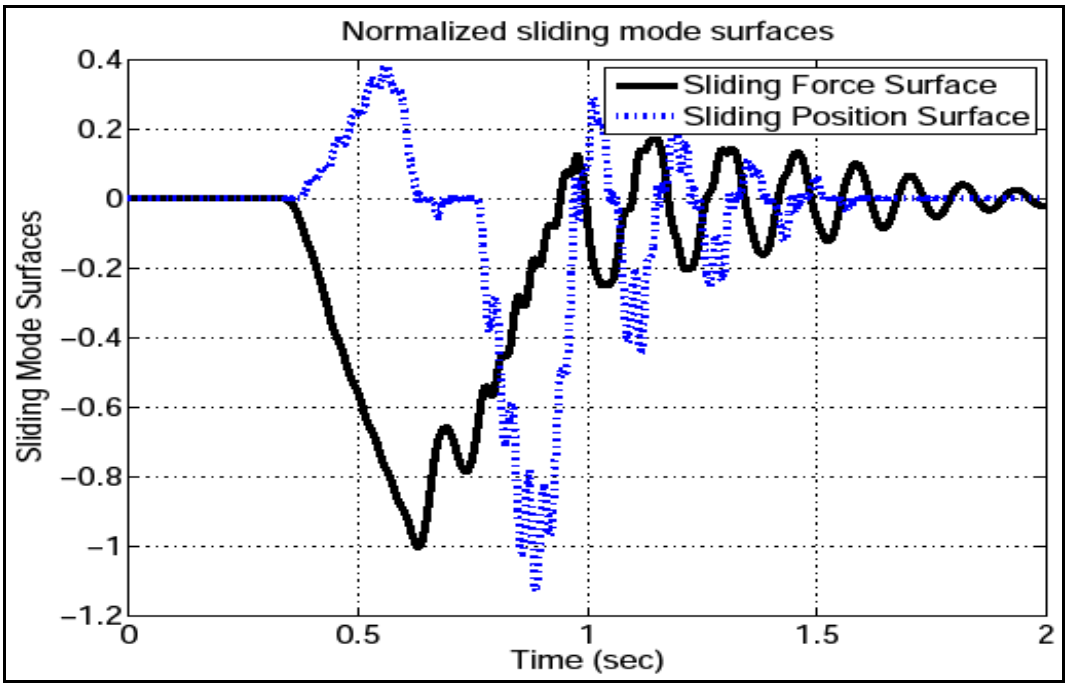

Figure 3.15 Sliding surfaces

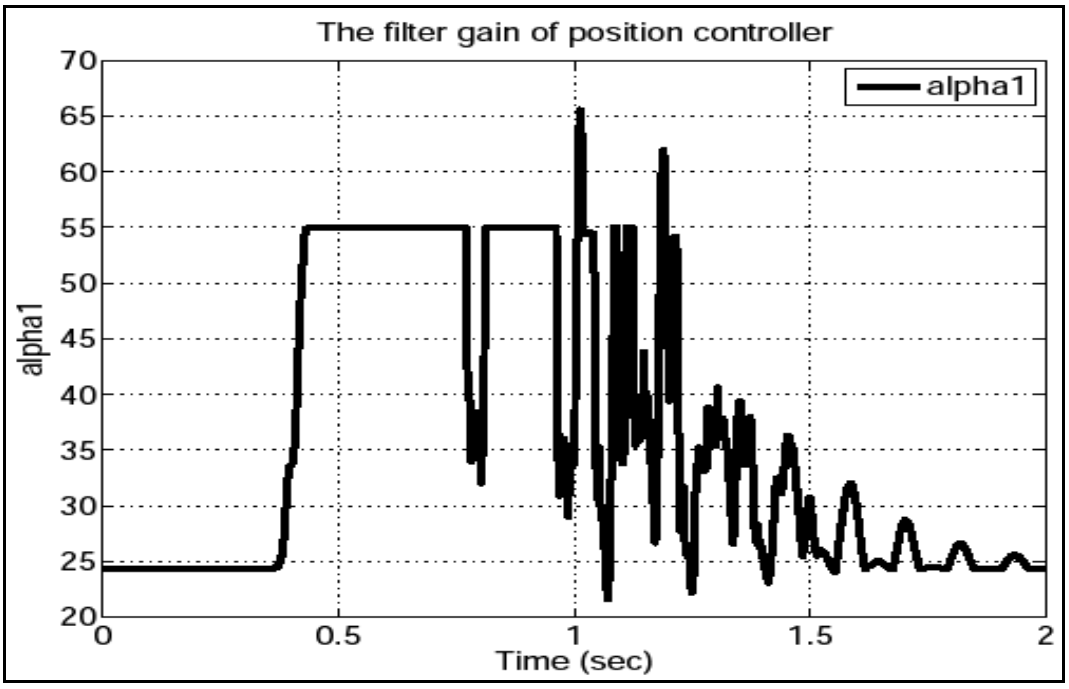

Figure 3.16 Position filter gain

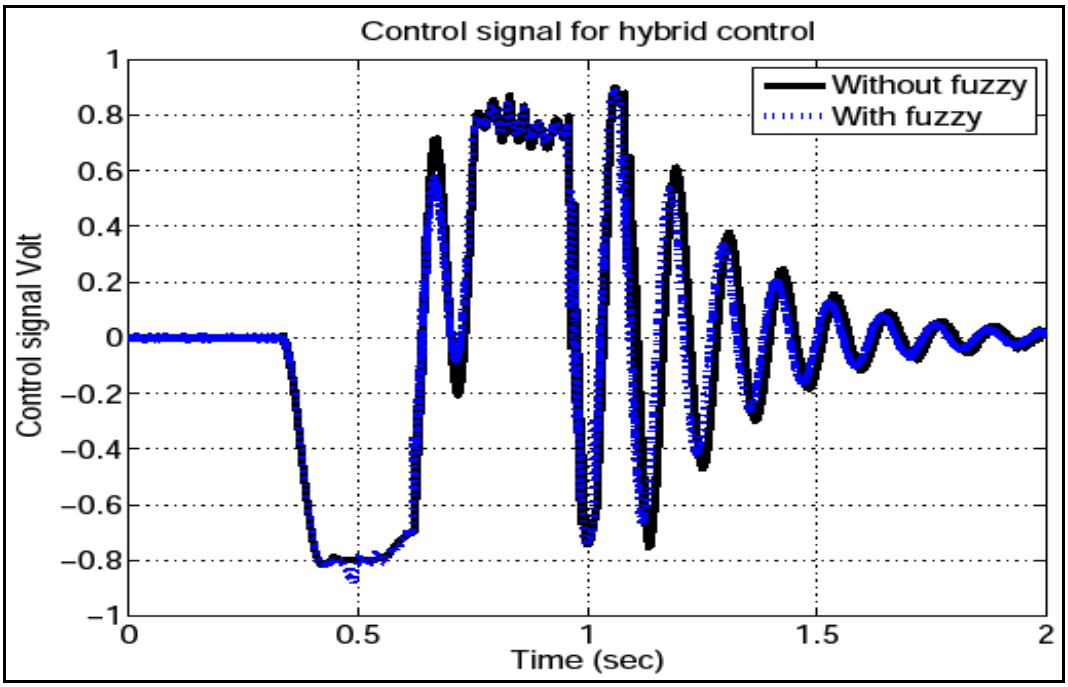

Figure 3.17 Control signal when fuzzy ERL hybrid controller and ERL hybrid controller are applied

3.4.4 Comparison with a PID controller

In this section, we will use a conventional PID to control the position of the sprung mass, and compare it with our proposed fuzzy ERL hybrid controller. We chose the PID controller because of its popular use in industry. The simulation results show that our proposed hybrid controller outperforms the PID by a significant margin. The PID gains were found using Ziegler Nichols. The resulting gains were not optimal, and so we modified them by trial and error to get the best performance. The PID controller was applied to the nonlinear model. The results of the simulation show that the passenger's vertical motion was reduced faster with our modified hybrid controller than with a PID (Figure 3.18). The PID controller reduced the perturbations to 50%, which was less than with the hybrid controller, at 87%.

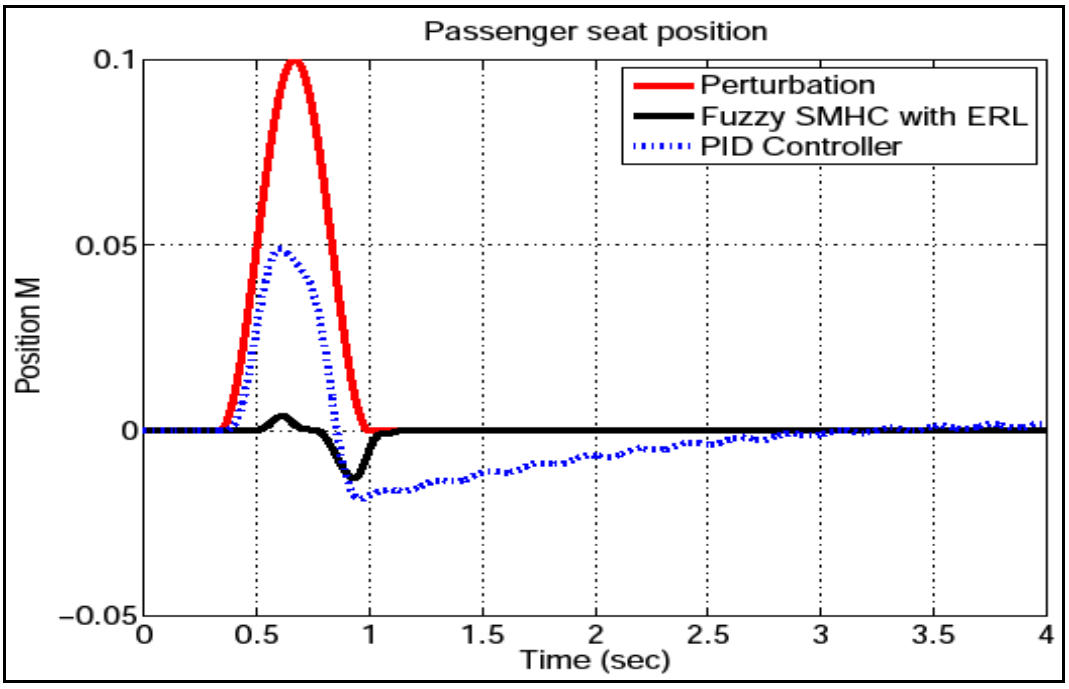

Figure 3.18 Sprung mass position when using the Fuzzy SMHC with ERL controller

The force transmitted to passengers with the PID had a longer settling time than what is seen with the SMC (Figure 3.18). In terms of the force amplitude, our controller produced a smaller transmitted force in comparison with the PID (1354 N), which is a very interesting improvement through its development process.

Practically, the new hybrid controller reduced the transmitted force from 2046 N (Figure 3.5) to 1304 N (Figure 3.19) by adding the ERL and fuzzy control to the main hybrid controller, which improved the performance by 37%. The tire deflection y_r with a PID controller oscillates with higher values than the fuzzy ERL SMHC controller. Figure 3.20 shows a better road contact with the fuzzy ERL SMHC controller. The lower the tire deflection, the better the vehicle handling.

The suspension travel y_3 for both controllers in Figure 3.21 is still within limits, but it takes more time to stabilize with the PID controller. The suspension travel with the fuzzy ERL SMHC controller has a bigger magnitude, due to the movement caused by the unsprung mass (tire). In other words, the hybrid controllers use the tire to dissipate the energy transferred from

road irregularities. The result is that higher forces are applied on the tire in order to better stabilize the car body.

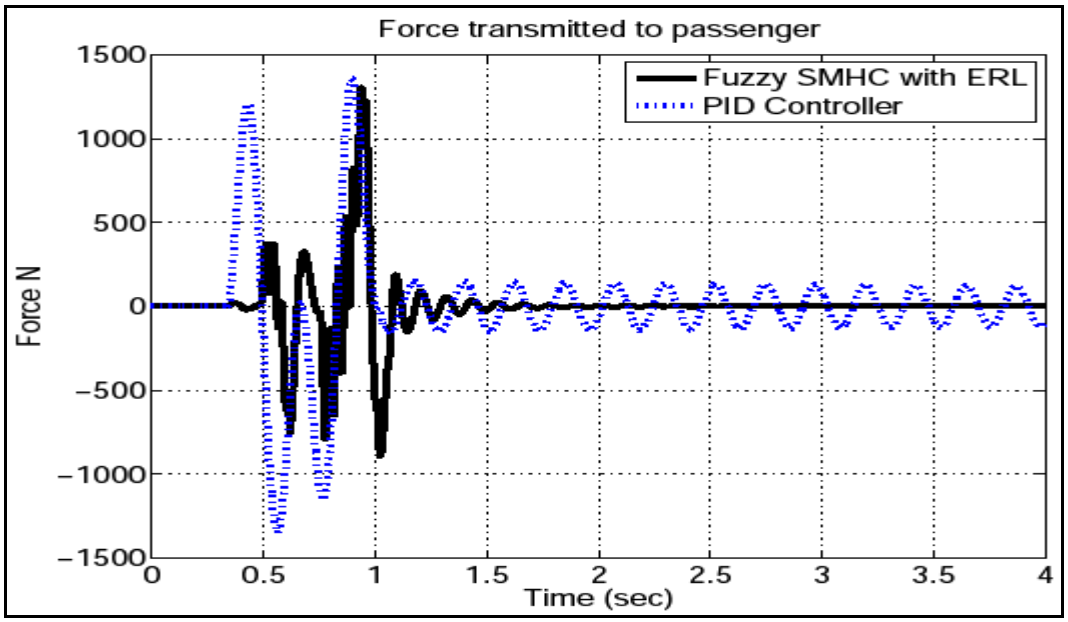

Figure 3.19 Force transmitted to passenger

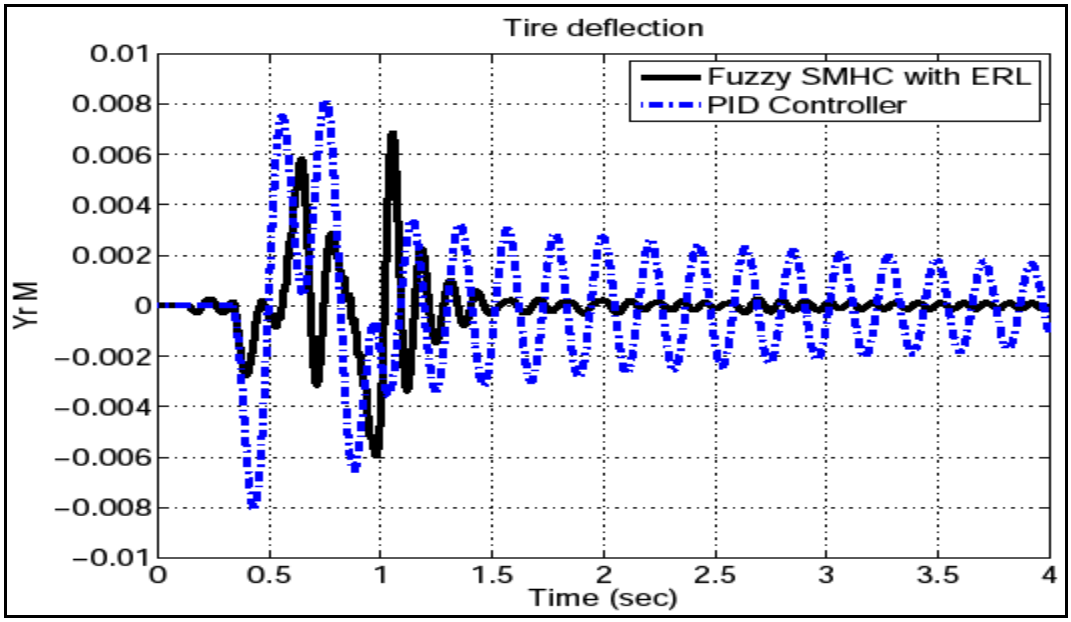

Figure 3.20 Tire deflection

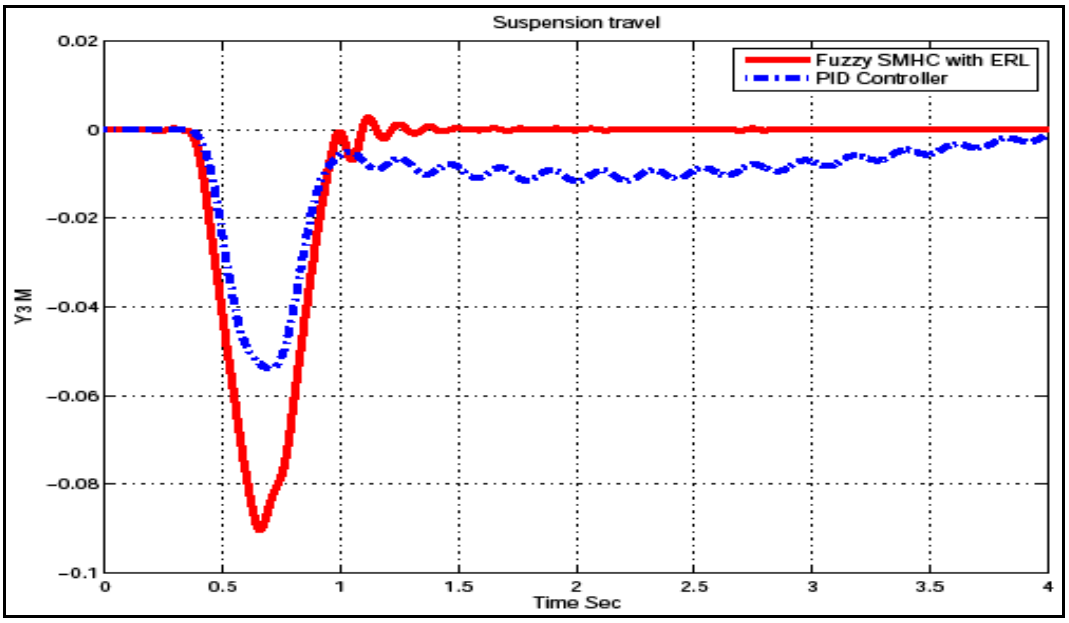

Figure 3.21 Suspension travel

The control signal of the PID controller (Figure 3.22) is smoother, with a longer settling time, in contrast to the Fuzzy ERL SMHC controller, which has an assertive behavior and a fast settling time to reach the desired position and force at the same time.

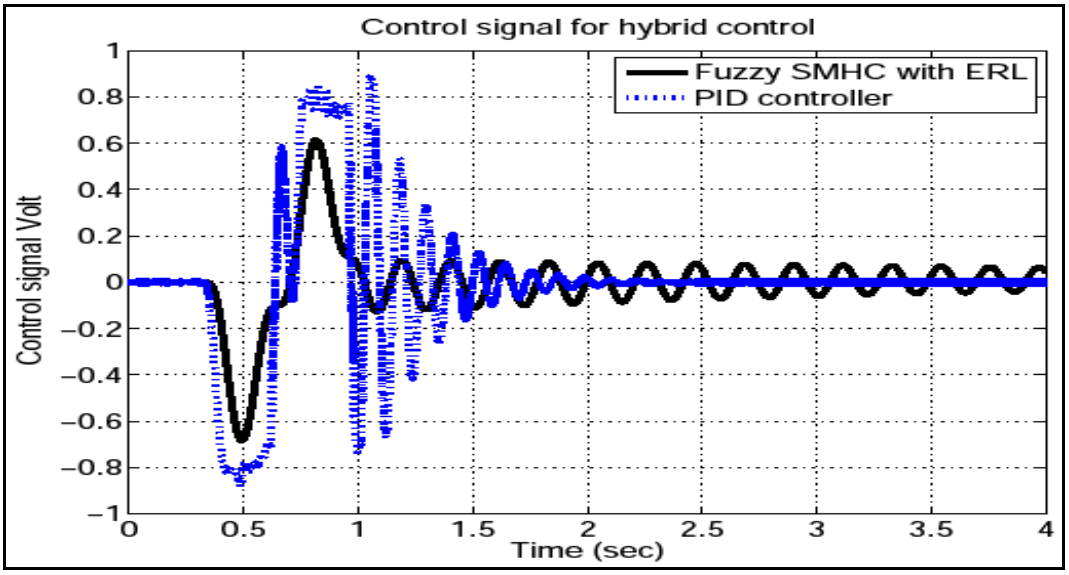

Figure 3.22 Control signal when a PID and Fuzzy SMHC with ERL controllers are applied

As the human body is sensitive to vibration between 25 rad/sec and 50 rad/sec (ISO 2631). A frequency response analysis, using the tool frequency estimation of simulink model, has been conducted to describe the steady-state response of a system to sinusoidal sweep input of road profile. The frequency analysis is applied with fixed step on both PID and Fuzzy SMC with ERL controllers. In Figure 3.23, the fuzzy SMHC with ERL controller overcomes the performance of PID controller against perturbations as it suppresses the perturbations due to its negative gain in (dB). The acceleration, in Figure 3.24, is reduced by our nonlinear proposed controller for all frequencies. The suspension travel frequency response of PID controller is better than the proposed controller which corresponds with suspension travel showed in Figure 3.24.

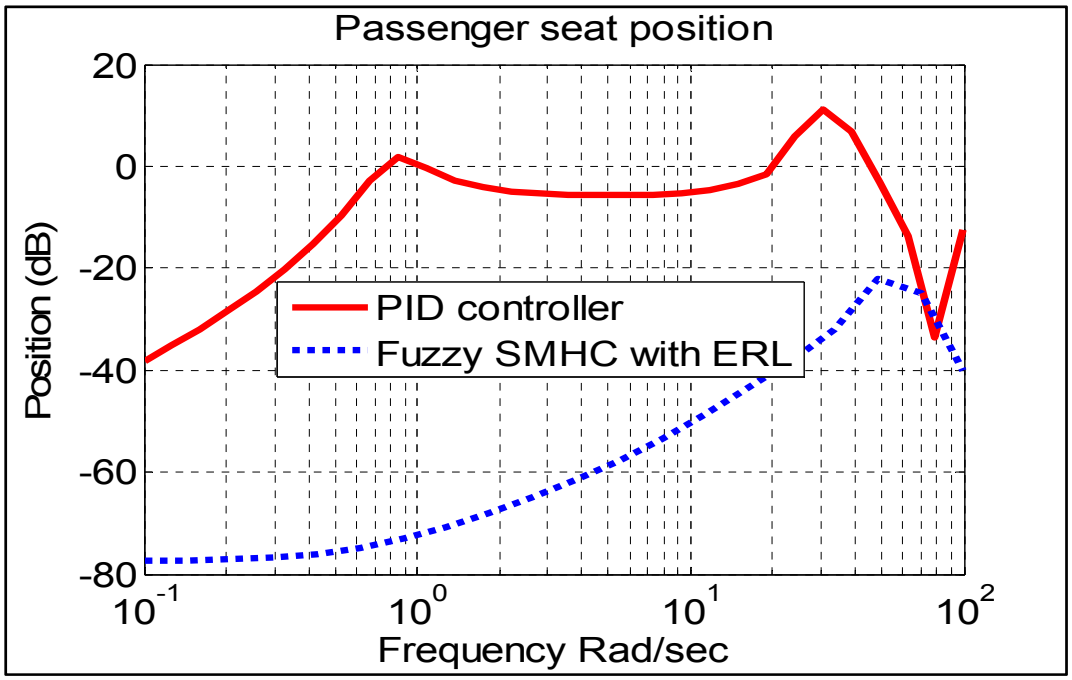

Figure 3.23 Frequency response of passenger seat position

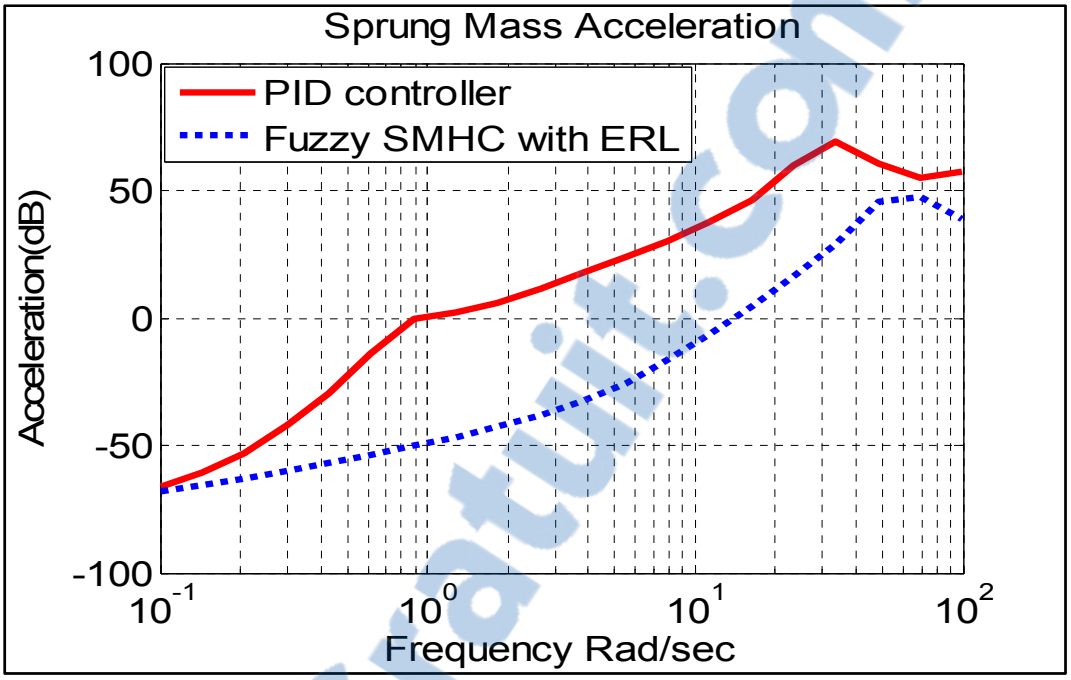

Figure 3.24 Frequency response of sprung mass acceleration

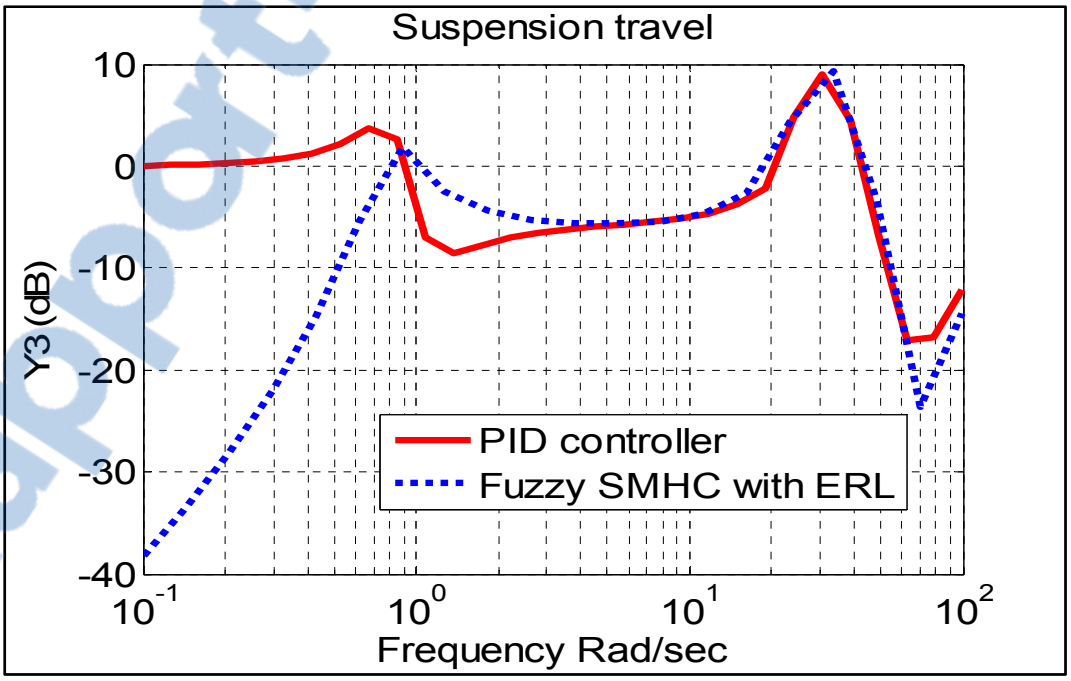

Figure 3.25 Frequency response of suspension travel

3.5 Experimental study

As the results of the simulation are good, the proposed structure is validated and applied to the hydraulic workbench in Figure 3.26. A hydraulic pump, driven by an electrical motor, feeds three electrohydraulic servovalves with oil stored in the tank. The servovalve 1 is used to drive the cylinder representing the road disturbances. The servovalve 2 is connected to the cylinder 2 which controls the active suspension. The servovalve 3 is connected to the cylinder 3 that represents the weight of the passengers and loading. The relief valve limits the maximum pressure in the system. A Linear Variable Differential Transformer (LVDT) is installed on the cylinder 2 in order to measure its linear position. Two pressures sensors are used for the two cylinder's chambers. The acquisition I/O card, is a National Instrument NI PCI 6014 . This card is a low-cost 200 kS/s, 16-Bit, 16 analog inputs multifunction data acquisition (DAQ).

In the Figure 3.27, the perturbation is presented as a semi sinusoidal bump of 5cm, the controller should reduce the perturbation effect on the passenger's seat. The sliding mode based hybrid controller SMHC reduced the perturbation from 5cm to 3.3cm (34%) with repetitive oscillations while the PID reduced the perturbation to 3.62cm (27.6%). The sliding mode based hybrid controller with ERL (SMHCERL) gave the best results as it reached a maximum of 1.768cm (64.2%). The transmitted force to passenger has reached a maximum of 4026N by the hybrid controller which is better than the PID 4553N in Figure 3.28. The SMHCERL has reduced the force to 3513N where we have about 1040N (22%) as a difference with the PID controller.

In Figure 3.29, the control signal of the hybrid controller is accompanied by chattering which could damage the cylinder. Thus an exponential reaching law is applied as done in the simulation. The experimentation showed that the hybrid structure made a better performance than all the controllers. The hybrid controller achieved its objective by making a compromise between the position and the force using low pass filters.

The ERL is applied to fasten the system response and reduce the chattering as its variable gain N(s) is reduced in Figure 3.30.The low pass filter has an additional influence by cutting the

high frequencies control signals issed from the SMHCERL controller. On the other side, the PID controller, as a classical controller, was not able to track both the position and force as it is designed to track one variable and does not have any influence on the other variables. The PID is designed with only one control signal in order to minimize the error of the passenger seat position; whereas the hybrid controller uses adaptive combination of controller outputs to produce its own control signal.

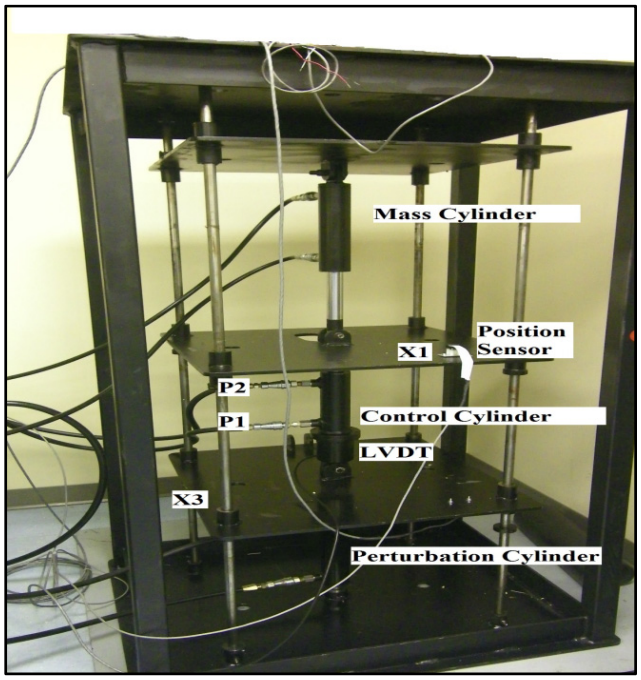

Figure 3.26 Active suspension workbench

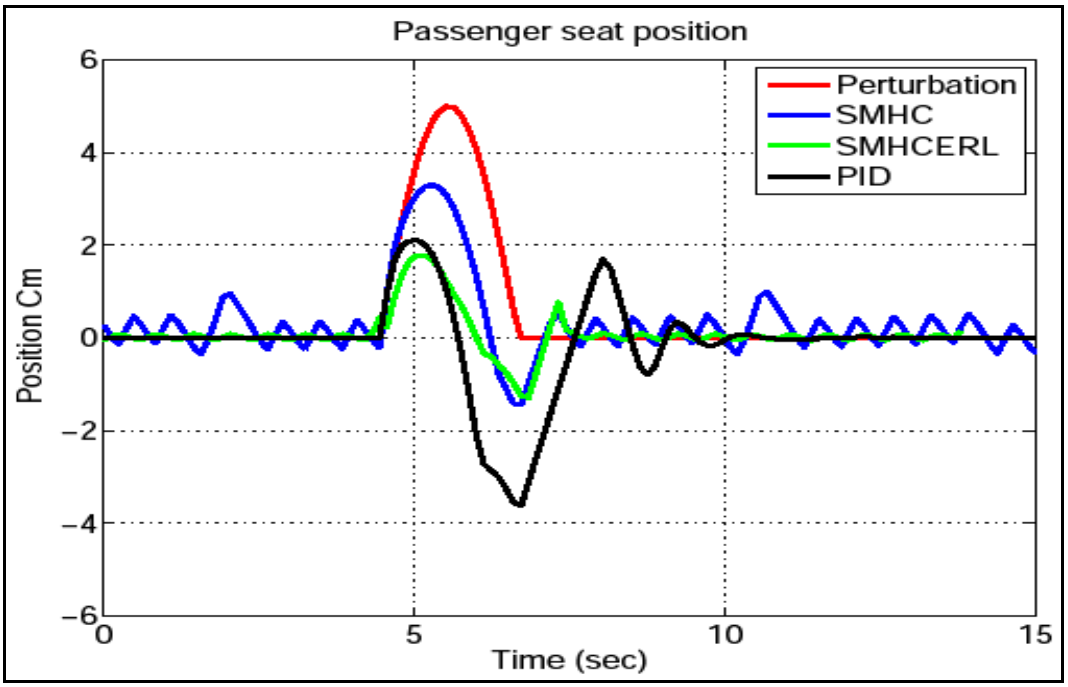

Figure 3.27 Sprung mass position, when SMHC with ERL controllers, SMHC without ERL and PID position controllers are applied

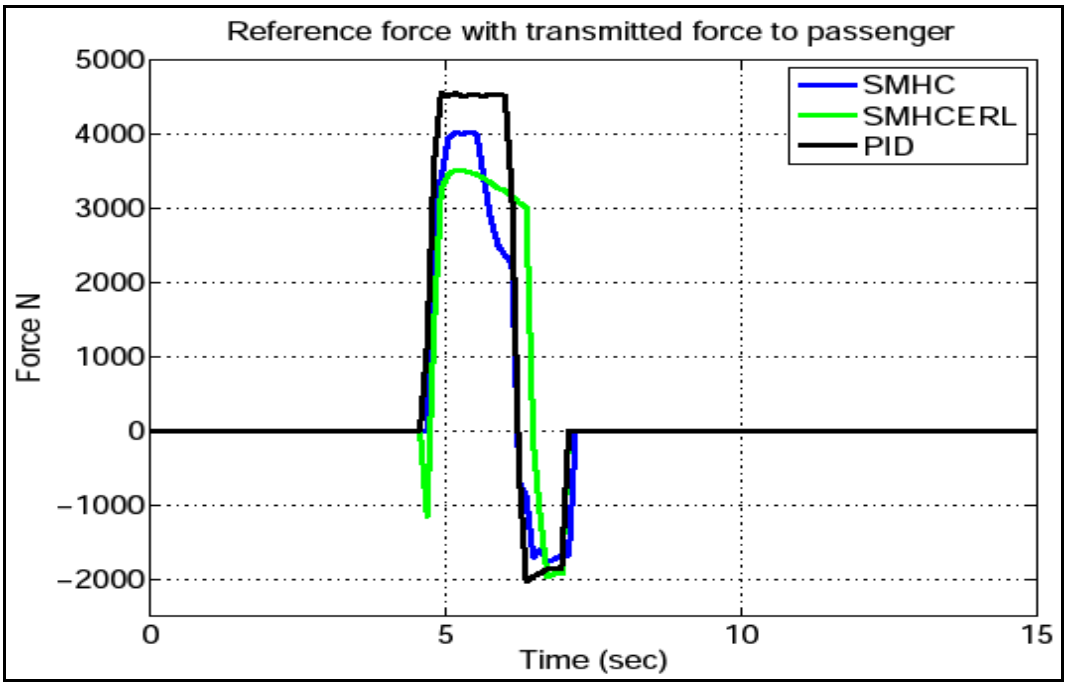

Figure 3.28 Force transmitted to passenger

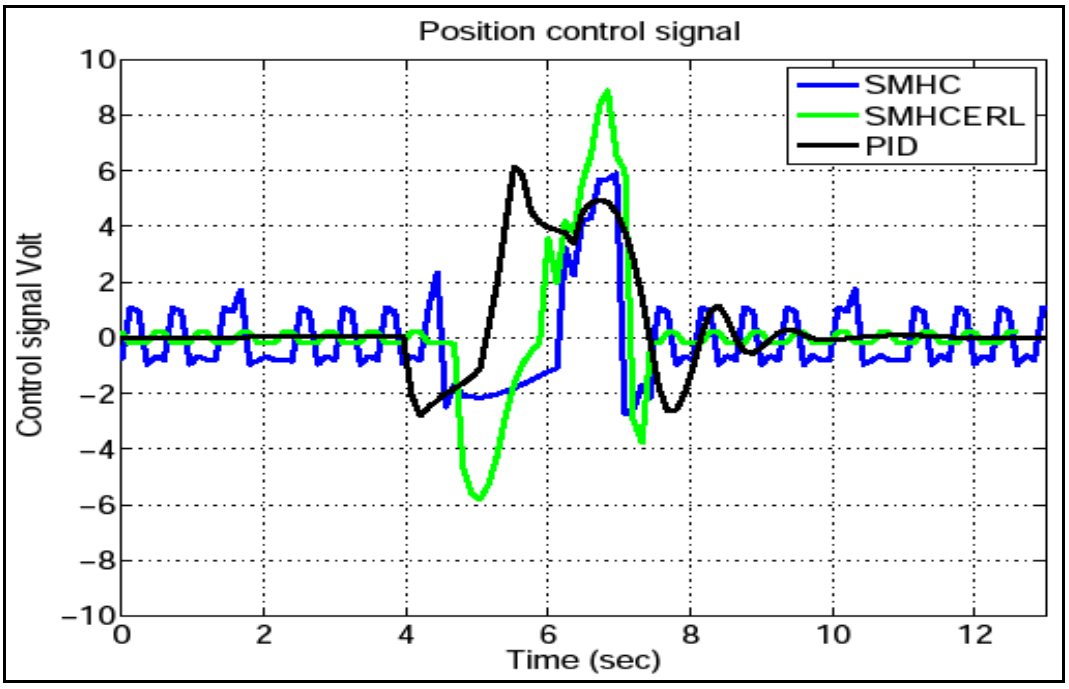

Figure 3.29 Control signal when SMPIDHCERL controllers, SMPIDHC without ERL and PID position controllers are applied

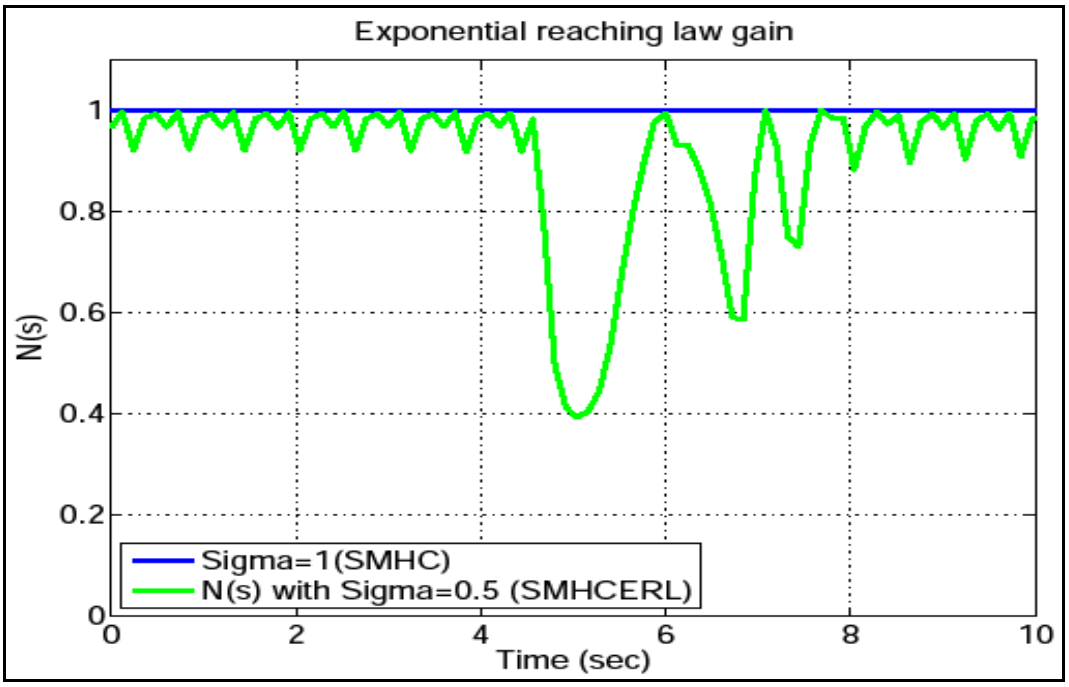

Figure 3.30 Exponential reaching law

3.6 Conclusion

This paper has presented a free chattering hybrid force/position controller for an electrohydraulic active suspension system. The proposed structure is tested and applied to suspension workbench in simulation and real time.

Achieving both good position tracking as well as good force tracking with separate position or force controllers is difficult. Thus, a hybrid force/position controller was developed and applied. Good force tracking was achieved with an attenuation of vertical seat perturbations. Using the proposed hybrid controller, the passenger seat was isolated from road irregularities. This combination was realized by two low-pass filters with variable gains. With a hybrid controller, two objectives were achieved by integrating the advantages of each controller (position, force). The chattering accompanying the control signal in the hybrid control was also removed by using an exponential reaching law.

A fuzzy logic controller was also used to change the filter's gains of an exponential reaching law based sliding mode hybrid controller. The fuzzy control was developed and based on the sliding position and force surfaces, which are relatively recent principles. The filter's gains improved the performance of the last controller. A frequency analysis for system variables has been conducted to evaluate the system response with the proposed controllers. In a future work, it will be worthwhile to consider different hybrid structures, different operating and loading conditions in real time validation.

CHAPITRE 4

REAL-TIME HYBRIDE CONTROL OF ELECTROHYDRAULIC ACTIVE SUSPENSION

Bassel Shaer[1], Jean-Pierre Kenné[1], Claude Kaddissi[1] and Honorine Angue Mintsa[2]

[1]*Département de Génie mécanique, École de technologie supérieure, 1100 rue Notre-Dame Ouest, Montreal QC H3C 1K3, Canada*
[2]*Département de Génie Électromécanique, École Polytechnique de Masuku, Franceville Gabon*

Article publié dans le journal «International Journal of Robust and Nonlinear Control», Juin 2017.

SUMMARY

Electrohydraulic actuators are an attractive choice for active suspension, because these systems provide a high power-to-weight ratio. However, their dynamics are highly non-linear. In addition, the use of one simple controller for both position and force is complicated, because there is a compromise between them in the case of active suspension. Most existing controllers do not efficiently fulfill the requirements, because only one state variable is considered.

In this paper, we address these problems by developing a new hybrid controller for both position and force, and implementing it in a real-time test bench. Our goal is to control the vertical position of the passenger seat while tracking the force transmitted to passengers and keeping it within tolerable and comfortable limits. Therefore, the proposed controller is a combination of two controllers. Its flexible structure redirects the control signal to control the proper controlled state-variable. The real-time results of the newly designed hybrid controller are compared to those obtained using a classical Proportional Integral Derivative (PID) controller, because this is the most widely used controller in the industry. As expected, the proposed controller demonstrates better performance in real-time operation.
Keywords: Real-time control, active suspension, hybrid control, position and force control, sliding mode control.

4.1 Introduction

An active suspension system is a system that allows for control of a vehicle's vertical position and softening of the force transmitted to passengers. Active suspension systems have become one of the most vigorous research subjects in recent years, as automobile manufacturers seek to improve ride quality and passenger comfort. Electrohydraulic systems have proven to be the ideal solution for active suspension systems, because the hydraulic components are already available in all vehicles. Having the proper active suspension system rewards drivers and passengers with improved safety, better road handling and more comfort. Considering the non-linearity of the system and the non-differentiability within the mathematical model, controlling electrohydraulic active suspension is a significant challenge. Active suspension control is approached by researchers as force control, position control or both. Some works are designed to limit the acceleration and suspension travel of active suspension systems. These works cannot be considered either force control or position control, because they do not track force or position references.

As in the work of [1], the objective of the controller is to prevent suspension travel from reaching its limits. Suspension travel is controlled through backstepping, in which a variable-bandwidth filter is used to change the stiffness setting of an active suspension system. The bandwidth filter is used with one state variable to change other system parameters. The controller shifts between its conflicting priorities, such as ride quality and suspension travel, in order to allow only a limited increase in the vertical acceleration of the vehicle.

Force control is usually presented as pressure control or acceleration control. In [2], a Lyapunov function with a variable gain is suggested in order to construct a control law. Tuning this gain allows the system control to be extended to a wide range. Although the Lyapunov theory guarantees stability, the performance is limited outside of the equilibrium points. This has led researchers to develop a hybrid serial controller, in which the inner loop is used to track a reference force that is produced by the outer loop [3]. The performance of this controller is

good in the case of force tracking, but not adequate for the vertical displacement of the car body.

In general, the structure of a hybrid control is limited by the capacity of the hydraulic elements. In light of this, [4] attempted to combine a pressure and flow rate feedback. The pressure control is used in an outer loop and the flow rate control is used in an inner loop to decrease the reciprocal action between them. Two control signals are issued from the controller to track both pressure and flow at the same time. This control strategy achieved the desired tunneling performance. Similarly, another structure consisting of four loops is suggested by [5], which focuses on a novel method for a real-time hybrid force controller, in which the dynamic system is regulated through the feedback loops. Only low-frequency perturbations are suppressed.

In order to achieve improved force control within a servo-hydraulic press system, [6] combined a relief valve and a flow servovalve as the control actuator. The fuzzy logic controller achieved very good force control within the imposed limits. The control methods used in force control, such as simple controllers, hydraulic element control and hybrid controllers, are also applied in the same way in position control.

Due to the stringent requirement for high-precision positioning, position control represents a challenge in electrohydraulic systems. The early control strategies used in [7] developed a time-scale separation and input decoupling transformation for the rear and front suspension forces in a 4-DOF active suspension system. Low- and high-pass filters were used in the inner loops to reduce the perturbations forces, while the pitch and heave displacements were controlled and rendered stable by the outer loops. The simulation results demonstrated inadequate damping for frequencies higher than the wheel frequency.

As with most controllers, the position controller can be integrated using adaptive methods. This is the area of position controller development where the parameters are estimated or tuned in order to achieve better performance. Adaptive methods are crucial, because they update the

controller with the proper values for the system parameters. Parameter uncertainty in electrohydraulic systems is mainly due to high operating temperatures and pressures.
In order to resolve this problem, [8] used a universe self-adjustment with a fuzzy-PID controller to control the electrohydraulic servo system position within a steam turbine governor and to suppress chattering. Position controller development reached a new level in the work of [9], which integrated two parallel controllers to form a hybrid controller. The transition between these two controllers was accomplished using a switch, where the position error is primordial in the transition process. The switch flips between controllers when the error exceeds a set point error.

In general, most researchers suggest solutions that range from simple controllers to adaptive controllers to hybrid controllers. The addition of special parameters to system models as variables is one of the aspects that are applied when controlling the position of electrohydraulic systems [10]. The idea of using an adaptive technique is extended to hybrid controllers. Therefore, [11] suggested a hybrid fuzzy-PID controller with coupled rules for positioning a hydraulic system. The controller achieved position control with a relatively fast response time accompanied by high force transmitted to passengers. In the case of the above-mentioned literature studies, the force controllers and position controllers are developed separately in order to track the force and the position successively.
Both controllers are supplied with adaptive methods in order to overcome the variation of parameters during operation.

Recently, the hybrid structure has entered into the scope of researchers. This refers to control structures where two or more controllers are combined to track multiple variables at the same time. In applications involving electrohydraulic systems, where position and force control are of equal importance, hybrid controllers have proven to be more efficient and produce better results.
In this field, [12] developed three control laws for force/position control for an electrohydraulic servo system using the backstepping technique. Other researchers, including [13], used two independent gains to form a hybrid controller, with each of the controllers forming the hybrid

controller having its own fuzzy logic development. The control law is applied to a hydraulic press during three stages. During these phases, position and force control is achieved using fixed gain.

Although using such a fixed gain with a precise vision system produced good results, other researchers preferred to use variable gains in order to achieve faster response times with variable PID gains. This was accomplished by [9], who designed a hybrid controller for position tracking, with the controller divided into two layers. The upper layer is designed with a gain scheduling Takagie-Sugeno fuzzy logic controller, and the lower layer is designed with a fuzzy controller to control the locally linearized manipulator system.

In [14], the authors developed a quasi-sliding mode-based single-input fuzzy self-tuning decoupled fuzzy PI control for robot manipulators with uncertainty. In this sliding-mode-based controller, the switching law is removed and replaced by a PI fuzzy controller. The stability is then guaranteed in the sense of Lyapunov, and by doing so, there is no chattering, because the original cause of chattering is removed. The tuning process employs a varying output gain decoupled fuzzy proportional integral sliding mode control approach using an approximate line equation. The results are good for the position tracking of the robotic arm for every joint, but the perturbation should be slowly time-varying in order to guarantee global asymptotic stability. The tuning process is complicated enough, because of the many controllers required for the tuning process, and it is not stable in the case of fast time-varying perturbations.

Using variable gains might produce good performance, but an adaptive control strategy becomes necessary when parameter uncertainty exists. This was achieved by [15], in which double loops were constructed with an online distribution rejection. The double-loop Auto Disturbances Rejection Control (ADRC) algorithm comprises three blocks: a transient block, an observer block, and finally, a block to calculate the control signal, which is a combination of the transient and estimated state-variables. In terms of control, the system is decoupled into two loops for position and force control. The ADRC achieved robust, adaptive and accurate performance for both position control and force control.

Despite all of the control theories for controlling both force and position in electrohydraulic systems, the main idea of decoupling a control structure is widespread in the control field.
This was recently accomplished by [16], in which two parallel hybrid control diagrams were built in order to create a force/position control, with the adaptive controllers considered with variables gains. The position controller is a proportional derivative controller. On the parallel branches, a force controller is designed in the same manner, with force identification block. The force block is necessary in order to update the force model. With such a complex controller, the position is well tracked, but the force error becomes significant at higher frequencies.

In this paper, we present a hybrid force/position controller design and the real-time experiment for electrohydraulic active suspension. The step-by-step design of this hybrid controller demonstrates the importance of the individual force and position controllers. The objective of the filter for the hybrid structure is similar to the filter used in [1]. The difference is that our filter is used at the control-signal level (high layer), whereas the filter in [1] is used to change the system variables (low layer).

The objectives of the filter in a hybrid structure are to ensure a smooth transition between controllers and to filter the undesired high-frequency control signals. The hybrid structure that was developed features the flexibility of integrating linear and non-linear controllers for either the position controller or the force controller. We began using the sliding mode technique as a non-linear position controller, due to its robustness. In Section 4.5.2, it is replaced by a Proportional-Integral-Derivative (PID) controller in order to form a classical hybrid controller of PID controllers. By doing so, we were able to test the efficiency of using non-linear and linear controllers in the proposed structure.
This is more difficult to achieve in the case of the force controller, because the force undergoes sharp changes, especially when the actuator changes the direction of movement. The force reference is chosen as a skyhook damping force, and therefore, a PID controller is used for force tracking. The objective of the hybrid controller is to find a compromise between keeping

the vertical motion of the vehicle's body near zero and reducing the force transmitted to passengers to a minimum, because one is accomplished to the detriment of the other.

Achieving both objectives is crucial, and by using a hybrid structure, we are able to achieve excellent performance. The hybrid controller achieves this compromise thanks to two low-pass filters. Depending on which controller is activated, the hybrid controller delivers the appropriate control signal, which then forces the actuator to fulfill the requirements in terms of force and/or position. The hybrid controller structure resolves the problem of coupling two controllers through the possibility of tuning the filter parameters. In addition, this structure can use classical controllers, such as PID or non-linear controllers, which gives the controller more flexibility in terms of integrating all types of controllers.

The designed hybrid controller is achieved through the following three steps, which constitute our main contribution to the field:

1- A sliding mode position controller is constructed and validated in order to isolate the vehicle from road perturbations.
   1.1- A recently developed algorithm for reducing chattering is integrated into the sliding mode controller to test how a new exponential reaching law (ERL) [17] can influence the famous sliding mode problem.
   1.2- The SMC controller is replaced with a PID controller in order to prove that the hybrid structure can include linear controllers and non-linear controllers.
2- A PID force controller is developed separately in order to track a skyhook reference force. The force transmitted to passengers is reduced to standard values. Ride quality is improved at this level.
3- Finally, the contribution represented by the hybrid controller structure is tested in real time using the controllers developed in Step 1 and 2, in order to verify the validity of the approach and to achieve efficient force and position tracking. Therefore, a sliding mode hybrid controller (SMPIDHC) and a PID hybrid controller (PIDHC) are used to achieve hybrid position and force tracking.

The paper is organized as follows:
Section 4.2 describes our motivation for applying the proposed controller in real time. In Section 4.3, we demonstrate the electrohydraulic active suspension workbench that was used in the real-time tests. The modeling of the electrohydraulic workbench is presented in Section 4.4. In Section 4.5, we present the controller design. In this section, we developed and applied the sliding mode hybrid controller. An exponential reaching law was tested as a new technique for removing the chattering caused by the SMC controller. Also in Section 4.5, we achieve best force tracking with minimum position error by developing PID hybrid controllers for force and position. Finally, we conclude with a summary of the results and future work.

4.2 Motivation

In the automobile industry, electrohydraulic systems are essential for passenger comfort and road handling while driving. For this reason, a compromise is requited between passenger comfort and road handling, regardless of the control strategy, because one is improved to the detriment of the other. Electrohydraulic systems are known to be highly non-linear and non-differentiable due to their non-linear components, and therefore, robust and efficient controllers for these systems should be designed in such a way as to handle these aspects – for example, by using the non-linearity to increase the stability of the system instead of eliminating it, as in classical controllers.

This paper is an extension of our previous work [18], in which the simulation demonstrates that the hybrid controller can track a desired force while maintaining the position of the passenger seat near an initial value. This has motivated us to validate this hybrid controller on a hydraulic active suspension system, and to test the effectiveness of the chattering suppression through an exponential reaching law [17] integrated into the sliding mode control.

The workbench that is presented in Figure 4.1 is missing some elements in terms of becoming an electrohydraulic active suspension system, which is why there will be a discussion (Section 4.4) pertaining to how to develop the workbench model when certain elements are missing. The PID hybrid controllers are developed for position control as well as for force control and

integrated into a hybrid structure. PID controllers are in widespread use in the industry, and therefore, PID hybrid controllers are more likely to be applied within embedded systems.

4.3 Description of the electrohydraulic active suspension workbench

Figure 4.1 shows the electrohydraulic active suspension workbench that is being studied. Figure 4.2 presents a functional diagram for the workbench. A hydraulic pump driven by an electric motor feeds three electrohydraulic servovalves with oil that is stored in the tank. Servovalve 1 is used to drive the cylinder that represents road disturbances. Servovalve 2 is connected to Cylinder 2, which controls the active suspension. Servovalve 3 is connected to Cylinder 3, which represents the weight of the passengers and the load. The relief valve limits the maximum pressure in the system. A Linear Variable Differential Transformer (LVDT) is installed on Cylinder 2 to measure its linear position. Two pressures sensors are used for the two chambers of Cylinder 2.

The acquisition I/O card (National Instrument NI PCI 6014) reads signals from the sensors and transmits the control signal to the servovalves. This is a low-cost 200 kS/s, 16-Bit, 16-analog input multifunction data acquisition (DAQ) card. The signals that are acquired include pressures p1 and p2, the vertical position of the passenger seat (sprung mass) x1 and the tire position (unsprung mass) x3.

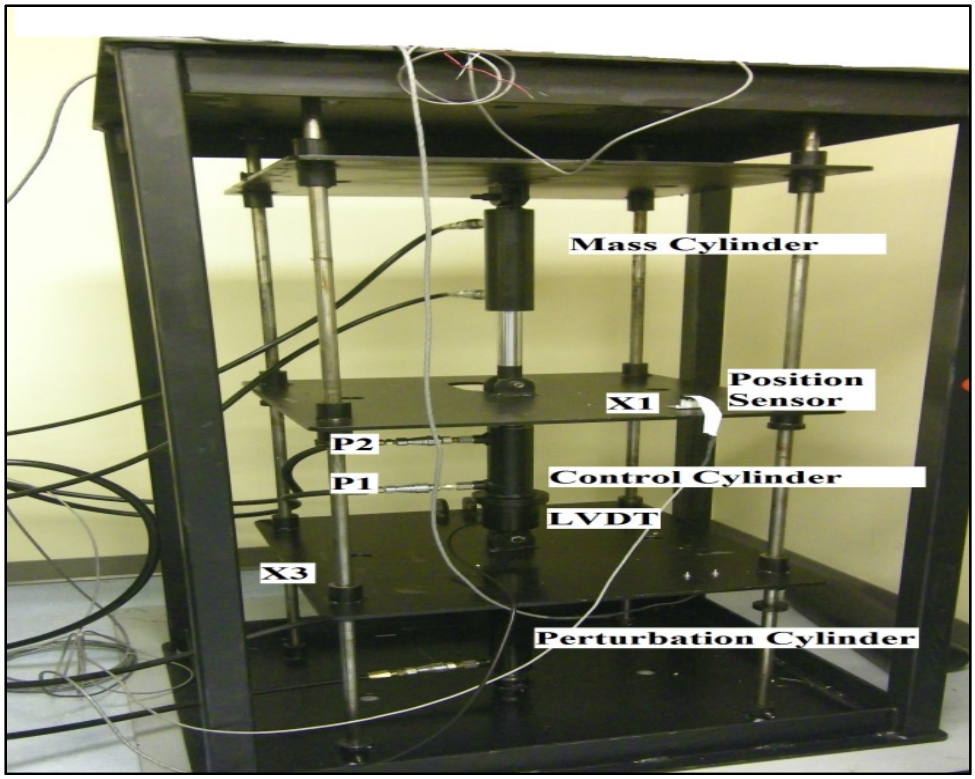

Figure 4.1 Active suspension workbench

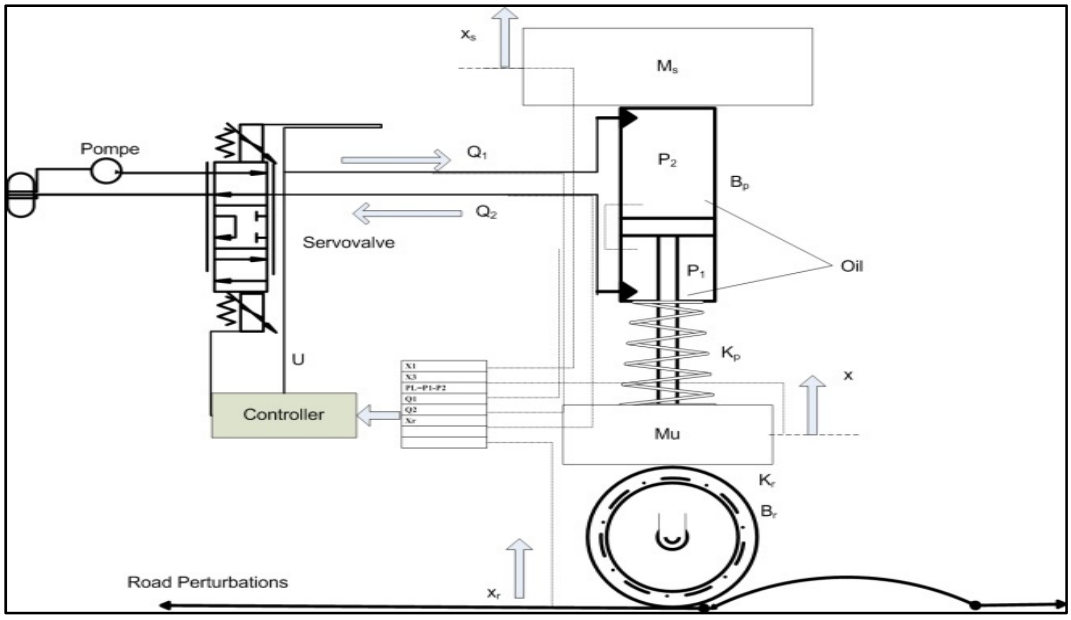

Figure 4.2 Active suspension schema

4.4 Dynamic model of the electrohydraulic active suspension system

In this section, we develop the mathematical model of the system in the state-space form. The relationship between the spool servovalve position $x_v(t)$ and the input control $u(t)$ is approximated by a first-order transfer function, where τ and k represent the time constant and the amplifier gain, respectively.

$$\dot{x}_v = \frac{1}{\tau}(-x_v + ku) \tag{4.1}$$

The expression of the flow across the servovalve, assuming symmetrical and matched orifices with minor leakage, is given by:

$$Q_1 = Q_2 = C_d x_v \sqrt{\frac{P_s - P_L * sigm(x_v)}{\rho}} \tag{4.2}$$

Where $P_L = P_1 - P_2$ is the load pressure differential, P_1 and P_2 are the pressures in the piston chambers, C_d is the flow discharge coefficient and ρ is the fluid mass density. The sign function represents the change in the fluid flow direction across the servovalve. This sign function is approximated to a sigmoid function, which is a differentiable function, in order to avoid numerical simulation problems, as suggested in [19]. The sigmoid function is defined as: $sigm(x_v) = \frac{1-e^{-\alpha x_v}}{1+e^{-\alpha x_v}}$

$$sigm\,(x_v) = \frac{1 - e^{-\alpha x_v}}{1 + e^{-\alpha x_v}} \tag{4.3}$$

This gives us: $sigm(x) = \begin{cases} 1 & if\ ax \to \infty \\ 0 & if\ ax \to 0 \\ -1 & if\ ax \to -\infty \end{cases}$ and $\frac{d\,(sigm(ax_v))}{dt} = \frac{2\,ae^{-\alpha x_v}}{(1+e^{-\alpha x_v})^2}$

The fluid dynamics in the cylinder are represented by the continuity equation:

$$\dot{P}_L = \frac{2\beta}{V_0}\left\{C_d x_v \sqrt{\frac{P_{s-}P_L * sigm(x_v)}{\rho}} - \mathrm{L} * P_L - A(\dot{x_s} - \dot{x})\right\} \tag{4.4}$$

The equations for the motion of the vehicle are found using Newton's second law (see Annexe II, Tableau-A II-1 for definition of the parameters):

$$\begin{aligned} M_s\ddot{x_s} = & -K_p\,(x_s - x) - B_p(\dot{x_s} - \dot{x}) + AP_L \\ M_u\ddot{x} = & K_p(x_s - x) + B_p(\dot{x_s} - \dot{x}) - k_r(x - x_r) \\ & -B_r(\dot{x} - \dot{x_r}) - AP_L \end{aligned} \tag{4.5}$$

The state variables are chosen as: $x_{1_{rt}} = x_s$, $x_{2_{rt}} = \dot{x}_s$, $x_{3_{rt}} = x_u$, $x_{4_{rt}} = \dot{x}_u$, $x_{5_{rt}} = P_L$, $x_{6_{rt}} = x_v$ and $x_{pert} = x_r$. This gives us the following state-space model, as in [19]:

$$\begin{aligned} \dot{x}_{1_{rt}} &= x_{2_{rt}} \\ \dot{x}_{2_{rt}} &= -a_0(x_{1_{rt}} - x_{3_{rt}}) - b_0(x_{2_{rt}} - x_{4_{rt}}) + a_1 x_{5_{rt}} \\ \dot{x}_{3_{rt}} &= x_{4_{rt}} \\ \dot{x}_{4_{rt}} &= d_0\left(x_{1_{rt}} - x_{3_{rt}}\right) + d_1\left(x_{2_{rt}} - x_{4_{rt}}\right) \\ &\quad -h_1\left(x_{3_{rt}} - x_{pert}\right) - b_1\left(x_{4_{rt}} - \dot{x}_{pert}\right) - c_1 x_{5_{rt}} \\ \dot{x}_{5_{rt}} &= \frac{J_1}{f(.)}\left(C_d\, x_{6_{rt}} g(.) + A(x_{4_{rt}} - x_{2_{rt}}) - L x_{5_{rt}}\right) \\ \dot{x}_{6_{rt}} &= \frac{1}{\tau}\left(-x_{6_{rt}} + k_{\mathrm{v}} u\right) \end{aligned} \tag{4.6}$$

Where:

$$a_0 = \frac{k_{\mathrm{p}}}{M_{\mathrm{s}}}, a_1 = \frac{\mathrm{A}}{M_{\mathrm{s}}}, b_0 = \frac{B_{\mathrm{p}}}{M_{\mathrm{u}}}, b_1 = \frac{B_{\mathrm{r}}}{M_{\mathrm{u}}}, c_1 = \frac{\mathrm{A}}{M_{\mathrm{u}}}.$$

$$d_0 = \frac{k_{\mathrm{p}}}{M_{\mathrm{u}}}, d_1 = \frac{B_{\mathrm{p}}}{M_{\mathrm{u}}}, h_1 = \frac{K_{\mathrm{r}}}{M_{\mathrm{u}}}.$$

As depicted in Figure 4.1, there are no springs in the electrohydraulic active suspension workbench that would make it an active suspension system, as shown in the schema in

Figure 4.2. The spring dynamics from the simulation complete the mathematical model for the electrohydraulic workbench, thus forming the hybrid structure of the electrohydraulic active suspension system. In order to remedy this problem, we integrated the workbench used in the simulation with the real workbench to form a hybrid workbench. Therefore, the hybrid workbench is composed of the hydraulic workbench and virtual springs.

The virtual springs reinforce the sliding mode control law and make it possible to apply it to the real hydraulic workbench. In other words, the control law that was developed for the ideal workbench is applied, because it is applied to the real hydraulic workbench without any modifications. The flexibility offered by this technique can be applied when certain elements are missing in real applications. With no springs installed, we propose: $a_0 = 0, d_0 = 0, h_1 = 0$. Replacing a_0, d_0, h_1 in (4.6) we get:

$$\begin{aligned}
\dot{x}_{1_{rt}} &= x_{2_{rt}} \\
\dot{x}_{2_{rt}} &= -b_0(x_{2_{rt}} - x_{4_{rt}}) + a_1 x_{5_{rt}} \\
\dot{x}_{3_{rt}} &= x_{4_{rt}} \\
\dot{x}_{4_{rt}} &= d_1\left(x_{2_{rt}} - x_{4_{rt}}\right) - c_1 x_{5_{rt}} \\
\dot{x}_{5_{rt}} &= \frac{J_1}{f(.)}\left(C_d\, x_{6_{rt}} g(.) + A(x_{4_{rt}} - x_{2_{rt}}) - L x_{5_{rt}}\right) \\
\dot{x}_{6_{rt}} &= \frac{1}{\tau}\left(-x_{6_{rt}} + k_{\mathrm{v}} u\right)
\end{aligned} \tag{4.7}$$

Where $x_{i_{rt}}$and $\dot{x}_{i_{rt}}$ represent the acquired sensor signals and their derivatives, while variable x_6 is estimated in Section 4.5. The derivatives of acquired signals are calculated using the system equations in (4.8), because the repetitive derivation of a variable adds considerable noise to the control signal, which would degrade the controller performance. This development is introduced in order to compensate for the missing elements in the hydraulic stations.

In Section 4.5.1, we will use the complete model in simulation to calculate the control law [18]. The terms $-a_0\left(x_{1_{rt}} - x_{3_{rt}}\right)$ and $d_0\left(x_{1_{rt}} - x_{3_{rt}}\right)$ are added to the derivative $\dot{x}_{2_{rt}}$, $\dot{x}_{4_{rt}}$

in order to model virtual springs. The constants $a_0$and $d_0$are chosen in such a way as to model the stiffness of virtual springs installed between the masses, as in Figure 4.2. The road level is the reference used for tire position and passenger seat position. We do not measure x_{pert}, but the term $h_1(x_{3_{rt}} - x_{pert})$ is considered to be a constant that is approximately near to zero $h_1(x_{3_{rt}} - x_{pert}) \approx 0$.

In light of this, we will not add the perturbations to the development of the control law. We also considered the initial value of all parameters to be equal to zero. Finally, the state-variables can be expressed by the intermediate variables $\dot{x}_{im}$:

$$\begin{Bmatrix} \dot{x}_{1m} \\ \dot{x}_{2m} \\ \dot{x}_{3m} \\ \dot{x}_{4m} \\ \dot{x}_{5m} \\ \dot{x}_{6m} \end{Bmatrix} = \begin{Bmatrix} \dot{x}_{1_{rt}} \\ \dot{x}_{2_{rt}} \\ \dot{x}_{3_{rt}} \\ \dot{x}_{4_{rt}} \\ \dot{x}_{5_{rt}} \\ \dot{x}_{6_{rt}} \end{Bmatrix} + Virtual\ springs \quad \Longrightarrow \text{ This gives:}$$

$$\begin{aligned} \dot{x}_{1m} &= \dot{x}_{1_{rt}} = x_{2_{rt}} \\ \dot{x}_{2m} &= \dot{x}_{2_{rt}} - a_0(x_{1_{rt}} - x_{3_{rt}}) \\ \dot{x}_{3m} &= \dot{x}_{3_{rt}} \\ \dot{x}_{4m} &= \dot{x}_{4_{rt}} + d_0\,(x_{1_{rt}} - x_{3_{rt}}) \\ \dot{x}_{5m} &= \dot{x}_{5_{rt}} \\ \dot{x}_{6m} &= \dot{x}_{6_{rt}} \end{aligned} \tag{4.8}$$

At this point, a variable change is required in order to include the suspension deflection and to lighten the system model. The new state-variables are:

$$y_1 = x_{1_m}, y_2 = x_{2_m}, y_3 = x_{1_m} - x_{3_m}, y_4 = x_{2_m} - x_{4_m}, y_5 = x_{5_m}, \\ y_6 = x_{6_m} \tag{4.9}$$

Replacing (4.8) and (4.9) in (4.7), we get:

$$\dot{y}_1 = y_2 \tag{4.10}$$

$$\dot{y_3} = y_4$$
$$\dot{y_4} = -A_1\, y_3 - A_2 y_4 + A_3 y_5 + b_1 \dot{y_r} + h_1 y_r$$
$$\dot{y_5} = \frac{J_1}{f(.)}(-A y_4 - L y_5 - C_d\, y_6 g(.))$$
$$\dot{y_6} = \frac{1}{\tau}(-y_6 + ku)$$

4.5 Controller design

In this section, we developed two essential hybrid controllers, namely the sliding mode PID hybrid controller (SMPIDHC) and the PID hybrid controller (PIDHC). These controllers comprise both position and force controllers.

In the SMPIDHC controller in Section 4.5.1, a sliding mode controller for position control and a force PID controller are integrated to achieve force and position tracking. In the PIDHC controller in Section 4.5.2, a position PID controller and a force PID controller are integrated to achieve force and position tracking.

4.5.1 Sliding mode PID hybrid control

The hybrid control is built using two parallel controllers (Figure 4.3). The sliding mode controller is the essential controller in this structure. The other controller is a classical PID (Figure 4.4). The combination of these controllers is called a sliding mode PID hybrid controller (SMPIDHC). This hybrid controller is designed for position control. Figure 4.3 shows the hybrid controller with its two loops.

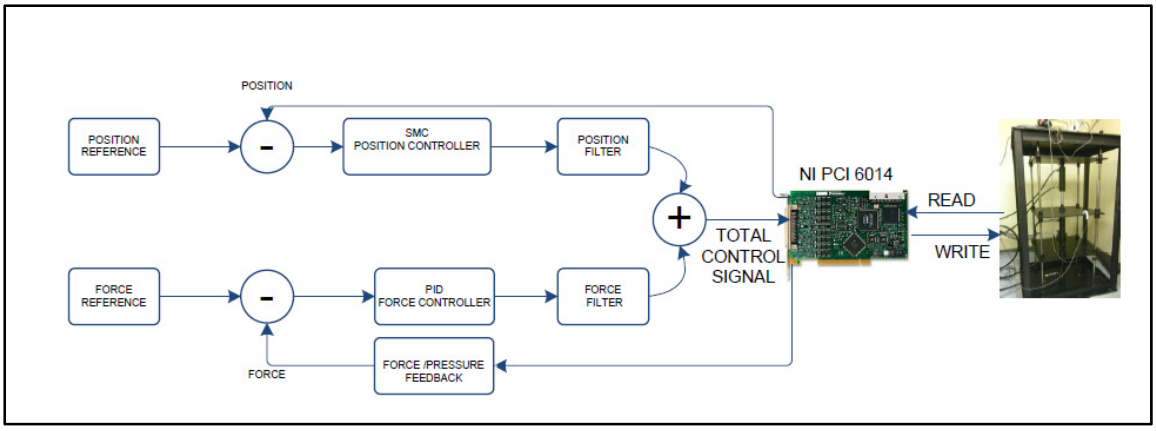

Figure 4.3 SMPID controller schema

The first loop is the position control loop, where a sliding mode controller is used for position control. The desired vertical position of the passenger seat is zero (i.e.: the rest position). The objective of the position controller (SMC) is to keep the passenger seat at this desired position, regardless of road perturbations. The second PID control loop is built as a force control loop, where its filtered output U_{f_f} is added to the total control U to create a hybrid control.

The reference force to be tracked by the PID force control is a skyhook damping force [20]. The structure of the controller overcomes the existing structures due to its flexibility of control, which is provided by the integration of two filters that can attenuate or magnify the control signals, as needed. In real-time control, this requires dealing with sampling frequencies, signal treatment and delay issues. The filters that have been chosen are low-pass filters, where $\frac{k_i}{s+p_i}$ is the transfer function. The control signal for the hybrid control is the sum of filtered outputs from both position and force controllers:

$$U_{tot} = U_{Lpf_p} + U_{Lpf_f}$$

The filtered outputs U_{Lpf_p} and U_{Lpf_f} are used for the position and force controllers respectively, and are described as follows:

$$U_{Lpf_p} = \frac{k_1}{s + p_1} * U_{P_{SMC}}$$
$$U_{Lpf_f} = \frac{k_2}{s + p_2} * U_{f_{PID}} \quad (4.11)$$

$U_{P_{SMC}}$and $U_{f_{PID}}$represent the position controller and force controller outputs, respectively. The low-pass filters are discretized as in [21, 22], giving us the following equation (4.11):

$$y_k = K\alpha x_k + (1 - \alpha)y_{k-1} \quad (4.12)$$

Where:

y_k is the discrete output (U_{Lpf_p} or U_{Lpf_f}).

x_k is the discrete input ($U_{P_{SMC}}$or $U_{f_{PID}}$).

k is the discrete time index.

Where:

$\alpha = \frac{f_{lp}}{f_{ls}+f_{lp}}$ is the smoothing factor, which should be $0 < \alpha < 1$.

$K = \frac{k_i}{p_i}$ is the filter gain.

f_{lp} is the frequency of loop execution in our real-time program.

f_{ls} is the sampling frequency.

The discretization is applied to both filters, giving discretized position and force controller outputs of:

$$U_{p_k} = U_{Lpf_p}$$
$$U_{f_k} = U_{Lpf_f} \quad (4.13)$$

Replacing (4.11) and (4.13) in (4.12), we get the discrete equations for the filters:

$$y_{p_{k+1}} = K_p \alpha_p U_{p_k} + \left(1 - \alpha_p\right) * y_{p_k}$$
$$y_{f_{k+1}} = K_f \alpha_f U_{f_k} + \left(1 - \alpha_f\right) * y_{f_k} \tag{4.14}$$

This gives the discrete total control signal as follows:

$$U_{tot} = y_{p_{k+1}} + y_{f_{k+1}} \tag{4.15}$$

The control law for sliding mode position controller $U_{P_{SMC}}$ is developed in the following equations. The $U_{f_{SMC}}$ is developed in the same manner:

From (4.10), we calculate the sliding surface S:

$$S = c_1 y_1 + c_2 \dot{y_1} + c_3 \ddot{y_1} + c_4 \dddot{y_1} \tag{4.16}$$

We then calculate the derivative of y_1 for use in (4.16):

$$\begin{aligned}
\dot{y_1} &= y_2 \\
\ddot{y}_1 &= \dot{y_2} = -a_0 y_3 - b_0 y_4 + a_1 y_5 \\
\dddot{y_1} &= \ddot{y_2} = -a_0 \dot{y_3} - b_0 \dot{y_4} + a_1 \dot{y_5} \\
&= -a_0 y_4 - b_0 [-A_1 y_3 - A_2 y_4 + A_3 y_5] + \\
a_1 \tfrac{J_1}{f(.)} &[-A y_4 - L y_5 - \quad C_d y_6 g(.)] \\
&= b_0 A_1 y_3 - \left(a_0 - b_0 A_2 + a_1 \tfrac{J_1}{f(.)} A\right) y_4 + \\
&\left(-A_3 b_0 - a_1 L \tfrac{J_1}{f(.)}\right) y_5 \\
&- \frac{a_1 C_d J_1 g(.) y_6}{f(.)}
\end{aligned} \tag{4.17}$$

Replacing (4.17) in (4.16) gives us:

$$S = c_1 y_1 + c_2 y_2 + (-c_3 a_0 + c_4 b_0 A_1) y_3 - (c_4 a_0 + c_3 b_0 - c_4 b_0 A_2 \tag{4.18}$$

$$+\frac{c_4 a_1 J_1 A}{f(.)})\, y_4 - \left(A_3 b_0 c_4 - c_3 a_1 + \frac{c_4\, a_1\, J_1\, L}{f(.)}\right) * y_5$$
$$-\frac{c_4\, a_1\, C_d\, J_1\, g(.)}{f(.)}\, y_6$$

The reaching condition must be verified:

$$S\dot{S} < 0$$

The Lyapunov function derivative is strictly negative when the reaching condition is verified, or in other words, when the sliding surface S converges to zero.

Therefore, $\dot{S}$ is chosen in such a way as to satisfy (4.19):

$$\dot{S} = -K_{sw}\, sign(S) \tag{4.19}$$

$$\begin{aligned}\dot{S} = {} & c_1 y_2 + c_2 \dot{y_2} + (-c_3 a_0 + c_4 b_0 A_1)\dot{y_3} - (c_4 a_0 + c_3 b_0 - c_4 b_0 A_2)\dot{y_4} \\ & - c_4 a_1 J_1 A \frac{\dot{y_4} f(.) - y_4\, \dot{f(.)}}{f(.)^2} - (A_3 b_0 c_4 - c_3 a_1)\dot{y_5} \\ & - c_4 a_1 J_1 L \frac{\dot{y_5} f(.) - \dot{f(.)} y_5}{f(.)^2} \\ & - c_4 a_1 C_d J_1 \frac{\left[g(.)\left[\frac{1}{\tau}(-y_6 + kU_{P_{smc}})\right] + \dot{g(.)} y_6\right] f(.)}{f(.)^2} \\ & + c_4 a_1 C_d J_1 \frac{g(.) y_6 \dot{f(.)}}{f(.)^2} = -K_{sw}\, sign(S)\end{aligned} \tag{4.20}$$

The function $\dot{g(.)}$ is highly non-linear, which complicates the process of finding the control law:

$$g\dot{(.)} = \frac{1}{\sqrt{\rho}} * \frac{-\left[sigm(\dot{y_6})y_5 + sigm(y_6)\dot{y_5}\right]}{2\sqrt{P_s - sigm(y_6)y_5}}$$

$$= \frac{1}{\sqrt{\rho}} * \frac{-\left[\frac{2a_2e^{-a_2y_6}}{(1+e^{-a_2y_6})^2}\frac{y_5}{\tau}\left(-y_6 + kU_{P_{smc}}\right) + sigm(y_6)\dot{y_5}\right]}{2\sqrt{P_s - sigm(y_6)y_5}}$$

$$= \frac{\frac{2a_2e^{-a_2y_6}}{(1+e^{-a_2y_6})^2}\frac{y_5y_6}{\tau}}{2\sqrt{\rho(P_s - sigm(y_6)y_5)}} - \frac{\frac{2a_2e^{-a_2y_6}}{(1+e^{-a_2y_6})^2}\frac{ky_5}{\tau}}{2\sqrt{\rho(P_s - sigm(y_6)y_5)}}U_{P_{smc}}$$

$$- \frac{sigm(y_6)\dot{y_5}}{2\sqrt{\rho(P_s - sigm(y_6)y_5)}}$$

$$= H(.) - I(.) - J(.)U_{P_{smc}}$$

$H(.)$, $I(.)$ and $J(.)$ are given by:

$$H(.) = \frac{\frac{2a_2e^{-a_2y_6}}{(1+e^{-a_2y_6})^2}\frac{y_5y_6}{\tau}}{2\sqrt{\rho(P_s - sigm(y_6)y_5)}}$$

$$I(.) = \frac{sigm(y_6)\dot{y_5}}{2\sqrt{\rho(P_s - sigm(y_6)y_5)}}$$

$$J(.) = \frac{\frac{2a_2e^{-a_2y_6}}{(1+e^{-a_2y_6})^2}\frac{ky_5}{\tau}}{2\sqrt{\rho(P_s - sigm(y_6)y_5)}}$$

To simplify (4.20) we choose:

$$A_{41} = -c_4a_0 + c_3b_0 - c_4b_0A_2$$

$$A_{42} = A_3b_0c_4 - c_3a_1$$

So $\dot{S}$ becomes:

$$\dot{S} = c_1y_2 + c_2\dot{y_2} + (-c_3a_0 + c_4b_0A_1)\dot{y_3}$$

$$-A_{41}\dot{y_4} - c_4a_1J_1A\frac{\dot{y_4}\,f(.) - y_4\dot{f(.)}}{f(.)^2} - A_{42}\dot{y_5} - c_4a_1J_1L\frac{\dot{y_5}\,f(.) - \dot{f(.)}y_5}{f(.)^2} \qquad (4.21)$$

$$-c_4a_1C_dJ_1\frac{kg(.)f(.)U_{P_{smc}}}{\tau f(.)^2} - c_4a_1C_dJ_1\frac{y_6f(.)\left[H(.) - I(.) - J(.)U_{P_{smc}}\right]}{f(.)^2}$$

$$-c_4 a_1 C_d J_1 \frac{\frac{-y_6 f(.) g(.)}{\tau} - g(.) y_6 \dot{f}(.)}{f(.)^2} = -K_{sw}\, sign(S)$$

Rearranging (4.21) to get $U_{P_{SMC}}$ gives us:

$$\begin{aligned}
\dot{S} &= c_1 y_2 + c_2 \dot{y}_2 + (-c_3 a_0 + c_4 b_0 A_1)\dot{y}_3 - A_{41}\dot{y}_4 \\
&- c_4 a_1 J_1 A \frac{\dot{y}_4 f(.) - y_4 \dot{f}(.)}{f(.)^2} - c_4 a_1 J_1 L \frac{\dot{y}_5 f(.) - \dot{f}(.) y_5}{f(.)^2} \\
&- A_{42}\dot{y}_5 + c_4 a_1 C_d J_1 \left[-\frac{k g(.)}{\tau f(.)} + \frac{y_6 J(.)}{f(.)} \right] U_{P_{smc}} \\
&- c_4 a_1 C_d J_1 \frac{y_6 [H(.) - I(.)]}{f(.)} \\
&- c_4 a_1 C_d J_1 \frac{\frac{-y_6 f(.) g(.)}{\tau} - g(.) y_6 \dot{f}(.)}{f(.)^2} = -K_{sw} sign(S)
\end{aligned}$$

Finally:

$$\dot{S} = \eta + \mu \mathrm{U}_{\mathrm{psmc}} = -K_{sw} sign(s) \implies U_{P_{smc}} = -\frac{\eta}{\mu} - \frac{K_{sw}}{\mu} sign(s)$$

Therefore, the total control signal $U_{P_{smc}}$ for the position control is:

$$U_{P_{smc}} = U_{P_{eq}} + U_{P_{sw}} \Longrightarrow \begin{Bmatrix} U_{P_{eq}} = -\frac{\eta}{\mu} \\ U_{P_{sw}} = -\frac{K_{sw}}{\mu} sign(s) \end{Bmatrix} \qquad (4.22)$$

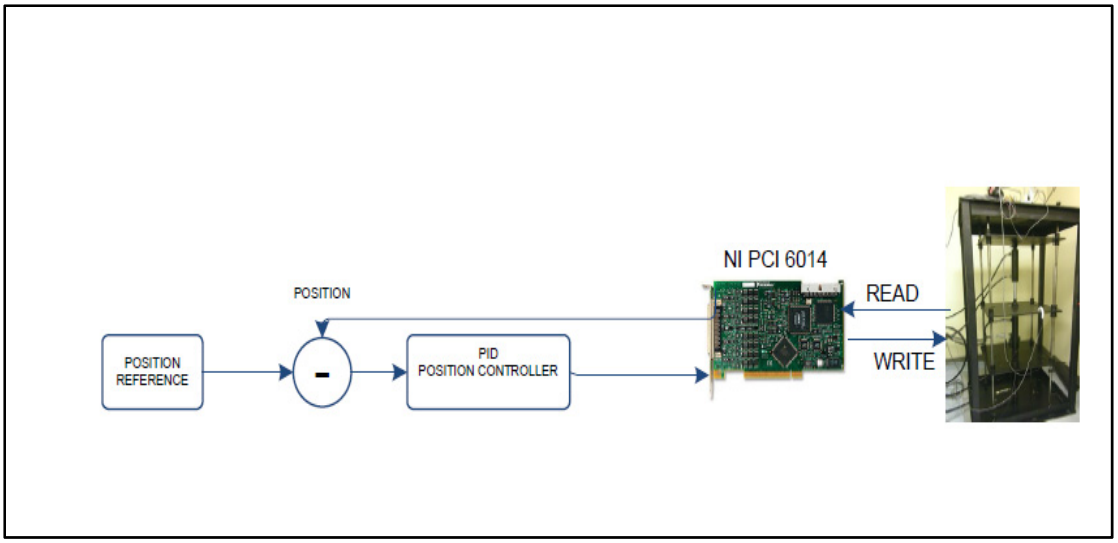

Figure 4.4 PID position controller schema

The PID control schema in Figure 4.4 represents a position controller. The position PID controller is used for comparison with the SMPIDHC controller. In Figure 4.5 (a), the position of the passenger seat has reached 3.3 cm with a perturbation of 5 cm. This represents a 34% improvement.

The force transmitted to passengers reached 4026 N with the SMPIDHC, which outperforms the PID (4553 N). This clearly demonstrates the performance and robustness of the SMPIDHC controller for position control. However, the SMPIDHC control signal is accompanied by chattering, which is inherent. This chattering could damage the hydraulic system and reduce the performance of the controller. It also provokes non-linear and undesirable terms in the system equations. In the next section, we will see how an exponential reaching law could solve the chattering issue.

4.5.1.1 Exponential reaching law sliding mode control

There are many sources of error in the real-time validation of the SMPIDHC controller in Section 4.5.1. As stated above with respect to the signals acquired from the workbench, the

flow Q and the spool valve position x_v are not measured directly, but are estimated from the mathematical model. We used the piston speed to estimate the flow Q.

$Q = V_1 * A$, the inflow for the extension phase.

$q = V_2 * (A - a)$, the inflow for the retraction phase.

Where:

A is the actuator piston area and a is the rod area.

V_1, $V_2$are the extension and retraction speeds, successively. This is calculated using the derivative of the vertical position of the passenger seat in real time.

$$V_1 = x_{2_{rt}} = \frac{\Delta x_1}{\Delta t} = \frac{x_{1_{rt_k}} - x_{1_{rt_{k-1}}}}{t_k - t_{k-1}}$$

Where: $\Delta t = 100\ ms$ is the loop period in labview. Therefore, the spool valve position is given by:

$$x_{v_{extending}} = \frac{Q}{C_d}\sqrt{\frac{\rho}{P_s - sign(V_1) * P_L}},\ x_{v_{retracting}} = \frac{q}{C_d}\sqrt{\frac{\rho}{P_s - sign(V_2) * P_L}}$$

The estimated value of x_v is:

$$\hat{x}_v = \begin{Bmatrix} x_{v_{extending}} & if & V_1 > 0 \\ -x_{v_{retracting}} & if & V_2 > 0 \end{Bmatrix}$$

The perturbations in masses at speeds $V_1$and V_2, due to derivations, yield to perturbations in the $\hat{x}_v$. Therefore, a chattering appears near zero speeds. Another chattering source is inherent in the sliding mode control, resulting from the switching control in conventional form (Figure 4.6 (a)):

$$\dot{S} = -K_{sw}\ sign(S)$$

Given that we have two chattering sources, a chattering removal strategy should beimplemented in order to improve the performance of the control. An exponential reaching law (ERL) for sliding mode control is suggested by [17] in order to reduce chattering and increase the reaching time. The comparison will be between the conventional reaching law and the ERL.

A sliding mode hybrid controller is applied with an ERL in order to verify the effectiveness of chattering suppression. The first test is conducted with a sliding mode PID hybrid controller with ERL, where: $N(S) = \delta_0 + (1 - \delta_0)e^{-\alpha|S|^p}$. The ERL is designed to be a generalized case of the conventional law. With the new law, $\dot{S}$ becomes:

$$\dot{S} = -\frac{k}{N(S)} sign(S) \text{ with} > 0 \ .$$

The second test is conducted with a sliding mode PID hybrid controller with the conventional reaching law (without ERL),
Where: $N(S) = 1$ or $\delta_0 = 1$.

The experimental results show that a reduction in chattering has been achieved with the ERL, but on the other hand, the new law made the system faster, with a reduction of 64.2%. The perturbations have been reduced from 5 cm to 1.768 cm, which is better than the other SMPIDHC (3.3 cm) (Figure 4.5 (a)). We can clearly see that the ERL removed most of these spikes, even if it did not eliminate the chattering entirely. However, the system response became smoother and more stable.

On the other hand, the transmitted force with the SMPIDHC (4026 N) is higher than with the SMPIDHCERL (3513 N) (Figure 4.5 (b)). This is normal, because the position controller with in the hybrid controller has a dominant role in the control process. This is attributed to the ERL which varies the switching gain (approaching law) in the total control signal, and therefore, the position error and the chattering are reduced (Figure 4.6 (a)).

Figure 4.6 (b) shows function $N(S)$, which is part of the switching gain. The higher the value of N(s), the larger the total control signals.

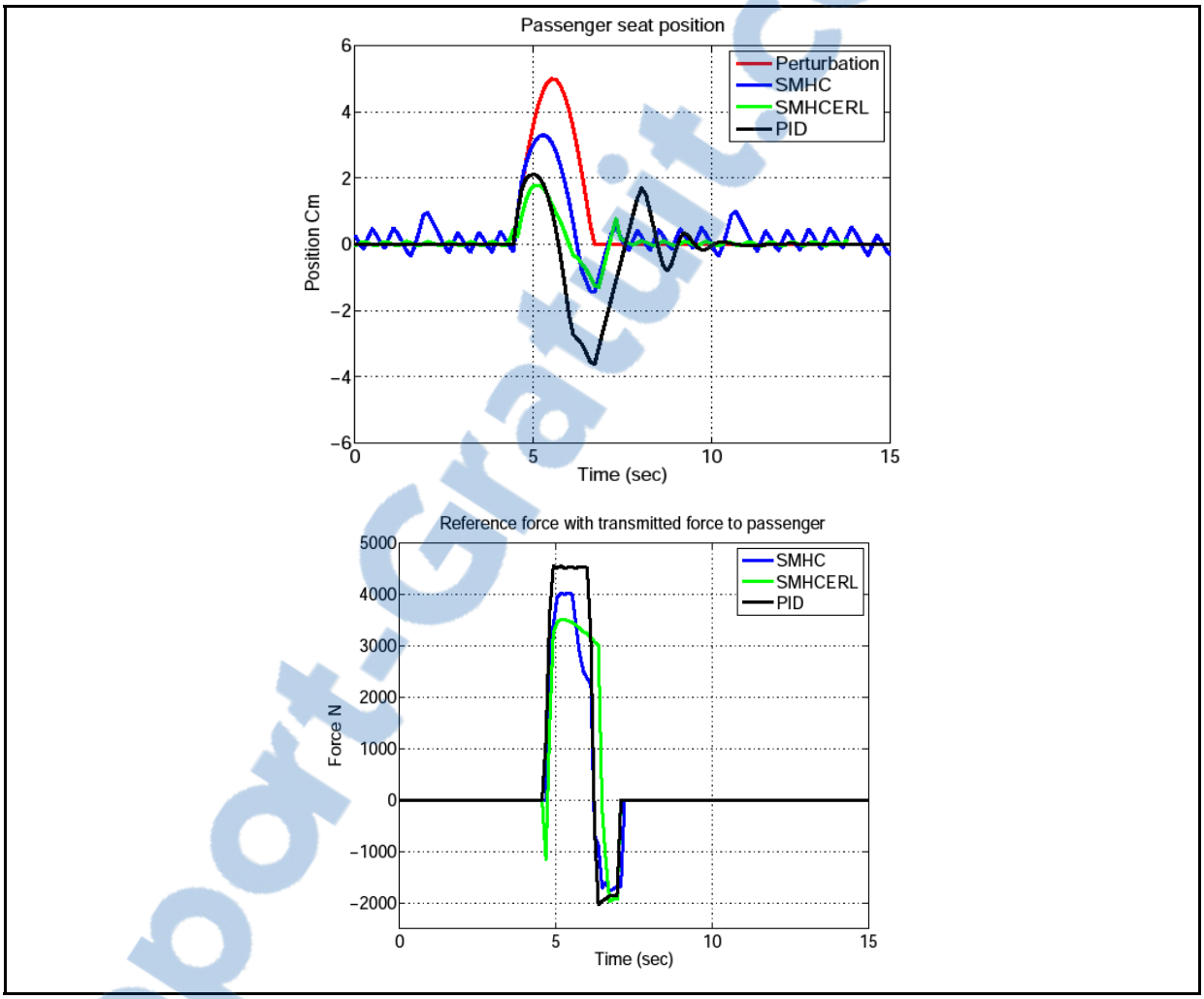

Figure 4.5 (a) Sprung mass position when SMPIDHCERL controllers, SMPIDHC without ERL and PID position controllers are applied (b) Force transmitted to passengers

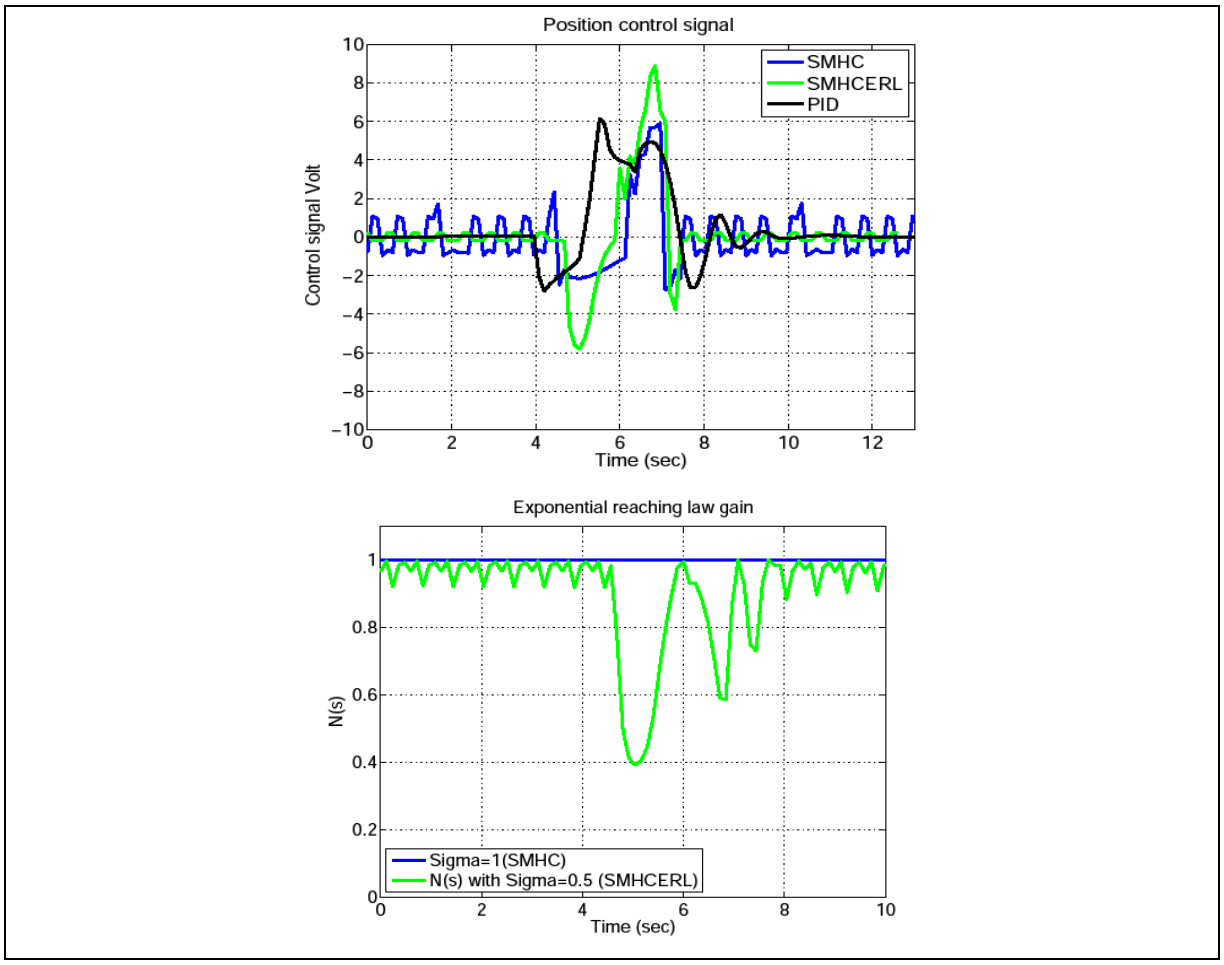

Figure 4.6 (a) Control signal when SMPIDHCERL controllers, SMPIDHC without ERL and PID position controllers are applied. (b) Exponential reaching law

4.5.2 PID hybrid controller

In this section, we develop a PID hybrid controller by tuning the filter parameters in the hybrid structure. To find the best filter parameters, we begin by tuning them to achieve the best performance in terms of the position of the passenger seat.

Secondly, we tune the parameters to achieve the best force tracking. Thirdly, in Section 4.5.2.3, we tune the parameters to achieve a compromised performance for position and force tracking. To find the best performance for both position and force, a compromise must be made between filter parameters (k_1, p_1) and (k_2, p_2).

The procedures are as follows:

1- Tune the parameters (k_1, p_1) and (k_2, p_2) in order to improve the vertical position of the passenger seat to maximum. In this step, force tracking will be degraded and the hybrid controller will be considered as a position controller.

2- Tune the parameters (k_1, p_1) and (k_2, p_2) in order to improve the force tracking to maximum. In this step, the vertical position of the passenger seat will be degraded, and the hybrid controller will be considered as force controller.

3- Find a compromise involving both pairs (k_1, p_1) and (k_2, p_2) in order to achieve the best results derived from the two previous steps. This step will determine the filter parameters to be used in the hybrid position and force controller.

4.5.1.2 Tuning the position control with the PID hybrid controller

As seen in the preceding section, the SMPIDHC controller produced good results, but the chattering, which influences the system performance, has led us to discuss this problem in this section, and to replace the SMC controller with a PID controller. Therefore, a PID hybrid controller (PIDHC) is built as a new controller in order to evaluate the impact of various controllers on overall performance. The schema in Figure 4.7 represents a hybrid controller with two PID controllers: the first is designed to keep the vertical position of the passenger seat at the desired (initial) position; whereas the other PID controller is designed to track a reference force signal.

The discretization equations are the same as in Section 4.5.1:

$$U_{Lpf_p} = \frac{k_1}{s + p_1} * U_{P_{PID}} \tag{4.23}$$

Where $U_{P_{PID}}$represents the output from the PID position controller.

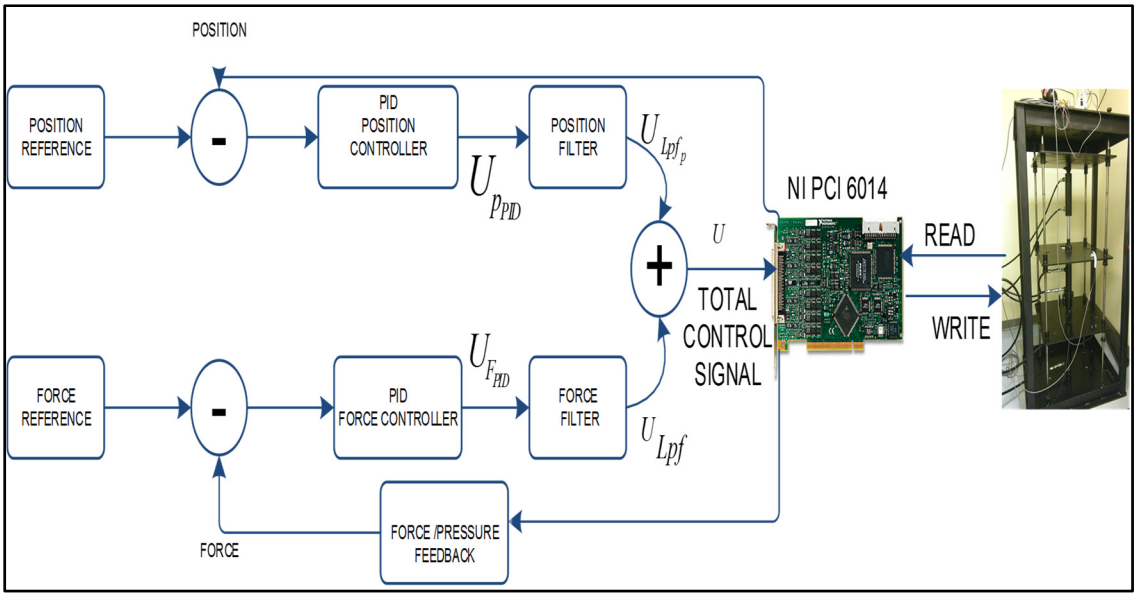

Figure 4.7 PID hybrid controller schema

It is evident that the parameters for the filters (k_1, p_1) and $(k_2, p_2)$are not the same for both controllers, and therefore, their discrete equivalent parameters are also different.

In Figure 4.8 (a), the PID hybrid controller reduced the position of the passenger seat to 2.3 cm with a perturbation signal of 5 cm, which is much better than 3.62 cm (PID).

The improvement with the PID hybrid controller (54%) is sufficiently significant in comparison with the PID controller (27.6%) to continue to use it for keeping the vertical seat position near zero.

As we see, the PIDHC doubled the performance and outperformed the PID position controller by isolating the position of the passenger seat with less force transmitted to passengers.

The PIDHC has a slightly lower force transmitted to passengers (4424 N) as compared to the PID (4553N) (Figure 4.8 (b)), which is too far from the skyhook force reference. Figure 4.9 (a) shows the control signal for both controllers. The PIDHC control signal is an oscillatory damped signal. Therefore, the workbench with PIDHC is considered to be an under-damped system, because the oscillations fade away.

In a detailed view, we see that this oscillatory form is attributed to the position control signal that brings the vertical position of the passenger seat to its initial state (position zero) (Figure 4.9 (b)).

At the final stage of perturbations (after 6 sec.), the total control signal for the PIDHC becomes the signal produced by the position controller. The filter's gain and phase for the position controller are $k_{p1} = 0.5$ and $\alpha_{p1} = 0.8$. The force controller filter parameters are $k_{f1} = 0.5$ and $\alpha_{f1} = 0.7$. As we can see, the same filter gains are used, but with different α_{p1} and α_{f1}, and the higher the value of α_{p1}or α_{f1}, the more the control identity is defined. Increasing α gives the corresponding controller priority when using the same filter gain. The parameter α has a significant influence on the filter phase, because it is based on sampling and filter frequencies.

As a result, in Figure 4.9 (b), the position control signal is seizing the overall performance. The question of the filter's influence on the other controlled variable, which in our case is force, is raised. In fact, the PIDHC control signal has reduced the transmitted force in comparison with the PID controller, due to the influence of the force filter output.

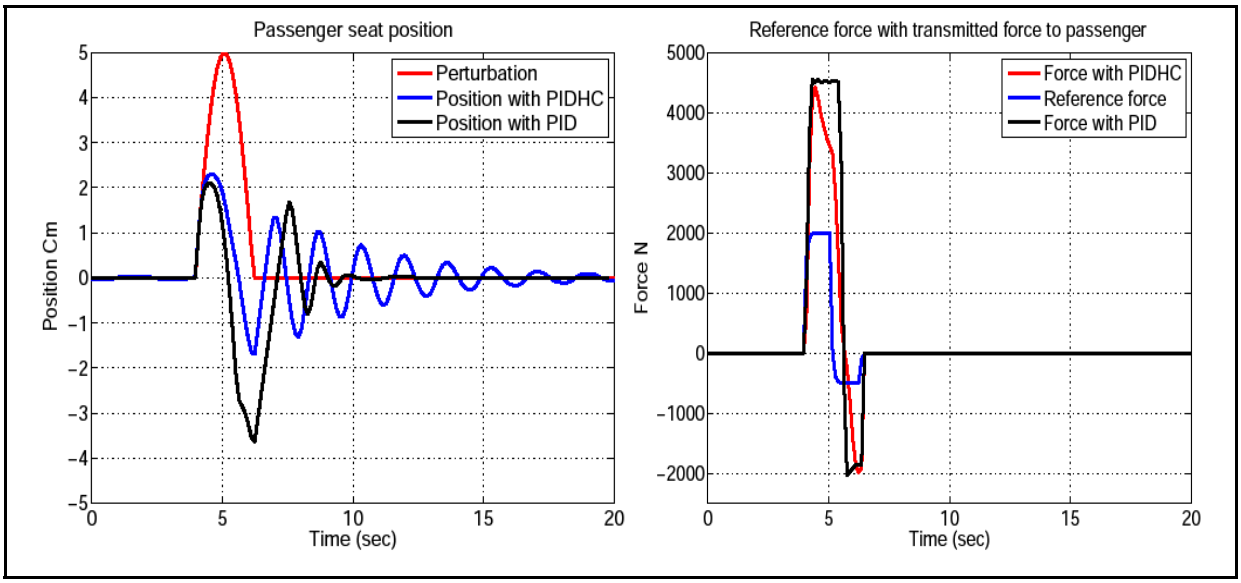

Figure 4.8 (a) Sprung mass position when PID and PIDHC position controllers are applied (b) Force transmitted to passengers

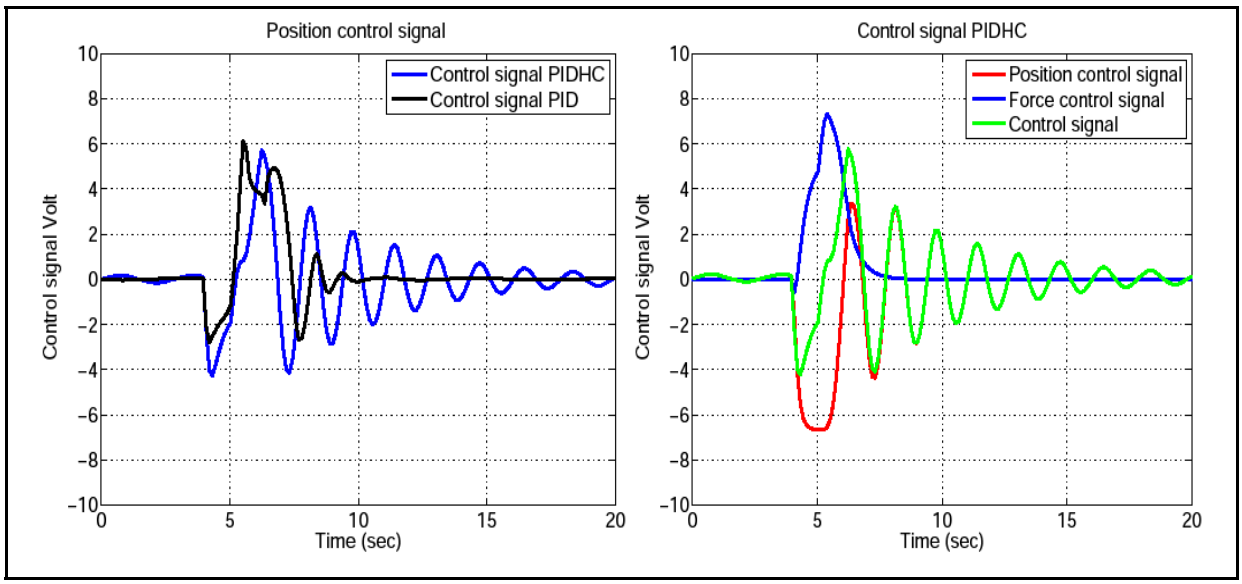

Figure 4.9 (a) Control signal when PID and PIDHC position controllers are applied (b) Control signals for PID controllers

4.5.1.3 Tuning the force control with the PID hybrid controller

The PID hybrid controller is tuned to achieve the best force tracking with the same structure illustrated in Figure 4.9. The parameters for the filter change the overall performance by making force tracking a priority and removing the position bias. Therefore, the parameters of the hybrid controller are chosen in such a way to fulfil two objectives: reduce the force error (force control) and force the passenger seat to return to its initial vertical position (position control). This is a different way of viewing a force controller by carrying out a new task, in addition to force tracking.

As a beginning, we have chosen a classical PID to achieve force tracking. The objective is to follow a reference force or a desired force. The tests in Figure 4.11 and Figure 4.12 were conducted in order to determine the best PID gains for developing a force control. These tests also show the position bias when tracking a reference force. In references [5, 20, 23, 24], they clearly demonstrate this position bias. In other words, when tracking a desired force, the

position of sprung mass is shifted gradually to hit one of its limits in non-symmetrical cylinders. Most works in the field of force control neglect the position bias, because it is not in their interest. In our proposed hybrid structure, we achieve force tracking while minimizing the position error to zero.

These gains will be used in the force control with the PID hybrid control. In the hybrid control, the reference force that was used is a skyhook damping force, which guarantees good ride quality. The PID gains are determined by trial and error in an effort to achieve the smallest possible tracking error $k_p = 0.00450, T_i = 0.001\ sec, T_d = 0.000054\ sec$. For this test, we applied a square signal with 60 sec as a reference. We chose a square signal in order to determine the best gains for tracking, which is not easy to do when using other references with small periods.

For the first part of test, which lasts less than 20 sec., the PID force controller follows the reference force with an overshoot with the gains of ($k_p = 0.00450, T_i = 0.001\ sec, T_d = 0.000054$ sec.) (Figure 4.11). For the second part of test, we have a smaller overshoot with the gains ($k_p = 0.00450, T_i = 0.005\ sec, T_d = 0.000054\ sec.$). When the integration time T_i, is increased, the overshoot becomes smaller. The force PID controller shows good tracking.

In Figure 4.12 (b), the position moves downward slightly with time, and after a while, the actuator will close completely due to the bias in seat position. This position bias has provoked the necessity of adding a position controller to keep the vertical position of the seat at a zero position when applying perturbations. The control signal in Figure 4.12 (a) also has a symmetric and square form. Therefore, considering its performance, we can use the PID as a force controller within the hybrid controller.

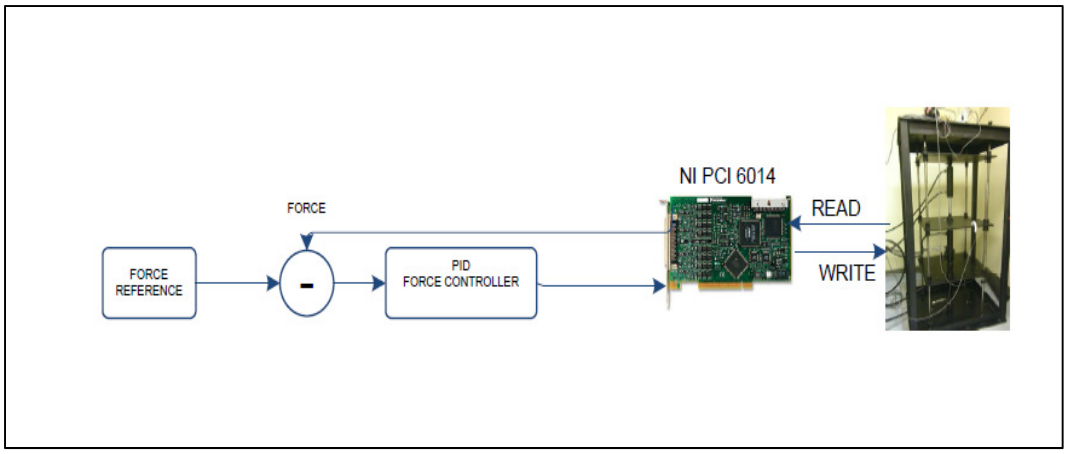

Figure 4.10 PID force controller schema

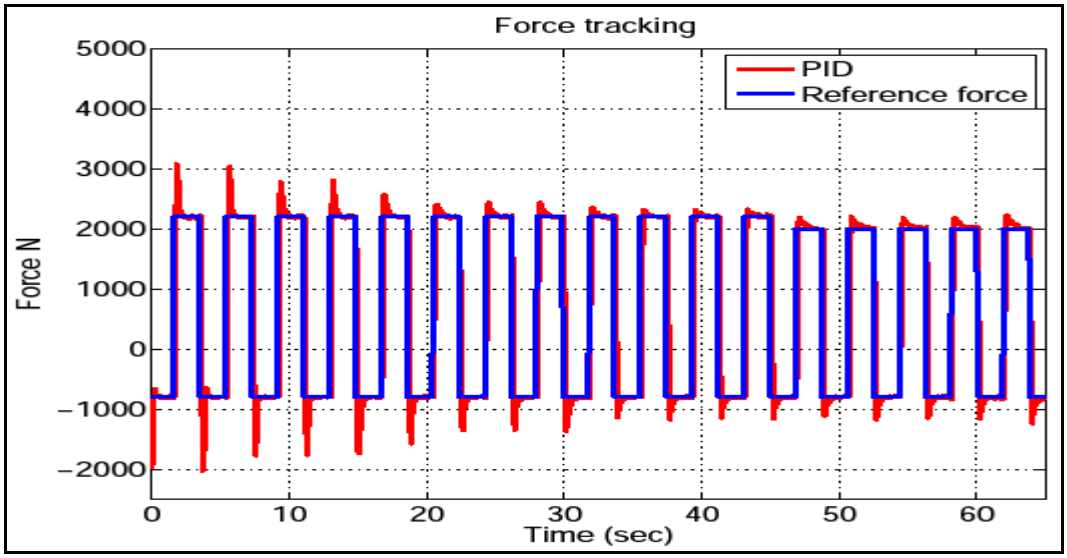

Figure 4.11 Force transmitted to passengers when the PID force controller is applied

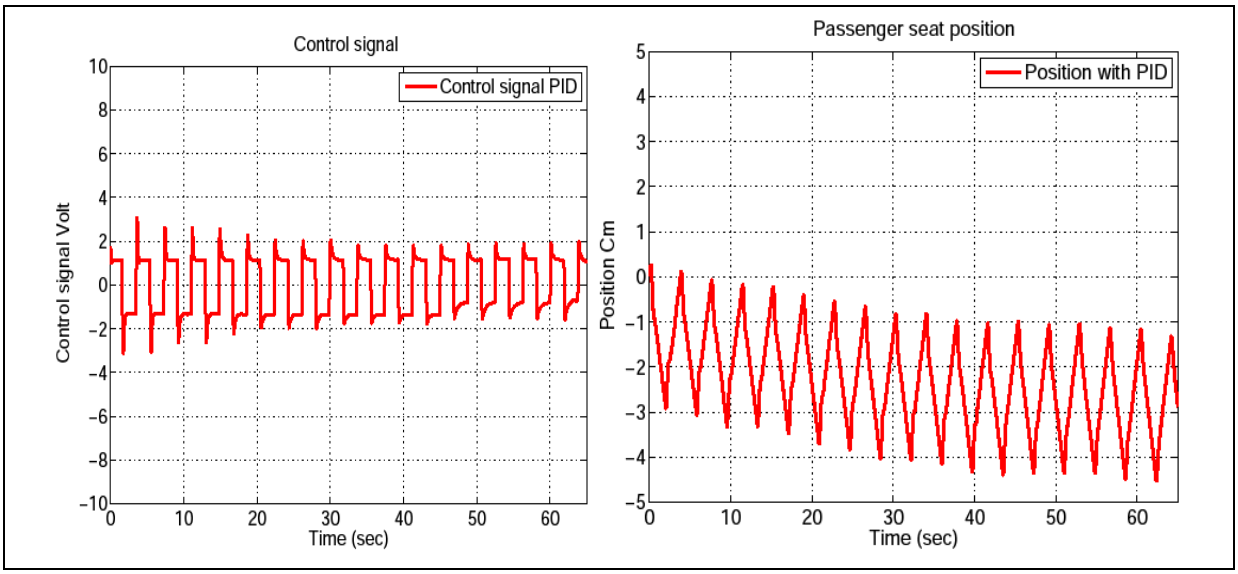

Figure 4.12 (a) Control signal when the PID force controller is applied (b) Sprung mass position

At this point, we apply the PID hybrid controller to the workbench with a skyhook force reference [20].

$$F_{des} = -\mathrm{B}_{sky}\dot{x}_s + \mathrm{K}_{sky}\,(\dot{x}_u - \dot{x}_s)$$

The desired force F_{des} is produced due to the movement of the two masses (sprung mass and unsprung mass). The force is calculated from the pressure variable, which has different values depending on the cylinder position. The calculated force has a non-zero initial value, and therefore, we will apply the force controller only when the perturbation is applied, since the force controller has no control on the position of the passenger seat tracking.

Consequently, it is normal to find a bias in this test, as before in Figure 4.12 (b). Therefore, we restricted the force control effect on the period when the perturbation is applied. The hybrid controller that is used to achieve force control is a combination of a PID position controller and a PID force controller. The signals for both controllers are merged by two filters, following the same approach as in Section 4.5.1.

The reference force is limited to (2000 N, -500 N). We have conducted two tests in order to determine the influence of the filters on the performance of the hybrid controller. With the first test, for the PIDHC T1 controller, the seat position returned back to its initial value, because the position controller, with $\alpha_{p1} = 0.8$, ensures position error correction (Figure 4.13 (b)).

This is not the case with the second test for PIDHC T2, where the position controller, with $\alpha_{p1} = 0.6$, has a smaller control signal, which in turn does not have a significant influence on the seat position in terms of forcing it to return to its initial value (Figure 4.13 (b)). In the first test for PIDHC T1, the filter parameters (K_{f1}, α_{f1}) are higher than their equivalent parameters (K_{p1}, α_{p1}) in the position controller. Higher values for α_{f1} shift the control focus to force control. In general, when we focus the control on the force transmitted to passengers, the position control is degraded, and when we focus the control on the vertical position of the passenger seat, the force control is degraded. This can be seen in Figure 4.13 (a) and (b) with the classical PID. This proves and confirms the importance of using a hybrid position/force controller in this type of application. Tableau 4.1 lists the parameters and results of the tests:

Tableau 4.1 PID hybrid control results

Controller type	PID parameters	Filter parameters	Maximum force values	Maximum position values
PIDHC T1	PID force controller: $k_p = 0.001966$ $T_i = 0.025233$ $T_d = 0.000141$ PID position controller: $k_p = 4$ $T_i = 0.006$ $T_d = 0.000111$	Position filter: $K_{p1} = 0.5$ $\alpha_{p1} = 0.8$ Force filter: $K_{f1} = 1$ $\alpha_{f1} = 0.9$	3314 N	(4.397-5)/5 cm 12.06%

PIDHC T2	PID force controller: $k_p = 0.001966$ $T_i = 0.025233$ $T_d = 0.000141$ PID position controller: $k_p = 4$ $T_i = 0.006$ $T_d = 0.000111$	$K_{p1} = 0.5$ $\alpha_{p1} = 0.6$ $K_{f1} = 1.5$ $\alpha_{f1} = 0.6$	3142 N	(4.563-5)/5 cm 8.7%
PID	$k_p = 0.00450$ $T_i = 0.001$ $T_d = 0.000054$	No filters	2595 N	(4.863-5)/5 cm 2.7%

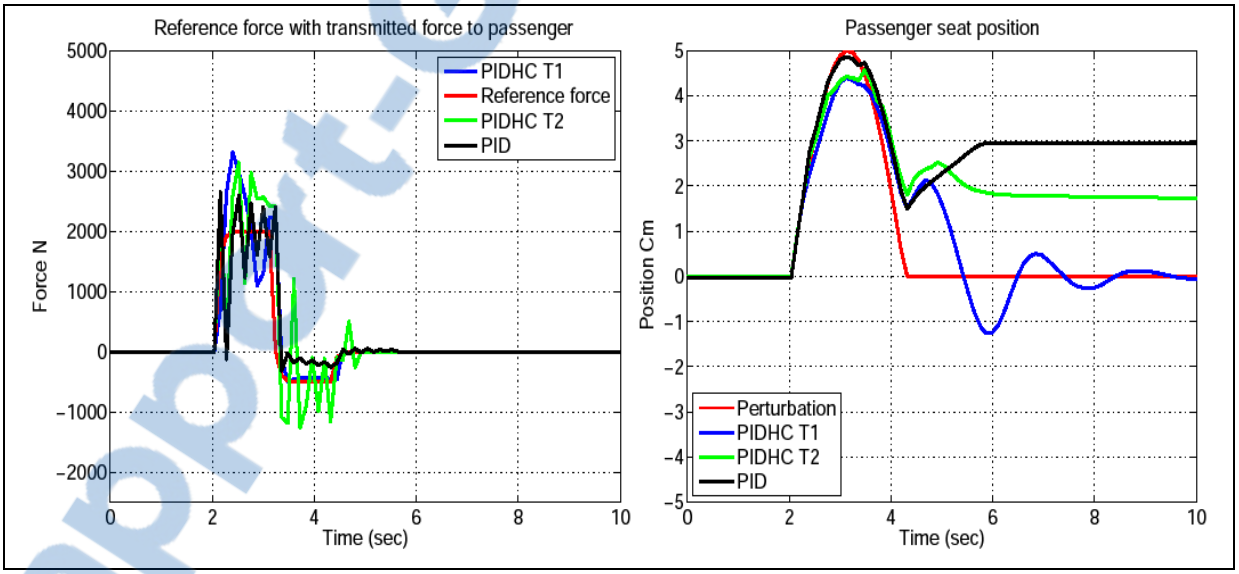

Figure 4.13 (a) Force transmitted to passengers when PID force controller is applied.
(b) Sprung mass position

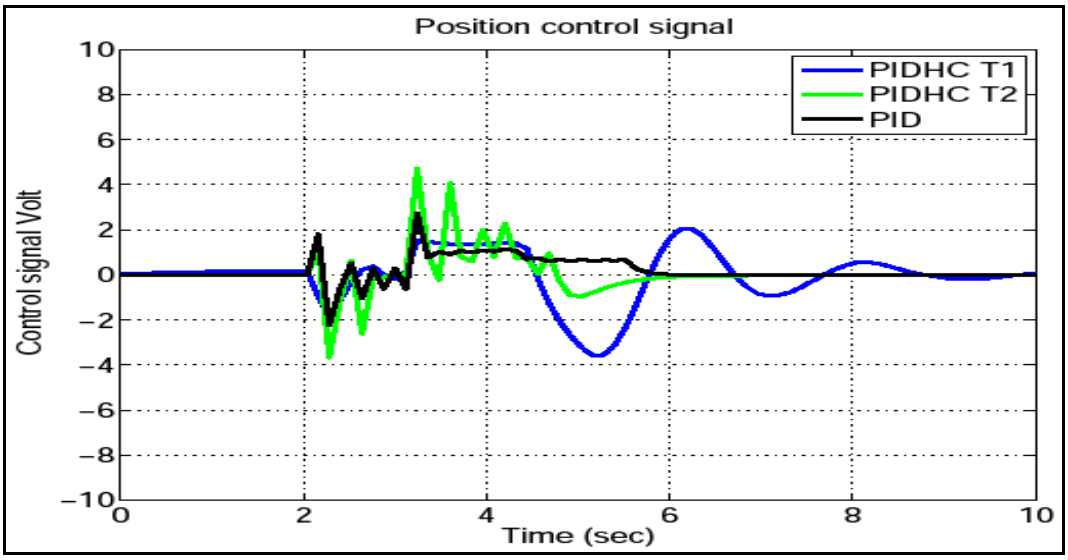

Figure 4.14 Control signal when force controller is applied

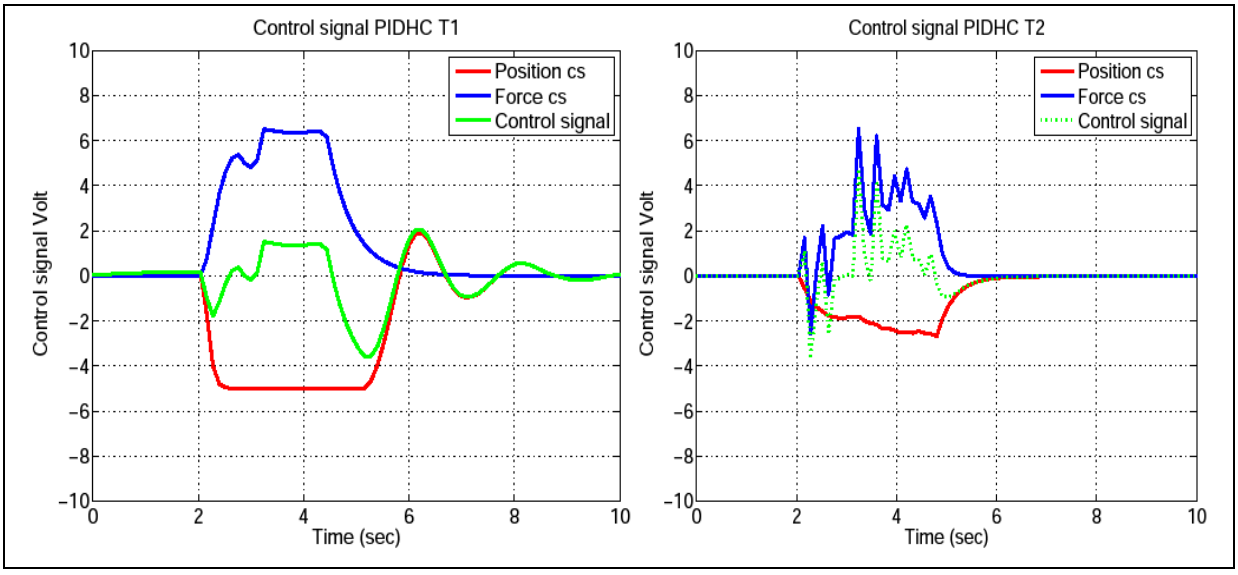

Figure 4.15 (a) Control signal when PID force controller is applied (Test 1).
(b) Control signal when PID force controller is applied (Test 2)

4.5.1.4 Position and force control with the PID hybrid controller

In this section, we use the hybrid controller in Figure 4.7, but with compromised parameters for the position and force filters. In order to achieve equilibrium between position and force control, we will attempt to determine the best force tracking while observing the seat position.

This means that the seat position should be as close to zero as possible, accompanied by good force tracking.
This objective can be summarized by partial isolation of the passenger seat from perturbations. To prove the validity of the hybrid structure, a comparison between PIDHC and PID controllers has been carried out. The results are excellent with this hybrid controller, where we compromised between the performances of the controllers to achieve a satisfying position and force control.

In Figure 4.16 (a), the seat position is reduced to 3.56 cm (28.2% of Test1) and 3.24 cm (35.2% of Test 2), which is slightly better than the PID controller (27.6%). For the position control, we can consider the PIDHC to be an efficient controller, but not as efficient as the SMPIDHCERL (63.2%). We also note the existence of some spikes in Figure 4.16 (a), due to the anticipation of the force controller in Figure 4.18 (a) and (b). These spikes are a direct response to the force control signal by the seat.

The hybrid controller negotiates the performance between the position and the force, especially when the force reference changes its signal. In Figure 4.16 (b), the force transmitted in test1 (PIDHC T1) (3536 N) is the lowest among these tests. An overshot is observed in Test 1, but the force tracking is acceptable (22% improvement) when compared to the PID controller. It is also worth noting that the force tracking with the PID controller in inadequate. The force is far enough from the reference force.

For test 2 (PIDHC T2), an oscillating performance is perceived, demonstrating a repetitive and insistent behavior on the part of the controller to reduce the force error tracking. This is due to the force controller parameters K_{f1}, α_{f1}, where $K_{f1} = 4$, $\alpha_{f1} = 0.33$. This choice of these parameters shows the intention of prioritizing the force controller, because the gain K_{f1} is higher than what is produced with other filter parameters $K_{p1} = 0.5$, $\alpha_{p1} = 0.8$.

The difference between Test 1 ($K_{f1} = 4, \alpha_{f1} = 0.33$) and Test 2 ($K_{f1} = 4$, $\alpha_{f1} = 0.22$) is the phase parameter α_{f1}, which increases the effect of the control signal in terms of creating a

change. The higher the value of α_{f1}, the smaller the force error and the higher the position error. The SMPIDHCERL outperformed all PIDHC and PID controllers when tracking force. For simplicity, we have summarized the results in Tableau 4.2.

Tableau 4.2 Force and position controller results

Controller	Force filter parameters	Position filter parameters	Maximum seat position	Maximum transmitted force
PIDHC Test1	$K_{f1} = 4$ α_{f1}=0.33	K_{p1}=0.5 α_{p1}=0.8	3.56 cm (28.2%)	(3536-3000)/3000= (17.8%)
PIDHC Test2	K_{f1}= 4 α_{f1}=0.22	K_{p1} =0.5 α_{p1}=0.8	3.24 cm (35.2%)	(3580-3000)/3000= (19.3%)
PID	No filter	No filter	3.62 cm (27.6%)	(4533-3000)/3000 =51.1%
SMPIDHCERL	K_{f1}= 4 α_{f1}=0.33	K_{p1}=0.5 α_{p1}=0.6	1.768 cm (64.2%)	(3513-3000)/3000 =17.1%
The best	SMPIDHCERL			

As seen in Tableau 4.1, the PIDHC performed better than a PID controller, especially in the area of force tracking.

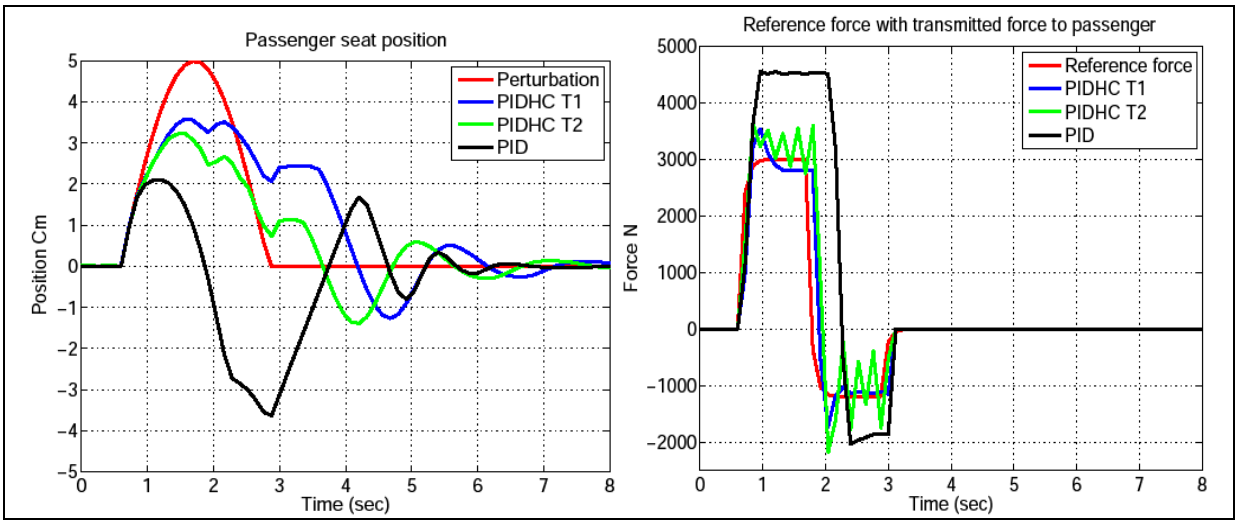

Figure 4.16 (a) Sprung mass position when PID and PIDHC position/force controllers are applied. (b) Force transmitted to passengers

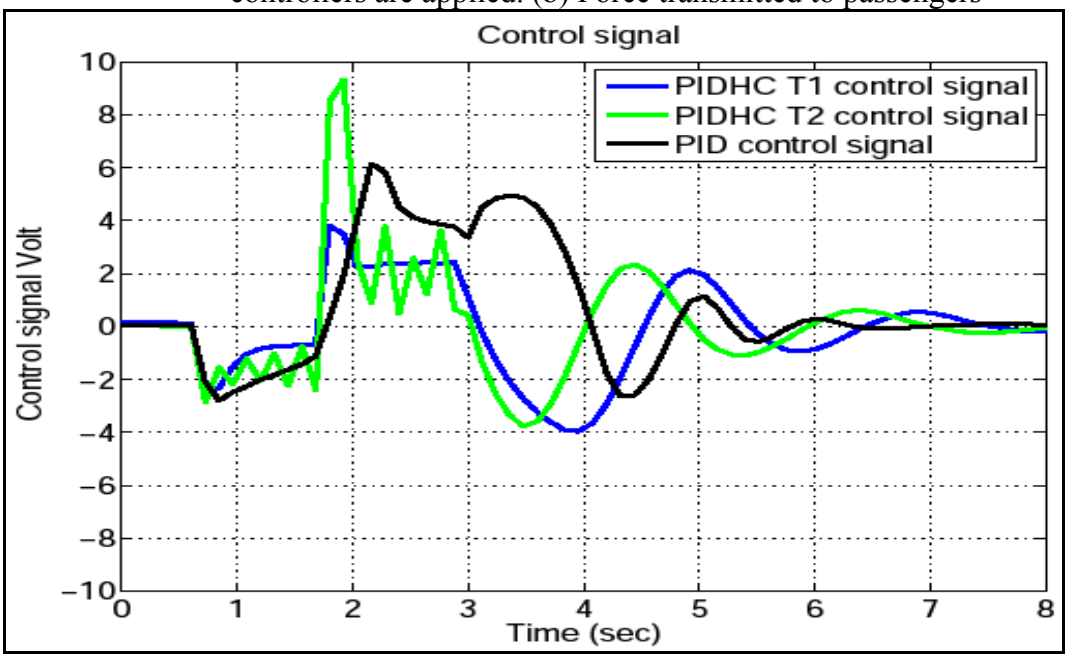

Figure 4.17 Control signal when PID and PIDHC Tests 1 and 2 position and force controllers are applied

In Figure 4.17, the control signal for Test 2 is the fastest and largest. This justifies the good results for either position or force control. A close look at Figure 4.18 (b) clearly demonstrates that the force control signal for Test 2 is dominant and the position control signal returns the seat position to zero after a while.

We see also the same trend in Figure 4.18 (a), except that the signal is oscillatory in nature. In the same Figure, the total control signal (green line) is composed of the position control signal (red line) and force control signal (blue line). Therefore, the position controller is responsible for returning the seat position to the initial state. In real time, the oscillatory response is observable by the operator during tests.

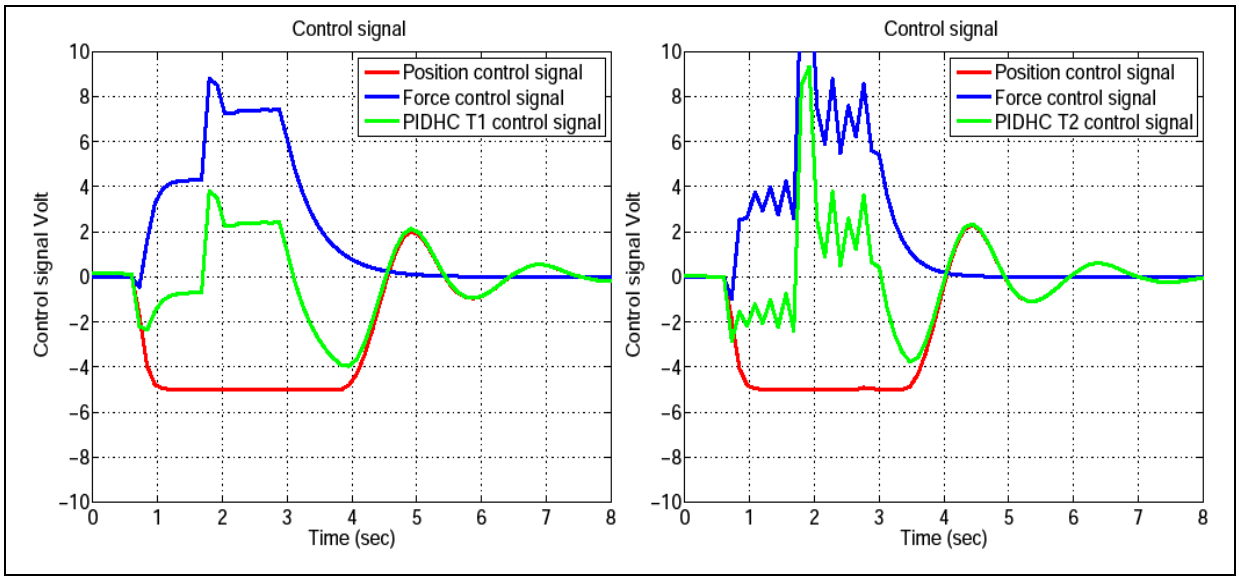

Figure 4.18 (a) Control signal when the PIDHC Test 2 position/force controller is applied. (b) Control signal when the PIDHC Test1 controller is applied

4.6 Conclusion

In this paper, we implemented an effective hybrid position and force controller in real time. The position controllers (either PID or SMC) achieved good and satisfactory results by stabilizing the position of the passenger seat with rapid and accurate response times, but with annoying high force transmitted to passengers.

To remedy this problem, we separately designed and implemented a PID force controller. The force transmitted to passengers is designed based on a skyhook damping force. Ideally, this force represents a comfortable and optimal force if it has been properly tracked. Although the

force has been significantly reduced to low levels, the position of the passenger seat is deviated to various levels far from zero or some stabilizing point.

To summarize, using the position controller, we achieved good position with high transmitted force. On the other hand, we achieved good force tracking with the force controller, but with a biased position for the passenger seat. Two separate controllers were not able to perform a multitask control, so a hybrid structure was proposed in order to achieve position and force control in real time. This hybrid structure is validated with an active suspension benchwork. The hybrid controller is a mixed pre-determined structure of two controllers. The combination is realized by using two low-pass filters with variable gain and poles.

The hybrid control proved the effectiveness of its structure by isolating the position of the passenger seat from perturbations and reducing the force transmitted to passengers to a minimum. In real-time tests, it was visually observed that there were two actions working together on the benchwork, which not the case when single controllers work separately. This has been verified by the distinct movement of the sprung mass when using the hybrid controller.

In the case of the sliding mode position controller, a chattering is observed with the conventional reaching law. To remedy this problem, an exponential reaching law was used to reduce the chattering and increase the system's response time.

In conclusion, the proposed hybrid controller with linear or non-linear controllers can achieve effective and accurate control for non-linear systems without implementing high costs and complex algorithms. The validation of this structure may help to make this structure common in industry, especially in the case of multi-variable systems where two variables are controlled in a coherent and integrated manner.

CHAPITRE 5

SERIAL FUZZY SELF TUNING PID DUAL LOOP POSITION CONTROLLER FOR ACTIVE SUSPENSION

Bassel Shaer[1], Jean-Pierre Kenné[1], Claude Kaddissi[1] and Ali Zaher[2]

[1]*Département de Génie mécanique, École de technologie supérieure, 1100 rue Notre-Dame Ouest, Montreal,QC, H3C1K3, Canada*
[2]*CNRS, PROMES Laboratory, Rambla de la thermodynamique, 66100 Perpignan, France.*

Article soumise à la revue «IEEE Transactions on Control Systems Technology», Juin 2017.

Abstract

The use of proportional integral derivative (PID) controllers is widespread in industry. This is due to their simplicity and efficiency. Faster PID controllers with faster response times are required for industrial applications. A number of adaptive and tuning methods are needed in order to achieve this objective. More complicated methods, such as fuzzy logic theory, optimization algorithms and multiple design structures are used for the tuning process. More recently, a PID dual loop (PIDDL) controller has been developed to overcome the performance of PID controllers.

In this paper, fuzzy tuning theory with a new structure is applied in order to tune PID and PIDDL controllers, but with a new structure. The proposed tuning structure uses the feedback principle, where the tuned gain transforms the estimated or predicted information derived from its future effect into other fuzzy sub-controllers in a successive manner. The online tuning structure is applied, in real time, to an electrohydraulic system, as represented by an active suspension bench. The results achieved in the testing highlight the simplicity and applicability of the tuning method in industrial applications with minor changes in hardware modules to get the best out of PID controller.

Keywords: PID Dual loop, position controller, real-time control, active suspension, feedback, fuzzy tuning

5.1 Introduction

Electrohydraulic systems are among the most used and developed systems in industry, and especially in heavy industry, where there is a significant demand for powerful systems due to space limitations.

Position controllers play an important role in controlling these systems, where precise positioning is an unavoidable objective in the fabrication of machines, hydraulic presses, robotics, etc. Classical or conventional controllers, including PID controllers, are more popular in this field, because the process for tuning their parameters is relatively simple.
A PID controller has three tunable gains, and a number of methods have been developed for achieving operational gains, such as the Ziegler-Nicols method. The research in this area been focused on the process of gain tuning where each gain is tuned in accordance with system performance.

Others use PID controllers as an introduction for other non-linear controllers (Jantzen, 1998). He began by transforming the PID into a fuzzy controller. He then used some developed non-linear tables to transform the linear controller into a non-linear fuzzy controller. Finally, with fine tuning, he achieved the proposed controller in order to produce the best configurations for rise time, overshoot and stabilization time for steady-state errors. Due to the importance and popularity of PID controllers, some researchers (Xu et al., 2000) found that simplifying the structure of these controllers could simplify tuning procedures and increase their integration in industry. The PID controller and its future have been studied with a view to determining the needs and requirements for expanding the use of these efficient controllers in industry.

For example, (Åström & Hägglund, 2001) suggested that new software should be developed, so that PID controllers could be used by individuals with moderate knowledge. This type of

software should include a PID controller with new tools for modeling and auto tuning. In addition, following methodological steps and simplifying the PID structure would lead to increased popularity. This was accomplished by (Xu, Hang et al. 2000), who designed a parallel combination of fuzzy PI and PD controllers. The tuning process, control rules and determination of controller parameters depend on the characteristics of the phase margin and gain margin. The controller produces higher gains when the system error is high, without exceeding the limits imposed on the control signal. The proposed fuzzy PID controller demonstrated better performance than conventional PID, due to the non-linear properties provided in the fuzzy PID control system. In applying a different way of thinking, (Almeida & Coelho, 2002) suggested a different gain-tuning structure. They proposed a systematic design for a fuzzy gain scheduling PID controller in order to tune the gains of a PID controller.

The mathematical models for both the process and controller are used to calculate the controller gains, where the controller parameters are chosen in such a way that the zeros of the controller cancel the process model poles. The normalized fuzzy output is the gain margin, which is used to calculate the PID gains online using a predefined law. The results are good, because the method is simple and guarantees system stability. Since the objective in tuning PID gains is to achieve the best gains, (Xu & Feng, 2004) developed an adaptive fuzzy PID tuner using an optimization method. They used a constrained optimization algorithm and sequential quadratic programming (SQP) to optimize the parameters of the fuzzy PID tuner. Based on the performance index, the minimum of cost function is achieved. The algorithm was applied as equal to linear and non-linear systems, and demonstrated good results in comparison with a classical PID controller.

In previous research into fuzzy tuning PID gains, the fuzzy controller essentially depends on the experience of experts. In order to remedy this problem, Callai et al (2005) developed an adaptive fuzzy PID controller, which is supposed to work over a wide range of different operating points, even with lack of expert feedback. There are no mathematical or formal laws for choosing fuzzy parameters, so the author added adaptive technique to tune the controller and improve the performance to maximum. Four adaptive techniques were developed in order

to make the fuzzy PID controller less dependent on expert knowledge. The first technique uses the standard least-square algorithm to calculate the mass centre of the membership function. Essentially, this structure is similar to the work done in (Jantzen, 1998), except for the way in which the membership functions are shifted. The second structure is interesting, because it uses an adaptive fuzzy PID (AFPID) with fuzzy compensation. A fuzzy compensator is used to compensate the control signal against various operating points. The third structure is similar to the second one, but with an inverse fuzzy model (IFM) compensator. The fourth structure is a conventional PID with a fuzzy compensator. The best results have been obtained with the AFPID with fuzzy compensator, because this structure does not modify the control model, but compensates the control signal when necessary.

In every PID-tuning process, the uncertainty in the system parameters represents a problem that must be resolved. In light of this, (Solihin, 2007) tuned the PID gains using fuzzy weighting factors, which are added to the fuzzy output in order to make the system robust against the uncertainty in system parameters. The tuning of the PID gains should be done online, so the learning process has a high chance of being applied. This was done by (Huang et al., 2009), who proposed a parameter auto-tuning method based on self-learning. Switching to a normal PID controller takes place when system performance is adequate. The input of the learning algorithm is the system error, and index evaluation is applied to determine whether a reward and punishment process should be applied to the fuzzy rules. This method is sophisticated, and requires more calculations. It proposes changing fuzzy rules by special block.

Another work that is similar to (Huang et al., 2009) is suggested by (Karasakal, et al., 2011), in which the membership functions have numbers corresponding with the phase system response zones. The algorithm demonstrated good performance, but it is time consuming and too complicated. Some researchers changed the method for following by introducing the system in different structures (Zheng et al., 2009). This control method uses the PID with auto-tuning fuzzy control. The tuning method is standard, but the change is applied to a new design of a volume-control hydraulic press driven directly by SRM. The dead zone and time lag in

hydraulic systems were taken into account in designing the controller. The results improved control accuracy against external perturbations. (Bakri et al., 2012) changed the fuzzy components in an interesting way in developing an adaptive fuzzy control. They shifted the membership function for outputs and inputs. The adjusted parameter is the universe of discourse (UOD), which determines how much the membership function is to be shifted. They proposed a method for tuning the UOD using a trial and error technique.

The adaptive fuzzy controller demonstrated good results, but was not robust against perturbations. With a view to remedying this problem, in a recent research project, (Maghfiroh, 2013) created a hybrid tuning structure in order to make the controller more robust against reference variations. The gain K_p is tuned online using a fuzzy controller. The controller showed improved performance in comparison with a fixed-gain PID controller.

In this paper, a new adaptive fuzzy gain tuning of a PIDDL controller is developed and applied in real time (Desantis, 1996). A PIDDL controller, which is an extension of a PID controller, has been developed by adding simple feedback loops. The philosophy behind the proposed structure depends on the feedback of predictive or estimated errors. An estimated error is the error produced by the system when applying these updated gains to the PID controller. The estimated error is generated by weighting functions from the first fuzzy controller output of the first gain. Subsequently, the estimated error and its derivative are added directly to their corresponding successive fuzzy controller inputs. These steps are repeated with subsequent PID gains.

By feeding the estimated error back to the other PID gain tuners, the objective is to send information concerning the change to be expected in the tuned gain from the previous step. The PID gains are tuned by varying the intermediary estimated error. The proposed adaptive method is applied using PID controllers and modified PIDDL controllers in real time to control the position of an active suspension system.

The paper is organized as follows: Section 2 presents the motivation and a description of the active suspension workbench. Section 3 presents a dynamic model of the active suspension

system. The proposed tuning methods and real-time tests are detailed in Sections 4 and 5. Finally, a summary of the work and other improvements are presented in Section 6.

5.2 Motivation and description of the active suspension workbench

In this section, the proposed tuned controller is applied to an electrohydraulic system in real time. It should be noted that the method used is not limited to these types of systems. Conventional controllers are still needed, and therefore, are still being developed. These controllers are being developed to adapt to the requirements of highly non-linear systems, such as active suspension systems. The workbench in Figure 5.1 shows an active suspension system.

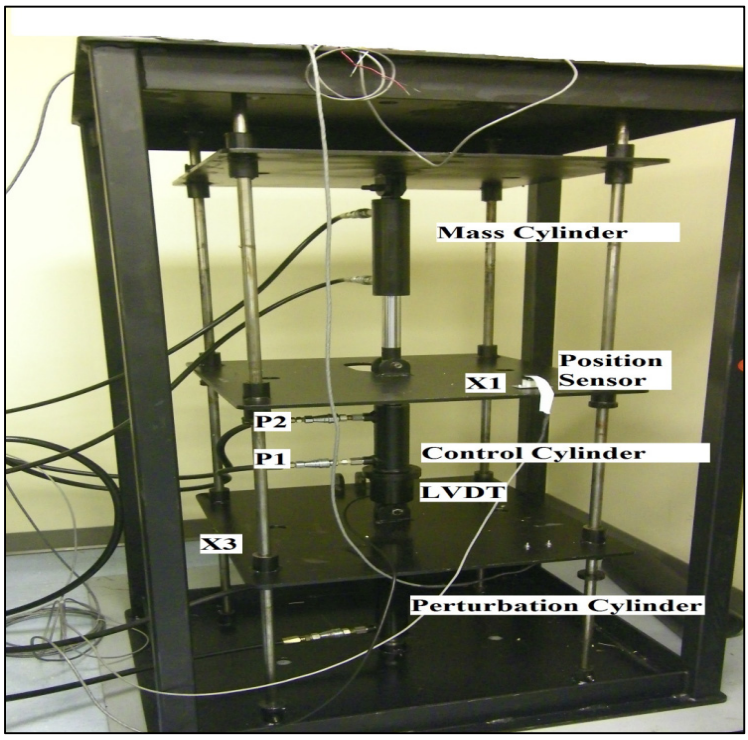

Figure 5.1 Active suspension workbench

The two metal sheets represent the mass of the car and wheels, successively. This hydraulic station is designed to be an active suspension system without springs. In a quarter-car model, the springs represent the passive suspension.

In a classical control using a PID controller, there is no need to model the system. The PIDDL technique suggested by (Desantis, 1996) is a novel extension of a PID controller. This

technique has not previously been applied on active suspension systems in real time. (Cornieles, 1998) applied a PIDDL controller to control the level and temperature of a tank. Our motivation for applying this technique in real time is reinforced by the new structure of feedback connections suggested for the fuzzy PID tuners.

The proposed method is also applied to the PIDDL controller, and is compared with other controllers. The new feedbacks in the proposed technique are promising and new. They can be developed in a variety of ways in any fuzzy tuning process. The techniques are validated using the electrohydraulic active suspension workbench in Figure 5.1. The main component, which is not shown in Figure 5.1, is a hydraulic positive displacement pump that is driven by an electrical motor. There are three servovalves. The first one is used to simulate road perturbations. The second servovalve is linked to the control cylinder in the middle, which is the active part of the active suspension system. A Linear Variable Differential Transformer (LVDT) is installed on the second servovalve to measure the valve's spool position. The third servovalve is used to control the mass cylinder and to change the passenger mass. The three servovalves are Parker BD15 models with 2.5 GPM and 3.6 VDC. These models have linear flow gain characteristics and pressure ranges of up to 3,000 psi.

The perturbation is produced by means of a position controller using an infrared sensor. The pressure sensors are mounted on the outlet and inlet ports of the servovalves. They are Omega px602 models, with a pressure range of 2,000 psig and sensitivity of 10 mV/V. The motor that drives the pump is an Emerson 5 HP Motor with a rated speed of 1,735 RPM. The hydraulic pump is a Marzocchi GHP1A-D-6 model with a maximum working pressure of 290 bar. The I/O card is a National Instrument NI PCI 6014 that reads signals from the sensors and transmits the control signal to the servovalves. This is a low-cost 200 kS/s, 16-Bit, 16 analog input multifunction data acquisition (DAQ) card. The acquired signals include pressures p1 and p2, the vertical position of the passenger seat (sprung mass) x1 and the tire position (unsprung mass) x3.

5.3 Dynamic model of the active suspension system

The model of the active suspension benchwork is similar to the model used in (Shaer et al., 2016), as follows:

$$\begin{aligned}
\dot{y}_1 &= y_2 \\
\dot{y}_2 &= -a_0 y_3 - b_0 y_4 + a_1 y_5 \\
\dot{y}_3 &= y_4 \\
\dot{y}_4 &= -A_1\, y_3 - A_2 y_4 + A_3 y_5 + b_1 \dot{y}_r + h_1 y_r \\
\dot{y}_5 &= {}^{J_1}/_{f(.)}\,(-A y_4 - L y_5 - C_d\, y_6 g(.)\,) \\
\dot{y}_6 &= \frac{1}{\tau}(-y_6 + k_v u)
\end{aligned} \tag{5.1}$$

Where:

$$f(.) = V_0^2 - A^2 y_3^2$$

$$\mathrm{g}(.) = \sqrt{\frac{P_s - sigm(y_6) y_5}{\rho}}$$

The variables and parameters for the model are defined in Tableau-A III-1 and Tableau-A III-2. The model is highly non-linear. The sign function integrated in $g(.)$ is a discrete function. In addition, $g(.)$ contains a square root of system variables. In other words, the system has many non-linear characteristics. Therefore, an adaptive controller with more feedbacks is required to deal with any changes in system parameters. The position of the sprung mass y_1 is the variable of interest to be controlled by the PID and PIDDL controllers.

5.4 Adaptive fuzzy tuning gain for PID and PIDDL controllers

PIDDL controllers have approximately the same gains as PID controllers, with the addition of new loops. The most common method for tuning PID gains is to use three fuzzy controllers for the three gains K_p, T_i, T_d. With traditional methods, there is no relation between the gain-tuning controllers.

For PIDDL controllers, a fourth gain K_3 is added into the structure. The choice of membership functions and other fuzzy parameters depends on the experience of the expert. Tuning by fuzzy

controller uses a parallel structure in order to tune each gain separately. The tuning of the gains usually starts with initial gains obtained using the Ziegler Nichols method. Adaptive PID and PIDDL structures will be described in detail over the next sections.

5.4.1 Design of a PID controller

The schema in Figure 5.2 depicts a conventional PID controller, where K_p, K_i and K_d represent the proportional, derivative and integral gains, respectively. The gains are fixed, and can be tuned using a variety of methods, including Ziegler Nichol. The gains applied to the active suspension benchwork are Ziegler Nicole gains, but they are not optimal. The number of channels and the loop frequency $f_s = 5 - 10$ Hz in LabVIEW are taken into account when applying the tuning method. Better performance can be achieved using the trial and error method based on the Ziegler Nichol gains.

The gains are $K_p = 4, T_i = 0.006$ and $T_d = 0.000111$. The results from the PID controller are compared with the results from other controllers in order to assess the efficiency of the other methods.

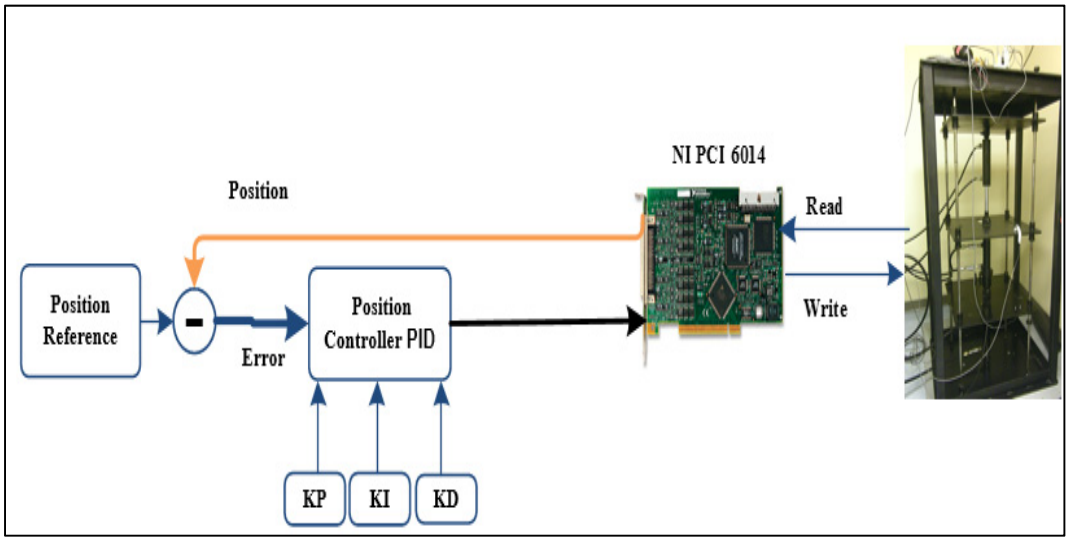

Figure 5.2 Conventional PID controller schema

5.4.2 Fuzzy tuning PID controller

Fuzzy controllers were developed in order to adjust the gains using position error and error derivation. The problem of tuning procedures is transformed into a fuzzy control design problem. Fuzzification is the first step, in which the membership functions are used to graphically describe the problem. These membership functions are designed based on system performance. The fuzzy rules are applied as a second step. The third step involves obtaining the crisp or fuzzy outputs using the defuzzification process. Therefore, the design of a fuzzy controller can vary due to the expert's knowledge of fuzzy tuning. The gains are tuned and applied to the controller at the same time. In the next instant, the system outputs resulting from the most recent tuned gains are used again to correct the gains until the position error vanishes to zero.

This principle is generally used in all tuned algorithms that use fuzzy controllers where there is no need for calculations or estimation of the effect of gain updates. In other words, a conventional fuzzy controller does not estimate the effect of any of its outputs or the outputs of other controllers on system performance at the same instant.

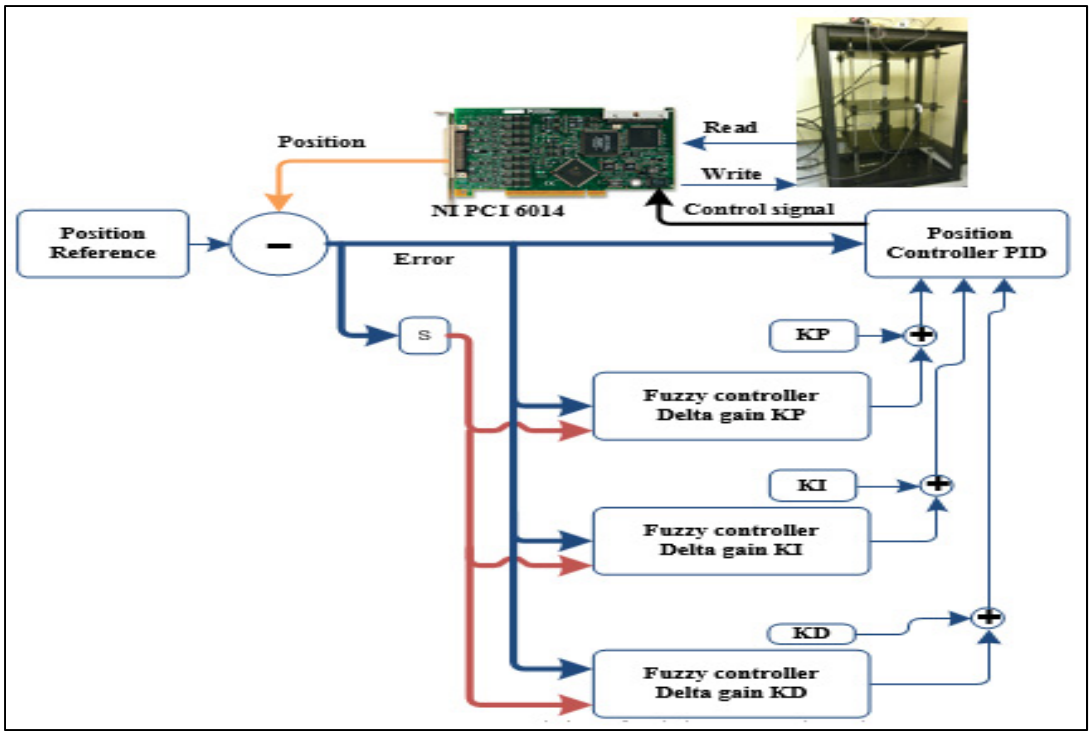

Figure 5.3 Fuzzy tuning PID (FPID) controller

The output from fuzzy controllers is the difference in gain to be added or subtracted from the initial values. In other words, $K_{p_r} = K_p + \Delta K_p$, where K_{p_r} is the new tuned gain applied to the PID controller. The basic range of input and output variables are:

$$e \in [-5\ cm, 5\ cm];$$

$$\dot{e} \in [-4\ cm/s, 4\ cm/s];$$

$$\Delta K_p \in [-5, 5]\ ,\ \Delta T_i \in [-0.05, 0.05]\ ,\ \Delta T_d \in [-0.05, 0.05].$$

The membership for the gain ΔK_p is represented in Figure 5.4. The corresponding fuzzy subsets are:

$e, \dot{e} = [\mathrm{NB}, \mathrm{NM}, \mathrm{ZERO}, \mathrm{PM}, \mathrm{PB}]$,

$\Delta K_p, \Delta T_i, \Delta T_d = [\mathrm{NB}, \mathrm{NM}, \mathrm{PM}, \mathrm{PB}]$.

Where:

- NB = Negative big;
- NM = Negative medium;
- Z = Zero;
- PM = Positive medium;
- PB = Positive big.

The fuzzy inference rules used in the calculations are:
If e is A_i and $\dot{e}$ is B_j, then ΔK_p is C_{ij}, ΔT_i is D_{ij},and ΔT_d is E_{ij}.

Where:
A_i and B_j are the fuzzy subsets of inputs.
C_{ij}, D_{ij}, E_{ij} are the fuzzy subsets of outputs, where $i = 1,2,3,4,5, j = 1,2,3,4$
The Mamdani operators used in fuzzy calculations are:

$$\mu_C(\Delta K_p) = \bigvee_{i,j} \left\{ [\, \mu_i(e) \wedge \mu_j(\dot{e})] \wedge \mu_{C_{ij}}(\Delta K_p) \right\}$$

Where: $\wedge$ is the minimum function and $\vee$ is the maximum function.
The centroid method is used to implement the defuzzification. The PID controller gain ΔK_p is calculated as follows:

$$\Delta K_p = \frac{\int \mu_C(\Delta K_p) * \Delta K_p * d(\Delta K_p)}{\int \mu_C(\Delta K_p) * d(\Delta K_p)}$$

The same calculation is applied to the gains ΔT_i, ΔT_d.

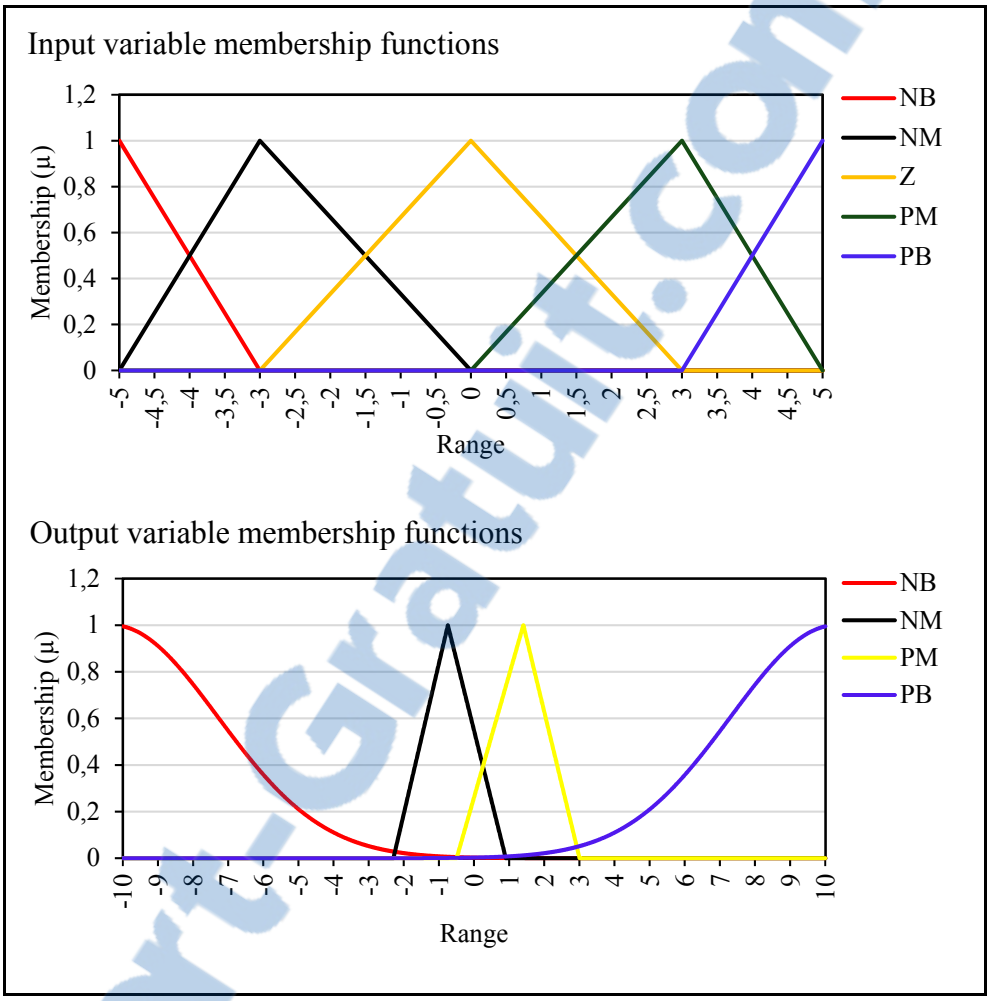

Figure 5.4 Membership functions for the gain ΔK_p

For T_{i_r}, the same development is used to get ΔT_i. T_{i_r} is used in the tuned PID controller, where $T_{i_r} = T_{i_r} + \Delta T_i$.

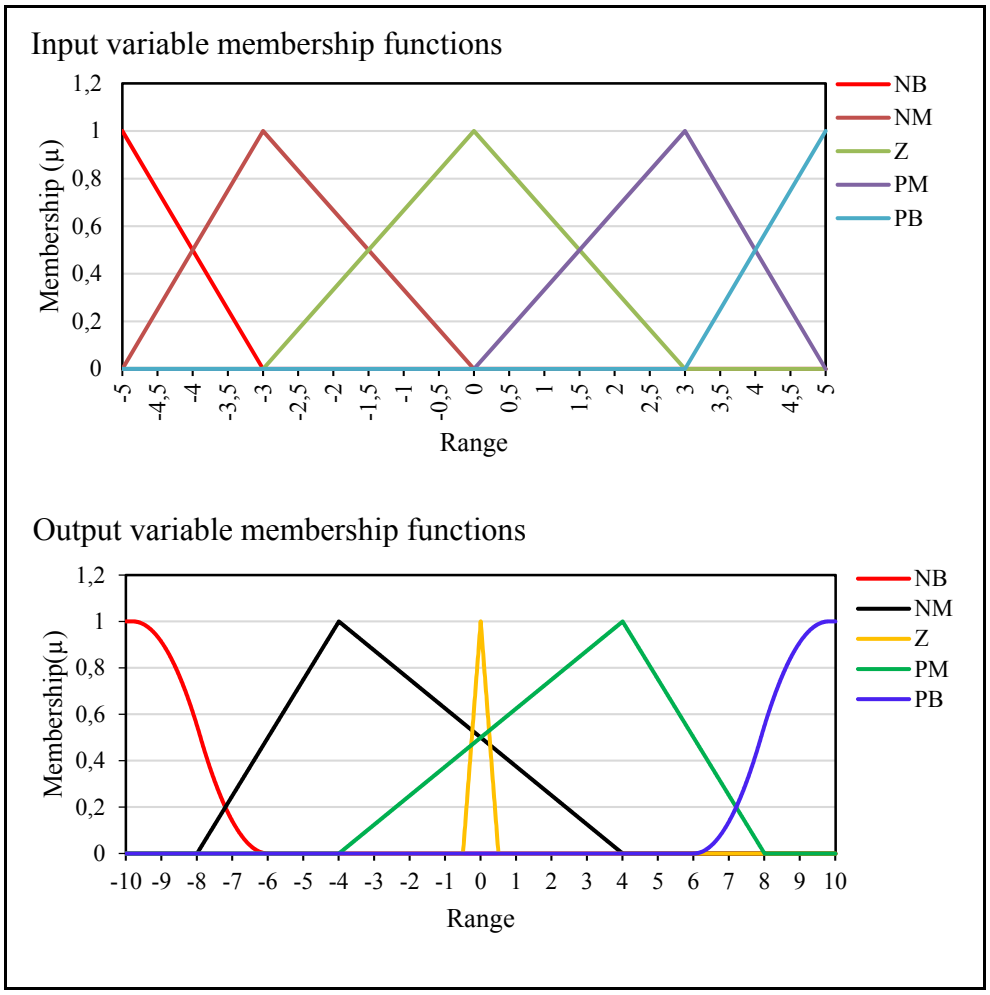

Figure 5.5 Membership functions for the gain ΔT_i

For T_{d_r}, the same development is used to get ΔT_d. The derivative time T_{d_r} is used in the tuned PID controller, where $T_{d_r} = T_d + \Delta T_d$. The membership is chosen using the trial and error method in order to produce the best system response.

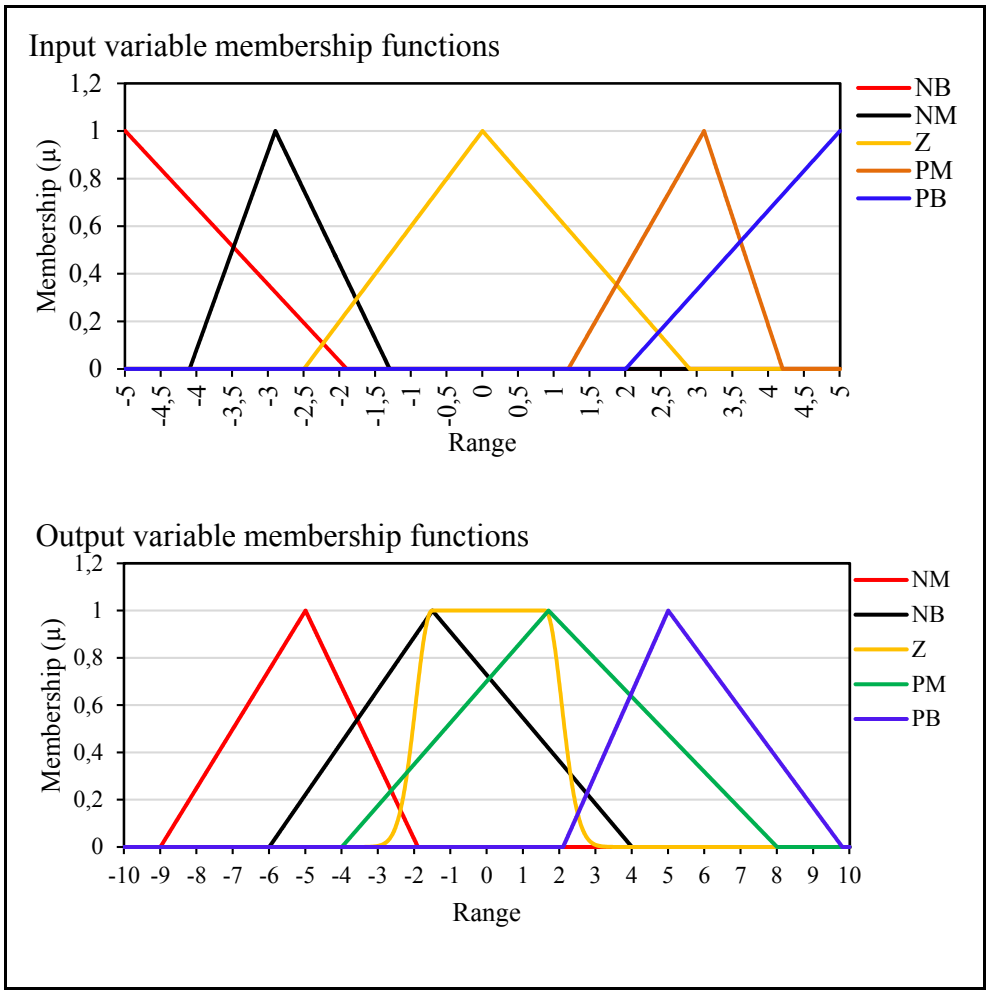

Figure 5.6 Membership functions for the gain ΔT_d

5.4.3 Adaptive fuzzy tuning PID controller

The updated gains for the fuzzy controller in Section 5.4.1 improve or degrade system performance. Every gain has a margin by which the PID controller can improve or degrade system performance.

Updating a single gain can degrade system performance, but the update process for the other gains may justify or improve performance. Therefore, a new method for adapting the fuzzy tuning of a PID controller in a new manner is proposed, in which an estimated error is returned as a feedback to the next fuzzy tuner. The adaptive structure actually returns the estimated error and its derivative resulting from the first fuzzy controller as feedback to the successive fuzzy

controller. The estimated error and its derivative represented in the schema in Figure 5.7 is produced by the functions $F_1(.)$ and $F_2(.)$. These functions are proportional functions with a phase. In other words, they are low-pass filters through which an estimated error is predicted by changing the gain and phase of this filters in order to achieve better system performance. The estimated error here is supposed to be the error that is produced when applying the adjusted $K_p(.)$ to the system.

The tuner ΔK_p is a fuzzy controller, where the outputs are ($\hat{e}_{K_P}, \dot{\hat{e}}_{K_P}$).

$$\hat{e}_{K_P} = F_1(\Delta K_p)$$

ΔK_p is the output of the fuzzy controller.

Where: $\hat{e}_{K_P}$ is the estimated error when adjusting K_p.

The same process is applied to the error derivation.

$$\dot{\hat{e}}_{K_P} = \mathrm{F}_2\left(\frac{(\Delta \mathrm{K_p})_{t2} - (\Delta \mathrm{K_p})_{t1}}{\mathrm{t_2} - \mathrm{t_1}}\right)$$

The variables $\hat{e}_{K_P}$, $\dot{\hat{e}}_{K_P}$ are fed back to the next tuner $\Delta \mathrm{T_i}$ (green).

For the next tuner $\Delta \mathrm{T_i}$, the outputs are:

$$\hat{e}_{\mathrm{K_I}} = \mathrm{F}_3(\Delta \mathrm{T_i})$$

$$\dot{\hat{e}}_{K_I} = F_4\left(\frac{(\Delta T_i)_{t2} - (\Delta T_i)_{t1}}{t_2 - t_1}\right)$$

The variables $\hat{e}_{\mathrm{K_I}}$, $\dot{\hat{e}}_{\mathrm{K_I}}$ are returned as a feedback and added to the inputs for the fuzzy controller $\Delta \mathrm{K_d}$ (red).

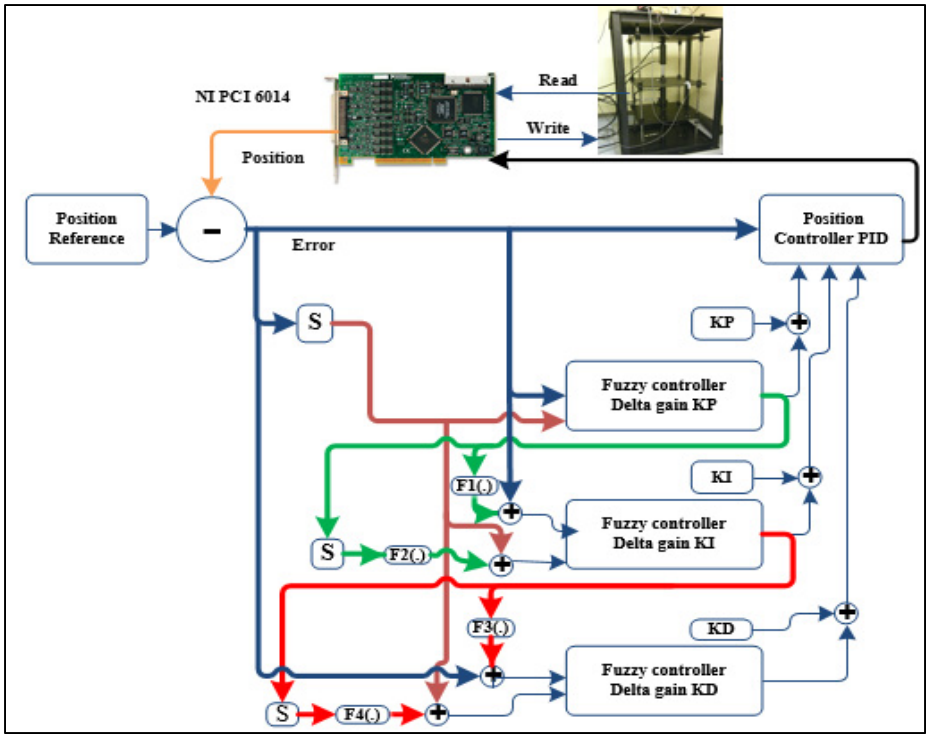

Figure 5.7 AFPID controller

5.4.4 PIDDL controller

The PIDDL controller is designed to be an improvement on the PID controller. The additional feedback loops and the gain-tuning method identify the PIDDL as an enhanced PID controller (Cornieles, 1998). The schema in Figure 5.8 (a) represents a PIDDL controller. Gains K_1, K_2 and K_4 represent the internal loop. Gains K_3, α_1 and α_2 represent the external loop.

The gain-tuning procedures are presented in (Desantis, 1996) for first-order systems, in which an analytical study is developed in order to achieve the best system response and rejection of perturbations.

The tuning process is divided into two steps:

1-Tuning the gain for internal loop K_1, K_2 and K_4.

2-Tuning the gain for external loop $K_3, \alpha_1$and α_2.

For position tracking:

Let $K_3 = K_4 = \alpha_1 = \alpha_2 = 0$. Gains $K_1$and K_2 should be modified in order to adjust the response time without overshot. Then, the values of $\alpha_1 \, and \, \alpha_2$ are determined in order to correspond to second-order coefficients. Gain K_3 should be increased in order to reduce the effects of perturbations without negatively affecting performance. A verification of the system response should be carried out in order to validate the gains of the PIDDL controller.

In this paper, a PIDDL controller is modified and then applied to non-linear systems. The reference position tracking is zero, so there is no need for gain K_4, Gains K_1, K_2 and K_3 are grouped together in a PID schema. Figure 5.8 (b) shows the gains independently (K_1 proportional, K_2 derivatives and K_3 integral). These gains are regrouped in a PID controller in order to facilitate the tuning and the tracking process (Figure 5.9).

Let $K_3 = \alpha_2 k_3$ and $\alpha = \alpha_1 k_3$ to get the final PIDDL schema (Figure 5.10). LabVIEW is used to test the controller in real time, and therefore, PID gains k_1, k_2, and k_3 are replaced by K_P, T_i and T_i, for reasons of simplicity.

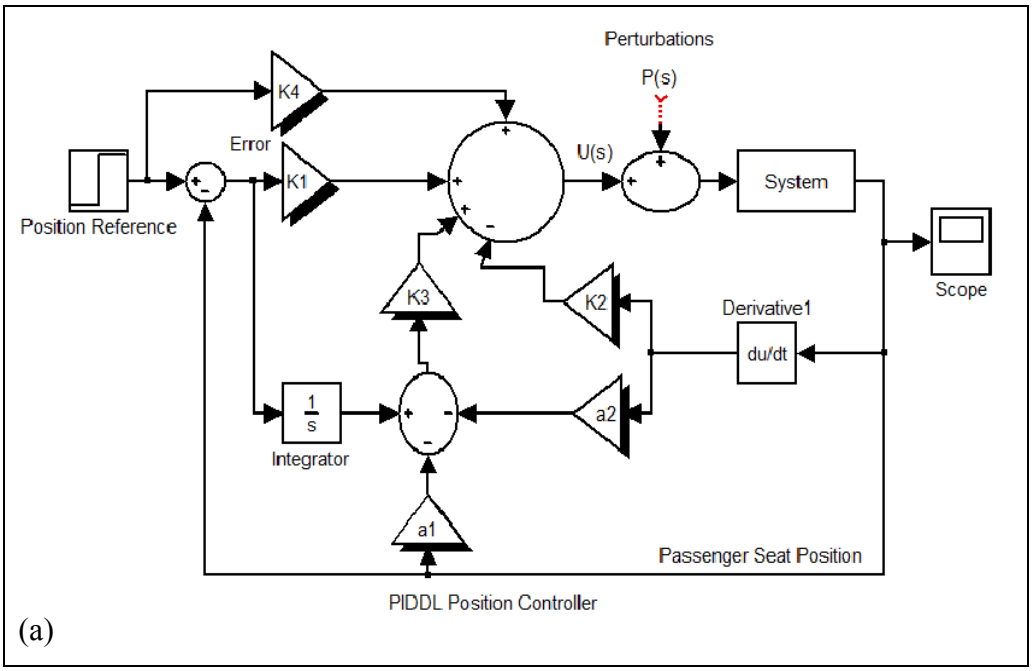

(a)

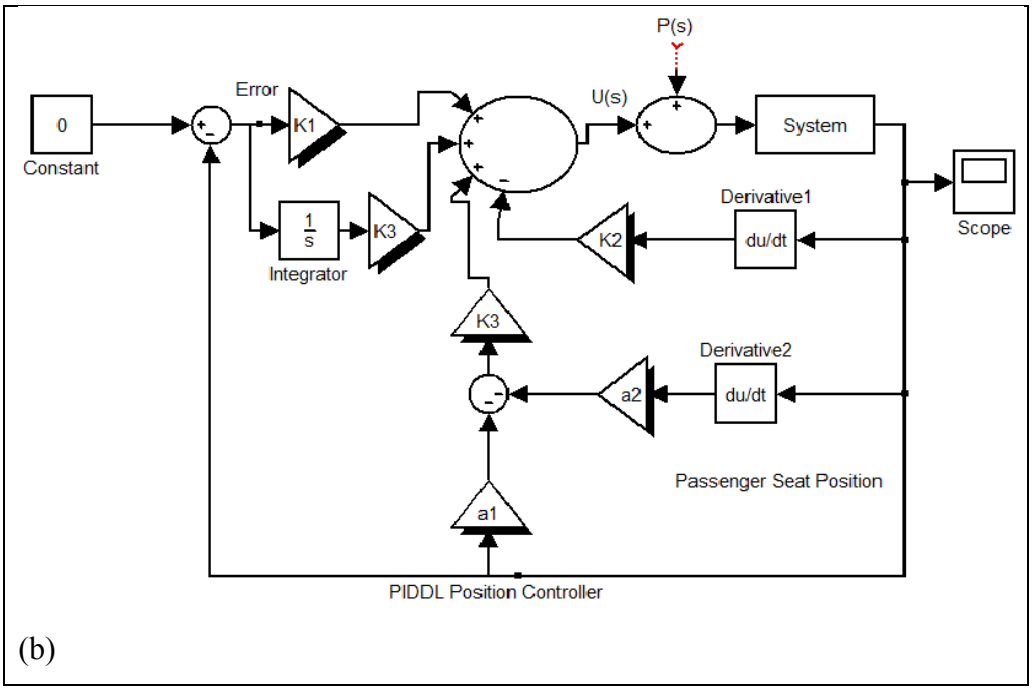

Figure 5.8 (a) PIDDL controller schema. (b) Modified PIDDL controller schema

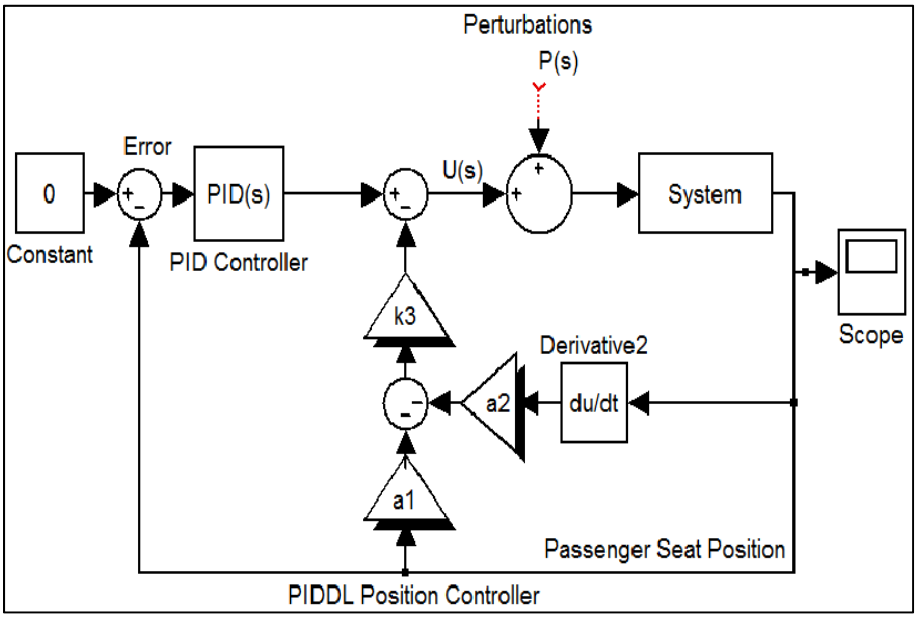

Figure 5.9 PIDDL controller with PID controller block

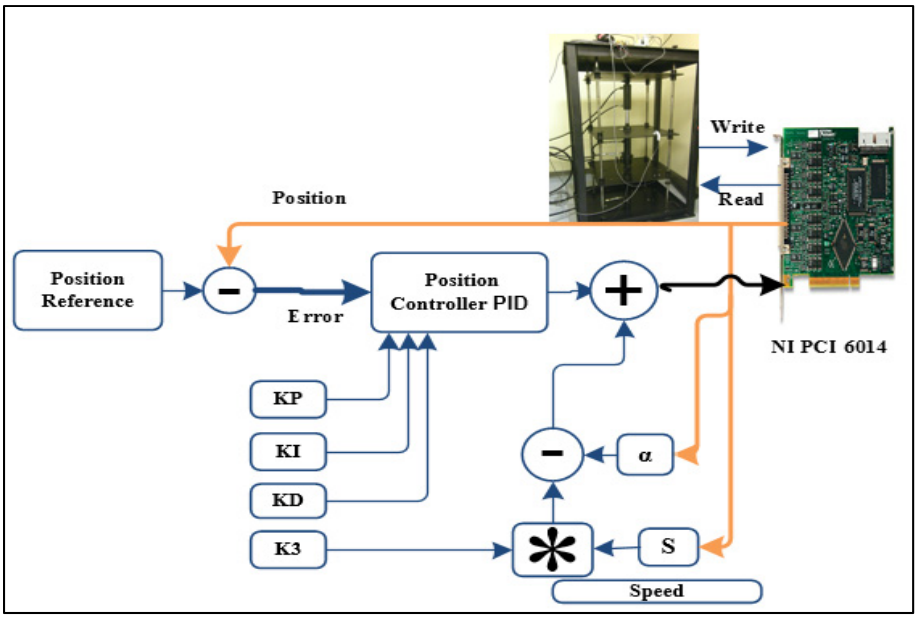

Figure 5.10 PIDDL schema

5.4.5 Fuzzy tuning PIDDL controller

PIDDL gains are tuned and applied using fuzzy controllers. The tuning method is developed using the predicted error resulting from gain tuners. The design is achieved in two steps:

(i) The first step involves tuning PIDDL gains $K_{p_r}, T_{i_r}, T_{d_r}$ as in Section 4.2 and gain K_{3_r} in order to produce a fuzzy PIDDL (FPIDDL) controller.

(ii) The second step involves applying the adaptive function $f_i(.): i = 1,2,3,4$ to return it as feedback to the inputs for the successive tuners of the fuzzy controller in Section 5.4.6.

Variable α is not within the tuning scope, because it does not have a significant influence on system performance. Gain $K_{3_r} = K_3 + \Delta K_3$ is tuned as an essential gain in the PIDDL controller in the same way as gain K_{p_r}.

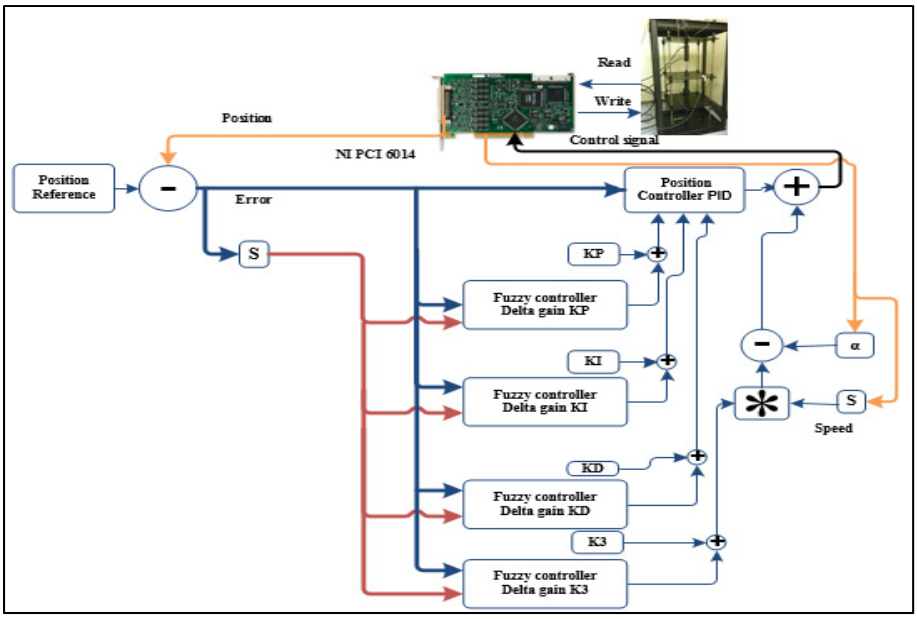

Figure 5.11 Fuzzy PIDDL gain tuning

The results will be discussed in Section 5.5. The values of the PID gains are used as initial values for tuning.

5.4.6 Adaptive fuzzy tuning PIDDL controller

The adaptive FPIDDL (AFPIDDL) is the new proposed structure for integrating the PIDDL controller into industrial control processes. The tuning is achieved when gains ΔK_p and ΔT_i are returned as feedback (green and red lines in Figure 5.12) to the successive fuzzy controllers. The output of fuzzy controller ΔK_p and its derivative $\Delta \dot{K}_p$ are integrated and added to the fuzzy controller inputs ΔT_i using functions $F_1(.), F_2(.)$.

This feedback corrects the effect of the excessive ΔK_p online. In other words, the overshot generated by tuning ΔK_p is modified by increasing T_{i_r}, as illustrated in Tableau 5.1.

Tableau 5.1 Rules of thumb for PID gains (Jantzen, 1998)

Tuned gain	Overshot	Rise time	stability
Increase K_{p_r}	Increase	Smaller	Decrease

Decrease T_{i_r}	Increase	Smaller	Decrease
Increase T_{d_r}	Decrease	Bigger	Increase

Stability is achieved by compromising ΔK_p and ΔT_i such that, when K_{p_r} causes the performance to deteriorates, the ΔT_i tuner already has an estimation of the system tendency. Gain T_{i_r} should be decreased in order to achieve a faster response time and smaller tracking error.

The stability will be deteriorated, and an overshot increase will be guaranteed.
There are two ways to remedy this problem:

1-Reduce gain $\mathbf{K_{p_r}}$, which should slow the rise time.

2-Increase T_{d_r}, which may also negatively affect the rise time.

The same discussion can be applied in order to tune ΔT_d. The tuning occurs when gain ΔT_i (red lines) is returned as feedback to the successive tuner ΔT_d. The output of fuzzy controller ΔT_i and its derivative are integrated and added to the inputs of the fuzzy controller ΔT_d using functions $F_3(.), F_4(.)$.

This feedback justifies the effect of an immoderate ΔT_i. Increasing T_{i_r} should be accompanied by decreasing T_{d_r} and vice-versa when adjusting the overshot and rise time. Stability is achieved by compromising ΔT_d and T_i. The proportional inverse relation between T_i and T_d means that, at this level, the tuning process has a direct influence on the system.

$F_3(.)$ And $F_4(.)$ Are chosen in such a way as to increase/decrease the error in order to shift the it and its derivative successively on the fuzzy controller scale. In other words, function $F_3(.)$ Is used to shift the position error in real time in order to change the associated fuzzy membership. This shift leads to a shifted fuzzy output, which in turn changes the PIDDL control output.

The same discussion as for function $F_3(.)$ Is also applied to function $F_4(.)$, with the corresponding derivative of error. The focus should be on choice of $F_3(.)$ and $F_4(.)$ functions

in cases where they could be linear or non-linear. A fuzzy controller with normalized input (error and its derivative) is used to tune gain K_{3_r}, which is similar in effect to gain T_{d_r} (Desantis, 1996).

As previously mentioned, there is no need to tune gain α due to its negligible influence on system performance. The results in the next section clearly demonstrate that this gain is higher than others. It is also returned as a negative feedback in order to form the total control signal.

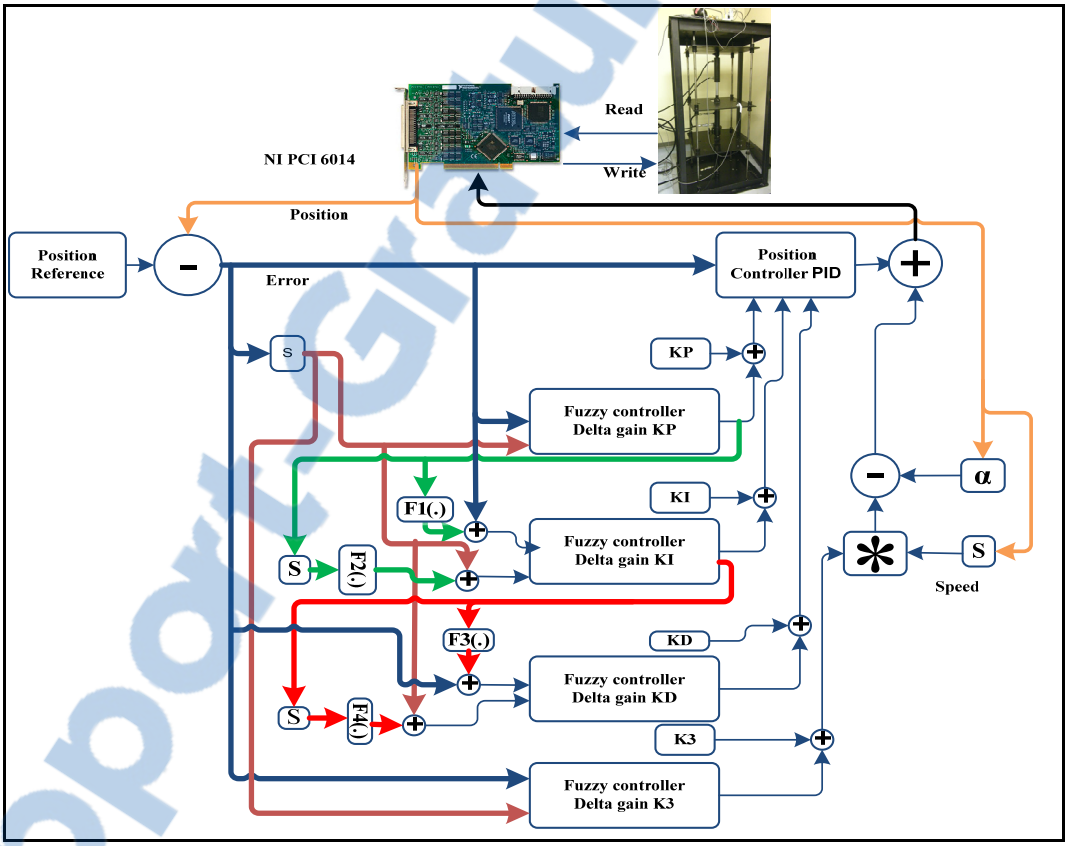

Figure 5.12 Adaptive fuzzy PIDDL gain tuning

5.5 Real-time results

The proposed structure is tested and applied to the active suspension benchwork in real time (Tableau-A III-2). The results clearly demonstrate the efficiency of adaptive fuzzy PIDDL controllers (Figure 5.13 (a)).

Tableau 5.2 Real-time results.

Sprung mass position				
AFPIDDL	AFPID	FPIDDL	PIDDL	PID
(1.99, -0.9) 82%	(2.153,-1.394) 72%	(2.032,-1.327) 73%	(2.049,-2.131) 57%	(2.11,-3.628) 27%

Tableau 5.2 illustrates the improvement achieved by applying the adaptive fuzzy structure to a PIDDL controller. 82% is a significant improvement compared to the PID controller (27%). The negative part of the sprung mass position is used to compare the results. For the positive part of the system response, the sprung mass position is situated between 1.99 and 2.11 cm. This is due to the delayed response of the system to perturbations and the non-symmetricity in the piston design. Similar results were achieved using AFPID and FPIDDL controllers.

This demonstrates the efficiency of PIDDL loops when the best gains are chosen by fuzzy controllers. The PIDDL controller demonstrated better results than the PID controller. The force transmitted to the passenger is reduced to its smallest values with fast response times when using an AFPIDDL controller (Figure 5.13 (b)).

The control signal reflects the performance of the controller in cases where the PID control signal is smallest. Not all control signals are saturated, which is primordial in making a fair comparison.

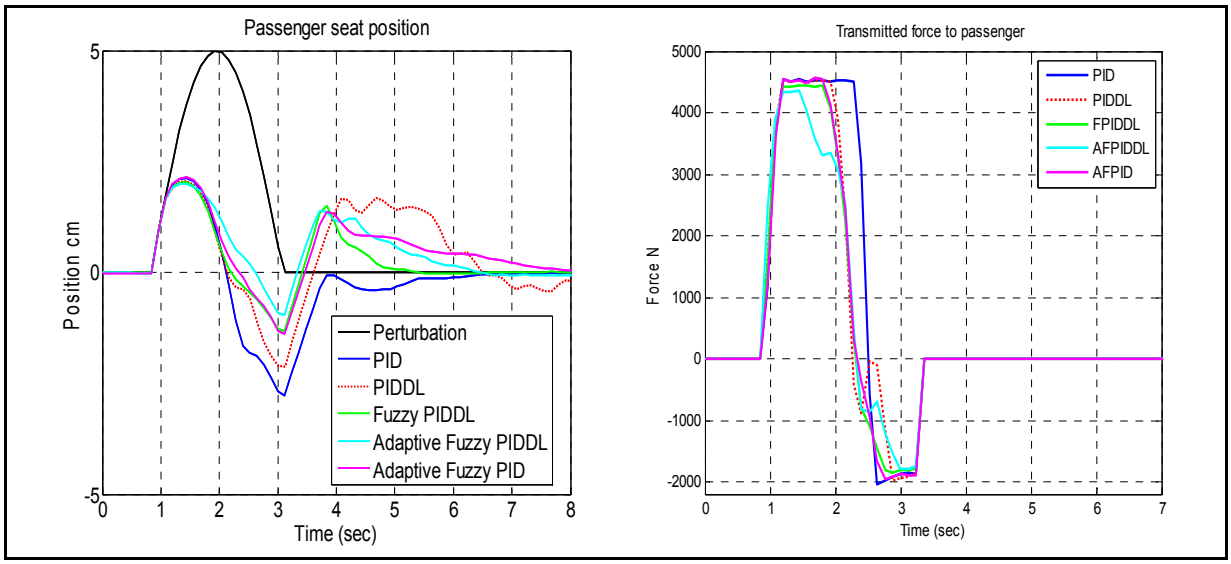

Figure 5.13 (a) Sprung mass position. (b) Force transmitted to the passenger

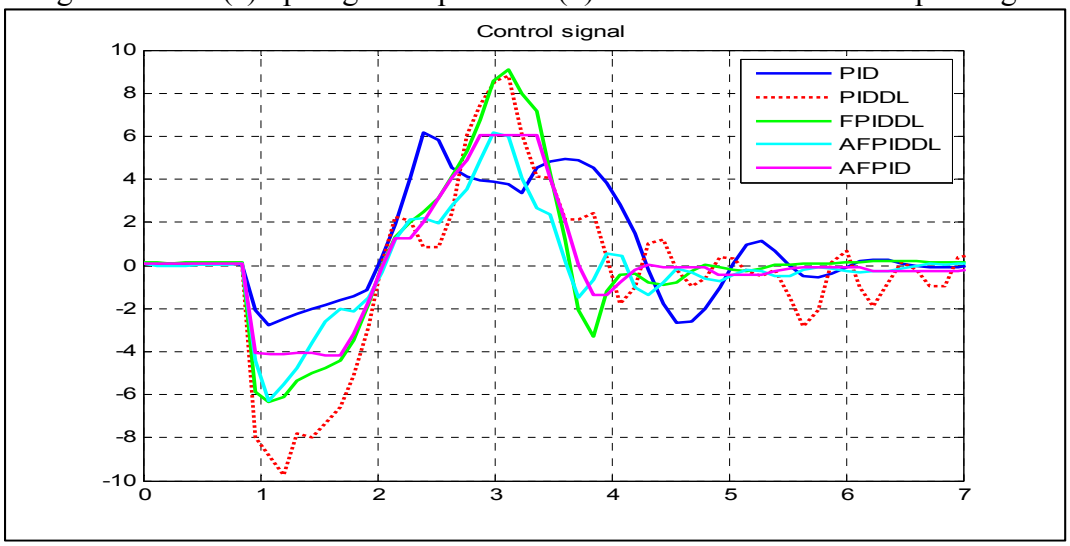

Figure 5.14 PIDDL control signal

Figure 5.15 (a) shows how to tune gain K_{p_r} based on the position error. The AFPIDDL controller demonstrates significant change ($K_{p_r} = 5$) during instants (1,2) sec and (3,4) sec. The PID gain is $K_{p_r} = 4$. For integral time T_{i_r} (Figure 5.15 (b)), the AFPID, FPIDDL and AFPIDDL controllers demonstrate variable integral times. The integral time for the PID controller is $T_{i_r} = 0.006$ sec. In Figure 5.16 (a), the AFPIDDL controller also demonstrates significant variations in the same period as with gain K_{p_r}. The derivative time for the PID

controller is $T_{d_r} = 0.000111$ sec. The essential gain K_{3_r} in the PIDDL structure is presented in Figure 5.16 (b). Gain K_{3_r} is doubled with the AFPIDDL controller as compared to the PIDDL controller, where $K_{3_r} = 30$.

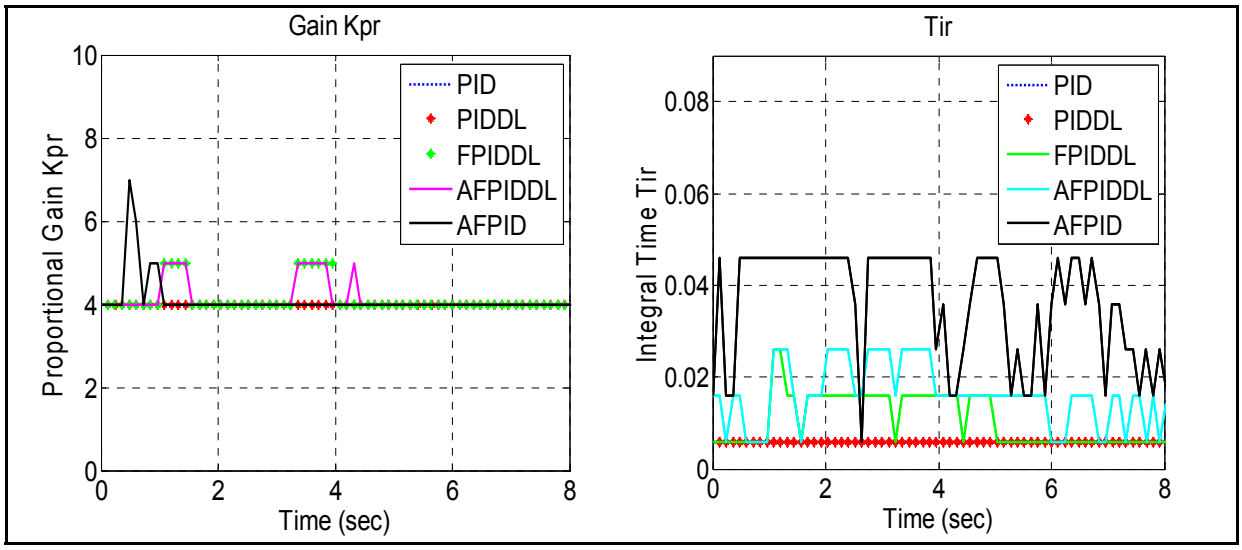

Figure 5.15 (a) PIDDL gain $\mathbf{K_{p_r}}$ (b) PIDDL $\mathbf{T_{i_r}}$

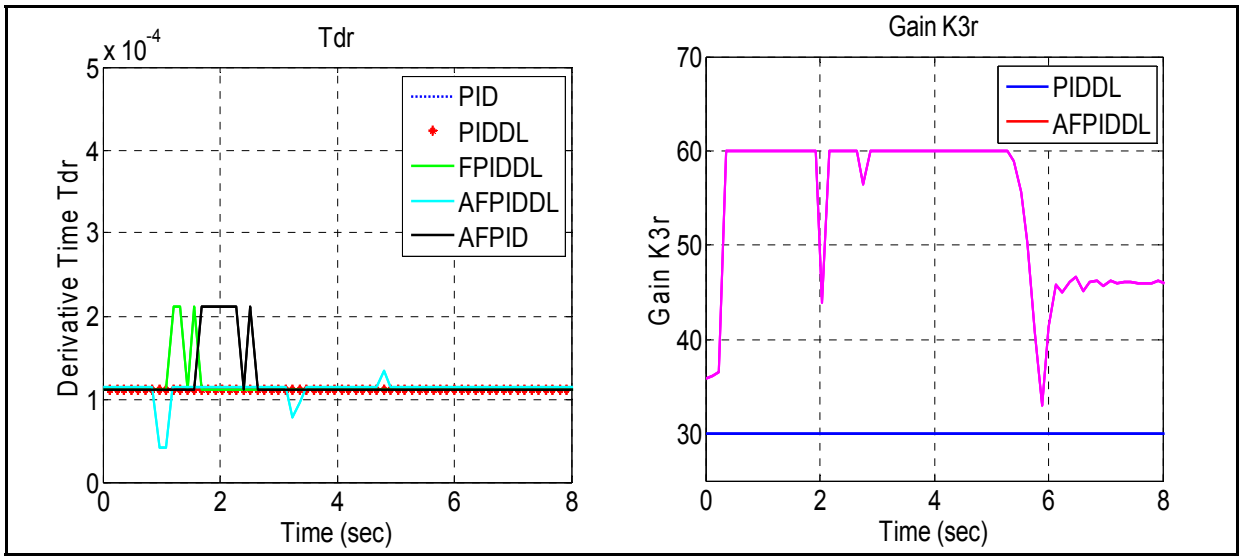

Figure 5.16 (a) PIDDL $\mathbf{T_{d_r}}$(b) PIDDL gain $\mathbf{K_{3_r}}$

In Figure 5.17 (a), the predictive error of $F_1(.)$ has a maximum of 2 cm for the AFPIDDL controller. The sign of the functions changed between instants (1,2) and (3,4) due to the need to correct the position error. The comparison between controllers is carried out in instants where the maximums are reached. In Figure 5.18 (b), the error derivative shows noticeable variations within instants (1,2) and (3,4), at which a meaningful action is taken by the controller.

The predictive error and its derivative are added to the inputs for the ΔT_d tuner using functions $F_3(.)$ and $F_4(.)$, as illustrated in Figure 5.18.

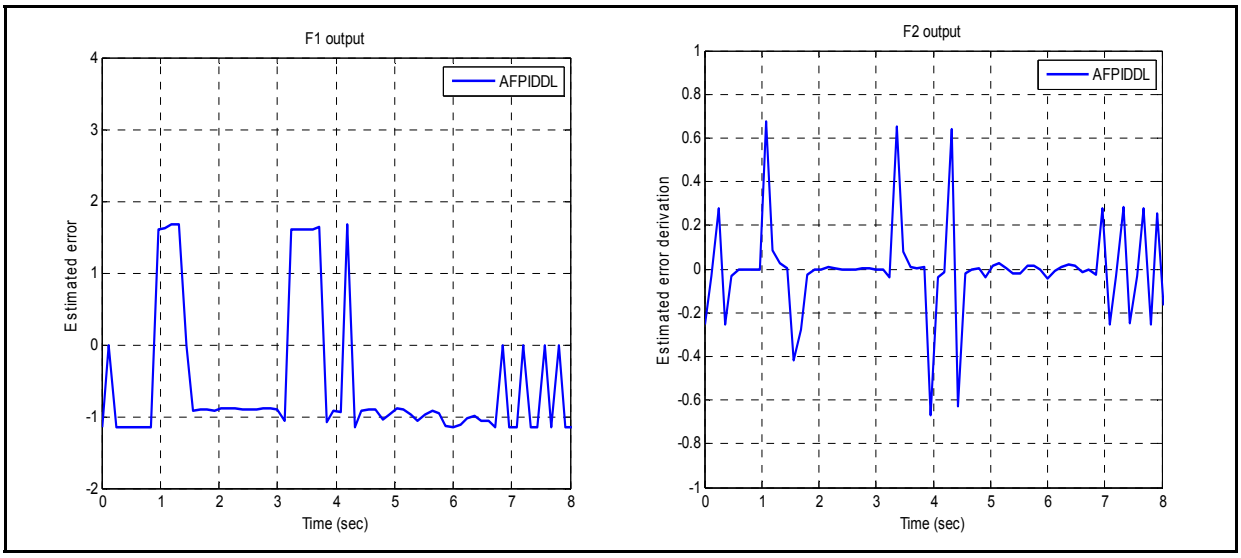

Figure 5.17 (a) $\boldsymbol{F_1}$ output (b) $\boldsymbol{F_2}$ output

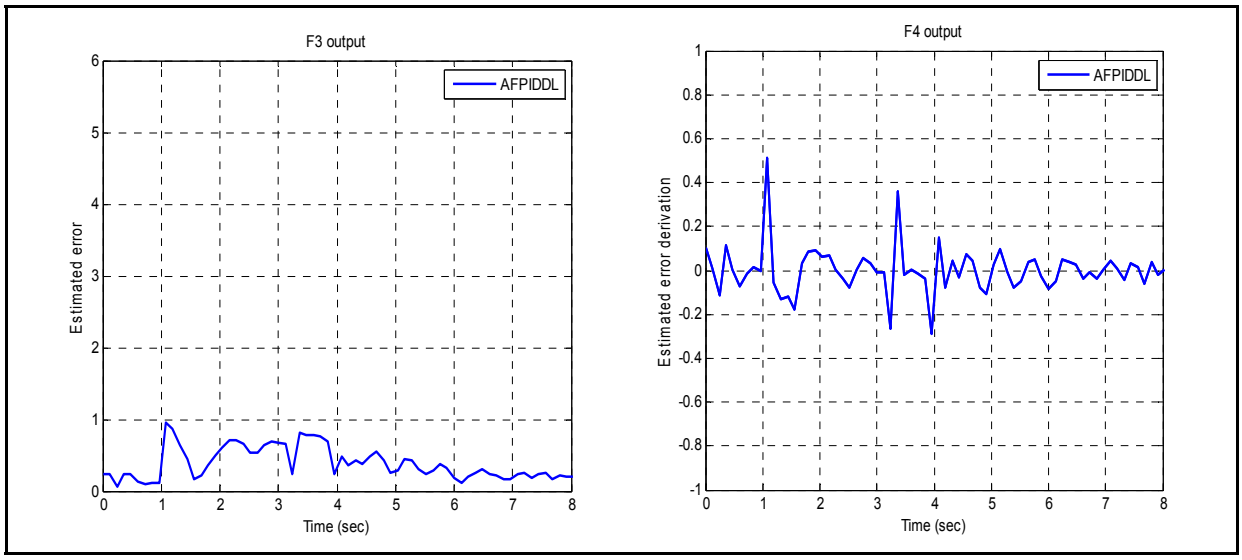

Figure 5.18 (a) $\mathbf{F_3}$ output (b) $\mathbf{F_4}$ output

The speed of the sprung mass in AFPID and AFPIDDL controllers results in a lower stabilization time than for PID controllers (Figure 5.19). Therefore, the passenger is subject to longer perturbations with the PID controller.

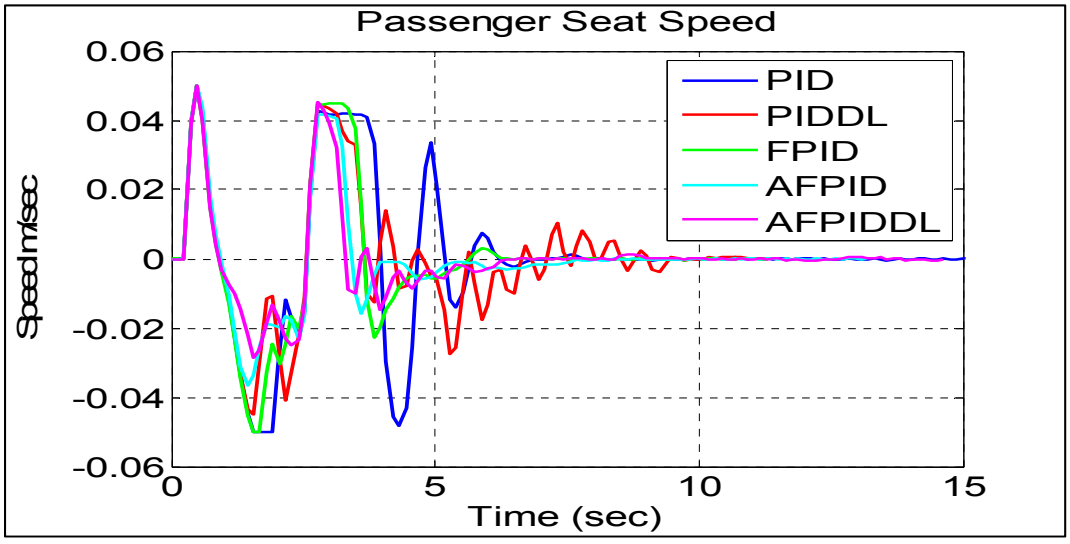

Figure 5.19 Speed of the sprung mass

5.6 Conclusion

An AFPIDDL controller was proposed and applied to an active suspension system. PID and PIDDL controllers were used to form the core of our proposed structure. The gains for the PIDDL controller were tuned using a fuzzy controller, the outputs of which are returned to intermediate functions as feedback in order to predict the errors produced by applying theses tuned gains to the system. In other words, the feedback makes a connection between tuned gains, which was not the case previously.

A comparison was carried out between AFPIDDL and FPIDDL controllers in order to prove the validity of the new structure. The tests conducted on the active suspension workbench in real time demonstrated improved performance as compared to conventional PID and other controllers. The AFPIDDL controller takes the speed of the sprung mass into consideration, which is not the case with PID controllers.

The proposed structure is able to use system information coming from sensors to tune the gains of the controllers using a fuzzy tuning process. This information can be fed back to successive inputs for the fuzzy controller using intermediate functions. In addition, the feedback functions can be replaced by non-linear functions. This proposed structure can also be modified to create a feedback connection between all the of PIDDL gains. The structure of the AFPIDDL controller can also be applied to industrial applications where fuzzy controllers and PID controllers are easy to apply.

CONCLUSION

Dans cette thèse, on a développé le modèle mathématique du système électrohydraulique à suspension active pour faire les tests en simulation et en temps réel. Le modèle du banc d'essai est développé et modifié pour que ça soit adapté pour des tests. Le modèle hybride est composé de modèle du banc d'essai et des éléments virtuels ajoutés pour réaliser les tests de validation.

La structure hybride pour contrôler la position du véhicule et la force produite transmise au passager est développées et appliquées en temps réel sur le banc d essaie. Les résultats ont prouvés la validité du contrôleur proposé par rapport aux contrôleurs conventionnels.
La structure hybride ne se limite pas aux contrôleurs nonlinéaires, elle regroupe également des contrôleurs conventionnels.

Dans la structure hybride plusieurs techniques sont utilisées pour éliminer le broutement comme la loi d'atteint exponentielle. En temps réel, le broutement est réduit au minimum avec un temps de réponse plus rapide. De plus, un contrôleur de logique flou basé sur les surfaces de glissement de la position et de la force est utilisée pour améliorer la performance.
Finalement, un contrôleur PIDDL basé sur le contrôleur PID a été modifié et adapté pour faire un contrôle de position sur le banc d'essai. Des contrôleurs de logique flou sont intégrés dans une structure pour mettre à jour les gains de contrôleurs PIDDL.
Les structures PIDDL générées sont testées sur le banc d'essai et comparées avec d'autres structures basée sur le contrôleur PID.

Les contrôleurs utilisés ne sont pas récents pourtant leur efficacités dans cette structure a fait une différence. Avec une telle structure, les portes sont ouvertes pour plus d'avancement concernant les structures hybrides où on peut faire une meilleure liaison entre les contrôleurs.
Les structures suggérées renforcent la tendance à l'industrie pour utiliser des contrôleurs confidentielle fiables.

RECOMMANDATIONS

Pour conclure cette thèse, des recommandations sont suggérées après avoir réalisé des tests en temps réel pour les trois articles. Les recommandations sont divisées en deux catégories.
La première catégorie concerne le banc d essaie hydraulique à suspension active.
La deuxième catégorie concerne la commande des systèmes électrohydrauliques.
Les améliorations suggérées pour le banc d'essai:

- La perturbation générée par un vérin du bas devrait utiliser une pompe indépendante vu que le vérin de perturbations devrait être isolé de vérin de contrôle. La performance s'améliore si une pompe plus grande est utilisée.
- Un débitmètre est nécessaire pour mesurer le débit au lieu de faire une estimation non précise.
- La position de tiroir de la servovalve est estimée. Pourtant s'il y avait une servovalve, avec un LVDT des résultats plus précis seront obtenus.
- Vu que le contrôle nonlinéaire emploie l'utilisation des équations discontinues et nondifférentiable, la carte utilisée n'est pas capable pour faire l'échantillonnage en temps réel. Un ralentissement est observé lors de tests en temps réel. C'est recommandable d'utiliser des Compact RIO Platform National Instruments en termes de rapidité et fiabilité
- L'installation des capteurs de force sera utile pour bien déterminer la force transmise au passager.

Par rapport à la commande des systèmes électrohydraulique, Nos recommandations sont les suivantes :

- Dans la structure hybride nous suggérons de développer une loi coopérative entre les contrôleurs en utilisant d'autre fonctions différentes des filtres passe bas. Ces fonctions devraient en principe être des fonctions de variables du système.

- Pour le contrôle adaptative utilisant le contrôleur PIDDL, les fonctions qui évaluent les effets des mis à jours des contrôleurs peut être remplacées par des fonctions pertinentes liées avec le modèle mathématique du système.
- La méthode de backstepping peut être investie en utilisant des fonctions lyapunov liées avec les trajectoires de position et de force pour réaliser un contrôleur qui lie entre les trajectoires désirées et les fonctions candidates de lyapunov.

ANNEX I

DONNÉES DE L'ARTICLE 1

Tableau-A I-1 System variables.

Symbol	Parameter	Value
$P_{1,2}$	Pressure at cylinder	$P_s = P_1 + P_2$
β	Effective bulk modulus	$7.995\text{e}8 N/m^2$
L	Coefficient of leakage	$9.047\text{e}-13 m^5/N_s$
A	Piston area	$3.35\text{e}-4 m^2$
P_L	Load pressure	$P_2 - P_1$
P_s	Supply pressure	$103.4\text{e}5 N/m^2$
ρ	Hydraulic fluid density	$867 kg/m^3$
V_0	Volume of actuator	$135.4\text{e}-6 m^3$
C_d	Low discharge coefficient	0.63
M_u	Unsprung mass	$59 kg$
M_s	Actuator mass	$290 kg$
K_r	Tire spring stiffness	$190{,}000 N/m$
K_p	Load spring stiffness	$16{,}812 N/m$
B_r	Tire viscous damping	$800 N_s/m$
B_P	Load viscous damping	$800 N_s/m$
τ	Servo-valve time constant	$0.01 s$

Tableau-A I-2 State variables.

Symbol	Parameter
x_r	External unknown perturbation
$\dot{x}_r$	Speed of perturbation signal
$x_1 = x_s$	Vertical position of the car body
$\dot{x}_s$	Piston speed
$x_2 = \dot{x}_1$	Vertical speed of the car body
$x_3 = x_u$	Vertical position of the car wheel
$x_4 = \dot{x}_3$	Vertical speed of the car wheel
$x_5 = P_L$	Pressure difference in the circuit
$x_6 = x_v$	Area of the servo valve orifice
U	Control signal

Tableau-A I-3 Controller parameters.

Symbol	Position control parameters	Value
c_1	Sliding surface gain	125000
c_2	Sliding surface gain	7500
c_3	Sliding surface gain	150
c_4	Sliding surface gain	1
α	Sigmoid function	2000
K_{sw}	Switching gain	330000
Force control parameters		
C_1	Sliding surface gain	150
ρ	Hydraulic fluid density	10000

ANNEX II

DONNÉES DE L'ARTICLE 2

Tableau-A II-1 System variables.

Symbol	Parameter	Value
M_s	Actuator mass	40 kg
M_u	Tire mass	32 kg
x_r	Perturbation	5 cm
B_p	Passive suspension damping	800 N_s/m
K_p	Passive suspension rigidity	16,812 N/m
B_r	Tire damping coefficient	800 N_s/m
k_r	Tire stiffness	190,000N/m
β	Bulk modulus	7.995e8 N/m^2
L	Leakage coefficient	9.047e-13 m^5/N_s
P_s	Supply pressure	500 Psi
A	Piston area	20.2683 e-4m^2
ρ	Hydraulic fluid density	867 kg/m^3
V_O	Volume of actuator	195.37e-6m^3
ρ	Hydraulic fluid density	857 kg/m^3
τ	Servo-valve time constant	0.0035 Sec.
k_v	Servovalve gain	1.3714eE-6 m^2/V
C_D	Low discharge coefficient	0.63
α	Sigmoid function	2000

ANNEX III

DONNÉES DE L'ARTICLE 3

Tableau-A III-1 System variables.

Symbol	Parameter/Value
y_1	Sprung mass position
y_2	Sprung mass speed
y_3	Unsprung mass position
y_4	Unsprung mass speed
y_5	Load pressure
y_6	Spool valve displacement
A_1	$a_0 + d_0$
A_2	$b_0 + d_1$
A_3	$c_1 + a_1$
J_1	$2V_O\beta$
a_0	$\frac{K_p}{M_s}$
b_0	$\frac{B_p}{M_s}$
a_1	$\frac{A}{M_s}$
b_1	$\frac{B_r}{M_u}$
c_1	$\frac{A}{M_u}$
d_0	$\frac{K_p}{M_u}$
d_1	$\frac{B_p}{M_u}$
h_1	$\frac{k_r}{M_u}$

Tableau-A III-2 Parameters Values.

Symbol	Parameter	Value
M_s	Actuator mass	40 kg
M_u	Tire mass	32 kg
x_r	perturbation	5 cm
B_p	Passive suspension damping	$800\ N_s/m$
K_p	Passive suspension rigidity	$16{,}812\ N/m$
B_r	Tire damping coefficient	$800\ N_s/m$
k_r	Tire stiffness	$190{,}000\ N/m$
β	Bulk modulus	$7.995e8\ N/m^2$
L	Leakage coefficient	$9.047e-13\ m^5/N_s$
P_s	Supply pressure	500 Psi
A	Piston area	$20.2683\ e-4\ m^2$
ρ	Hydraulic fluid density	$867\ kg/m^3$
V_O	Volume of actuator	$195.37e-6\ m^3$
ρ	Hydraulic fluid density	$857\ kg/m^3$
τ	Servo-valve time constant	0.0035 Sec
k_v	Servovalve gain	1.3714e-6 m^2/V
C_D	Low discharge coefficient	0.63
α	Sigmoid function	2000

LISTE DE RÉFÉRENCES BIBLIOGRAPHIQUES

Alleyne A, Liu R (2000) A simplified approach to force control for electro-hydraulic systems. *Control Engineering Practice* 8(12): 1347-1356.

Alexander GL, Jorge R, Yuri VO and Edgar T (2009) Robust Trajectory Tracking for An Electro-hydraulic Actuator. *IEEE Transactions on Industrial Electronics* 56(9): 3523-3531.

Almeida, O. d. & Coelho, A. A. (2002). A fuzzy logic method for autotuning a PID controller: SISO and MIMO systems. *15th IFAC World Congress on Automatic Control*.

Amer AF, Sallam EA, Elawady WM. Quasi sliding mode-based single input fuzzy self-tuning decoupled fuzzy PI control for robot manipulators with uncertainty. *International Journal of Robust and Nonlinear Control* 2012; 22(18): 2026-2054.

Angue-Mintsa H, Venugopal R, Kenne JP and Belleau C (2011) Adaptive Position Control of an Electrohydraulic Servo System with Load Disturbance Rejection and Friction Compensation. *Journal of Dynamic Systems, Measurement, and Control.* 133(6): 064506-1 -064506-8.

Assadsangabi B, Eghtesad M, Daneshmand F and Vahdati N (2009) Hybrid sliding mode control of semi-active suspension systems. *Smart Materials and Structures* 18(12): 1-10.

Aström, K. J. & Hägglund, T. (2001). The future of PID control. *Control engineering practice,* 9(11), 1163-1175.

Bakri, F. A., Mashor, M. Y., Sharun, S. M., Norhayati, M. N., Supardi, N. Z. & Saad, Z. (2012). A simple Adaptive Fuzzy Logic Controller base on shifting of the membership function. *IEEE 8th International Colloquium on Signal Processing and its Applications* (CSPA), 456-460.

Baumal AE, McPhee JJ and Calamai PH (1998) Application of Genetic Algorithm to the Design. Optimization of an Active Vehicle Suspension System. *Computer Methods in Applied Mechanics and Engineering* 163(1): 87-94.

Bonchis A, Corke P, Rye D and Ha Q (2001) Variable structure methods in hydraulic servo systems control. *Automatica* 37 (4): 589-595.

Callai, T. C., Santos J. E. S., Sumar R. R. & Coelho, A. A. R. (2005). Applying the potentiality of using fuzzy logic in PID control design. *Soft Computing: Methodologies and Applications, Springer,* 193-204.

Campos J, Davis L, Lewis FL, Ikenaga S, Scully S, Evans M. Active suspension control of ground vehicle heave and pitch motions. *Proceedings of the 7th IEEE Mediterranean Control Conference on Control and Automation* 1999; 222-233.

Çetin Ş, Akkaya AV. Simulation and hybrid fuzzy-PID control for positioning of a hydraulic system. *Nonlinear Dynamics* 2010; 61(3): 465-476.

Chapman K. Digitally removing a DC offset: DSP without mathematics. *Xilinx white paper* 2008; 279: 134.

Chantranuwathana S, Peng H. Force tracking control for active suspensions-theory and experiments. *IEEE Conference on Control Applications*; 1: 442-447.

Chen HM, Shen CS, Lee TE. Implementation of Precision Force Control for an Electro-Hydraulic Servo Press System. *Applied Mechanics and Materials* 2012; 190: 806-809.

Cornieles, E. (1998). Développement d'un module de réglage automatique d'un compensateur PID Dual Loop [Developing an auto-tuning module for a PID Dual Loop compensator] . (Ph.D. Thesis), École polytechnique de Montréal.

Desantis, R. M. (1996). Dual loop PID configuration. United States Patent. Patent number: 5481453, January 1996.

Edwards, C. Spurgeon, S. (1998) Sliding mode control: theory applications. London: *Taylor & Francis*.

Fainekos, G. E., H. Kress-Gazit and G. J. Pappas (2005). Hybrid controllers for path planning: A temporal logic approach. *Proceedings of the 44th IEEE Conference on Decision and Control*.

Fallaha C, Saad M, Kanaan HY, Al-Haddad K. Sliding-mode robot control with exponential reaching law. *IEEE Transactions on Industrial Electronics* 2011; 58(2): 600-610.

Fateh MM (2010) Robust impedance control of a hydraulic suspension system. *International Journal of Robust and Nonlinear Control 20 (Compendex)* 20(8): 858-872.

Ferreira JA, Sun P, Gracio JJ. Design and control of a hydraulic press. *IEEE Conference on Computer Aided Control System Design*, Munich, Germany, 2006; 814-819.

Fung RF and Yang RT (1998) Application of VSC in position control of a nonlinear electrohydraulic servo system *Computers & structures* 66(4): 365-372.

Gao W and Hung JC (1993) Variable structure control of nonlinear systems: a new approach. *Computers & structures* 40(1): 45-55.

Han G, Chen L, Shao J, Sun Z. Study of fuzzy PID controller for industrial steam turbine governing system. *IEEE International Symposium on Communications and Information Technology* 2005; 2: 1275—1279.

Hedrick J and Yip P (2000) Multiple sliding surface control: theory and application. *Journal of dynamic systems, measurement, and control* 122(4): 586-593.

Heinrichs, B., N. Sepehri and A. Thornton-Trump (1997). Position-based impedance control of an industrial hydraulic manipulator. *Control Systems*, IEEE 17(1): 46-52.

Huang, H., X. Yang, X. I., Deng, X. L. & Qiao Z. h. (2009). A Parameter Auto-Tuning Method of Fuzzy-PID Controller. *Fuzzy Information and Engineering Springer,* (2), 1193-1200.

Hwang C and Lan C (1994) The position control of electrohydraulic servomechanism via a novel variable structure control. *Mechatronics* 4(4): 369-391.

Hwang CL (1996) Sliding mode control using time-varying switching gain and boundary layer for electro-hydraulic position and differential pressure control. In Proceedings of IEE—*Control Theory Application* 143(4): 325–332.

Jantzen, J. (1998). Tuning of fuzzy PID controllers. Technical University of Denmark, Department of Automation, Report no 98- H 871, 30 Sep, 1-22.

Kaddissi C, Saad M, Kenne JP. Interlaced backstepping and integrator forwarding for nonlinear control of an electrohydraulic active suspension. *Journal of Vibration and Control 2009*; 15(1): 101-131.

Kalyoncu M, Haydim M. Mathematical modelling and fuzzy logic based position control of an electrohydraulic servosystem with internal leakage. *Mechatronics* 2009; 19(6): 847-858.

Karasakal, O. M., Guzelkaya, M., Eksin I. & Yesil, E. (2011). An error-based on-line rule weight adjustment method for fuzzy PID controllers. *Expert Systems with Applications,* 38(8), 10124-10132.

Karpenko M and Sepehri N (2012) Electrohydraulic force control design of a hardware-in-the-loop load emulator using a nonlinear QFT technique. *Control Engineering Practice* 20(6): 598-609.

Kim SW and Lee JJ (1995) Design of a fuzzy controller with fuzzy sliding surface. *Fuzzy Sets and Systems* 71(3): 359-367.

Kurfess, T. R. (2004). Robotics and automation handbook, CRC press.

Lane DM, Dunnigan MW, Clegg AC, Dauchez P and Cellier L (1997) A comparison between robust and adaptive hybrid position/force control schemes for hydraulic underwater manipulators. *Transactions of the Institute of Measurement and Control* 19(2):107-116.

Lin J-S and Kanellakopoulos, I (1997) A comparison between robust and adaptive hybrid position/force control schemes for hydraulic underwater manipulators. *Control Systems, IEEE* 17(3):45-59.

Lin JS, Kanellakopoulos I. Nonlinear design of active suspensions. *Control Systems, IEEE* 1997; 17(3): 45-59.

Maghfiroh, H., Oyas, W., Cahyadi, A.I. & Supriyanto, P. (2013). PID-Hybrid Tuning to Improve Control Performance in Speed Control of DC Motor Base on PLC. *International Conference on Instrumentation Control and Automation* (ICA), 233 - 238.

Mahmoodabadi M, Taherkhorsandi M, Talebipour M and Castillo-Villar K. (2014) Adaptive robust PID control subject to supervisory decoupled sliding mode control based upon genetic algorithm optimization. *Transactions of the Institute of Measurement and Control* 70(1): 110.

Merritt, HE (1967) Hydraulic control systems. New York: *John Wiley & Sons*.

Mihajlov M Nikoli'c V and Anti'c D (2002) Position control of an electro-hydraulic servo system using sliding mode control enhanced by fuzzy PI controller. *Facta universitatis-series: Mechanical Engineering*. 1(9): 1217-1230.

Mahmoodabadi M, Taherkhorsandi M, Talebipour M and Castillo-Villar K. (2014) Adaptive robust PID control subject to supervisory decoupled sliding mode control based upon genetic algorithm optimization. *Transactions of the Institute of Measurement and Control* 70(1): 110.

Priyandoko G, Mailah M, Jamaluddin H. Vehicle active suspension system using skyhook adaptive neuro active force control. Mechanical Systems and Signal Processing 2009; 23(3): 855-868.

Schlichthärle D. Digital filters. *Editorial Springer*: Berlin, 2000.

Shaer, B., J.-P. Kenné, C. Kaddissi and C. Fallaha (2016). A chattering-free fuzzy hybrid sliding mode control of an electrohydraulic active suspension. *Transactions of the Institute of Measurement and Control*: 0142331216652468.

Shao, J., Z. Wang, J. Lin and G. Han (2009). Model identification and control of electro-hydraulic position servo system. Intelligent Human-Machine Systems and Cybernetics, 2009. IHMSC'09. *International Conference on, IEEE.*

Shi M, Liu X, Shi Y. Research n enhanced ADRC algorithm for hydraulic active suspension. *Transportation, Mechanical, and Electrical Engineering (TMEE) on International Conference IEEE* 2011; 1539-1543.

Shi H, Gong G, Yang H. Pressure and speed control of electro-hydraulic drive for shield tunneling machine. *Proceedings of the IEEE/ASME International Conference on Advanced Intelligent Mechatronics, IEEE*, Xi'an, China, 2008; 314-317.

Shoorehdeli MA, Teshnehlab M and Shoorehdeli HA. Velocity control of an electro hydraulic servosystem. *IEEE International Conference on Systems, Man and Cybernetics* 2007; 1536—1539.

Slotine, J.-J. E. and W. Li (1991). Applied nonlinear control, prentice-Hall Englewood Cliffs, NJ.

Sohl GA and Bobrow JE (1999) Experiments and simulations on the nonlinear control of a hydraulic servosystem. *Control Systems Technology, IEEE Transactions* 7(2): 238-247.

Solihin, M. I. (2007). Fuzzy-tuned PID control design for automatic gantry crane. *IEEE International Conference on Intelligent and Advanced Systems ICIAS*, 1092-1.

Ursu I, Ursu F, Popescu F. Backstepping design for controlling electrohydraulic servos. *Journal of The Franklin Institute* 2006; 343(1): 94-110.

Utkin VI and Lee H (2006) Chattering problem in sliding mode control systems. *In International Workshop on Variable Structure Systems* (VSS'06), Alghero, Italy, 5-7 June 2006, pp.346-350.

Wang Z,Shao J, Lin J, Han G. Research on controller design and simulation of electro-hydraulic servo system. *IEEE International Conference on Mechatronics and Automation* 2009; 380-385.

Wos P, Dindorf R. Practical parallel position-force controller for electro-hydraulic servo drive using on-line identification. *International Journal of Dynamics and Control* 2014; 4(1) :1-7.

Wright PG (1983) The influence of aerodynamics on the design of Formula One racing cars. *International Journal of Vehicle Design* 3(4): 383-397.

Xu, J. & Feng, X. (2004). Design of adaptive fuzzy PID tuner using optimization method. *IEEE Fifth World Congress on Intelligent Control and Automation WCICA*, 2454—2458.

Xu, J. X., Hang, C. C. & Liu, C. (2000). Parallel structure and tuning of a fuzzy PID controller. *Automatica,* 36(5), 673-684.

Yahada MD, Hudha K. PI/PISMC control of hydraulically actuated active suspension system. *Proceedings the 1st international conference on natural resources engineering and technology INRET* 2006, Marriot, Putrajaya, Malaysia, 2006.

Young KD, Utkin VI and Ozguner U (1996) A control engineer's guide to sliding mode control. In *Proceedings of IEEE International Workshop on Variable Structure Systems*, (VSS'96), Tokyo, Japan, 5-6 December 1996, pp.328-342.

Zheng, J.M., Zhao, S. D. & Wei, S. G. (2009). Application of self-tuning fuzzy PID controller for a SRM direct drive volume control hydraulic press. *Control Engineering Practice,* 17(12), 1398-1404.

Zhiming J, Shengwei W and Tingqi L (2003) Variable structure control of electrohydraulic servo systems using fuzzy CMAC neural network. *Transactions of the Institute of Measurement and Control* 25(3): 185-201.